Coherent transport through potential barriers in a quantum channel in magnetic field

Student: Yu-yu Lin   Advisor: Chon-Saar Chu

Department of Electrophysics

National Chiao-Tung University

January 19, 2006

Abstract

In this thesis, we try to push our theoretical description of magnetotransport in a quantum wire to the high magnetic field regime. Two different approaches, namely, the mode matching approach and the partial Fourier transformation of the Lippmann-Schwinger equation approach, have been employed to cross check our results. We have plotted the transmission, the wavefunction, and the current density patterns and have interpreted them in light of the edge states. A simple criteria for the formation of edge states is reached, which is arisen from the comparison of the cyclotron radius and the effective width of the wire. For the case of a single repulsive barrier, a transmission dip is found at the threshold of a subband. For the case of a single attractive barrier, two transmission dips are found for incident energy that lies below a subband threshold. These are discussed in terms of the edge states and the evanescent modes.

摘要

　　在本論文中, 我們試著將所能得到的在量子導線的磁導率增促到高磁場的範圍。我們使用了兩種不同的方法、模態匹配近似法及 Lippmann-Schwinger 方程式的部分富立葉轉換近似方法、來交互比對確定我們的結果。接著我們對對穿透率、波函數、及電流密度作圖並解釋其中邊緣態的現象。經由比較比較磁場的迴旋半徑及通道的等效寬度, 提供了一個簡單度量邊緣態產生的方法。在通道含有一個排斥力的雜質時, 我們在次能帶底部之上可以發現一個凹陷。而在吸引的雜質時, 則在入射能量低於次能帶底部的地方發現兩個凹陷。我們也會討論邊緣態跟衰減態的現象。

誌謝

從專題研討開始，至今也已經四年有了。面對老師的時間，也不可所謂不長。除了在專業上的指導與討論，更應該感謝的是由老師本身所傳達的對學問的專注與熱情。尤其是在做學問的態度上，我能學的實在太多也得到太多。除了老師，也該感謝在這日子裡不斷給予指導叮嚀的唐志雄學長。總是能在我需要協助的時候，給予最好的建議。當然，伙伴是不能少的。從老王學長、淑維學姊到哲明、宇廷、靖航、淑娟及其他的朋友們。有你們的出現、陪伴才不會那麼孤單。尤其，要特別感謝老王學長，在實驗室裡的這段日子真的是多受到照顧了。另外，也要感謝許永昌學長及 Prof. Vidar Gudmundsson 的討論，特別是在數值程式方面的指導，這在我的研究上提供了最有力的協助。最後，我要感謝我的家人，這也是之於我最重要的支持力量。不管多麼困難，你們總是永遠無私的付出與體諒。

感謝所有。

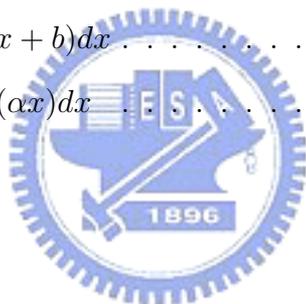# Contents

List of Figures

Chapter 1

Introduction and background

The discovery of the quantized conductance steps in two-dimensional electron gas(2DEG), micro-constrictions based on $GaAs/Al_xGa_{1-x}As$ heterostructures [1,2], the quantized conductance steps followed an increase of interest in the study of quantum ballistic transport through narrow channels in 2DEG [3]. In particular, the influence of impurities on the conductance attracted a great deal of attention since impurities inside or near the conducting channel may destroy the conductance quantization [4–21], The effect of the impurities is especially strong near the step, i.e. the thresholds where propagating modes are opened. And it is also known from experiments as well as from theory that near the steps even a single impurity may strongly affect the conductance.

The influence of a single impurity on the conductance of a 2DEG channel was studied theoretically in Refs. [12–14], [19] and [20]. The theoretical treatment of this program was based on two model potentials, of the channel and of the impurity. The simplest channel confining potential, which is an infinite uniform 2D wire with hard walls, was considered in papers [12–14]. Actually, for a wire, realistic narrow channels in split-gate devices cannot be taken as uniform wires, but rather as a parabolic constructions in the propagating direction. As to the impurity potential, the short-range δ-type potential was used in almost all papers. There are only a few exceptions: a infinite-long 2D wire with parabolic confinement in the propagating direction and a δ-type barrier cross the wire. [14]

It is shown that a single impurity produces fine-structure effects in the dependence of the conductance G on the Fermi energy E near the thresholds. For instance, an attractive impurity in an infinite uniform wire generates dips below the conductance. steps [12–14] These dips appear as a result of resonance reflection by quasibound states in the impurity potential. But in the case of repulsive potential, it do not have any resonance as long as it is only a δ-type barrier. There must be two or more δ-type barrier or finite-range barrier and the resonance happened.

Suppression of backscattering by a magnetic field is the basis of the theory of the quantum Hall effect developed by Marcus Büttiker (IBM, Yorktown Heights) [22]. Büttiker's theory uses a multi-reservoir generalization of the two-reservoir Landauer formula. The propagating modes in the quantum Hall effect are the magnetic Landau levels interacting with the edge of the sample. There is a smooth crossover from zero-field conductance quantization to quantum Hall effect, corresponding to the smooth crossover from zero-field wave guide modes to magnetic edge states.

The discovery of the quantum Hall effect [23] stimulated intensive theoretical and experimental research on magnetic field influence on low dimensional nano structures(see Refs. [24–28], and references therein). In particular, the resistances of a quantum channel with a finite barrier inside were calculated in the limit of very strong magnetic fields. [29] Oscillations which are periodic in the field, in the low-temperature magnetoresistance of a point contact in the two-dimensional electron gas were observed experimentally and explained theoretically as a tunneling between edge states across the point contact. [30] Conductivity of the many-terminal junctions of quantum wires was theoretically investigated, [31–33] and a rich structure of the Hall resistance deviating considerably from the wide-wire result was shown. Computational study of several different kinds of four-terminal junctions showed that the Hall and bend resistances are extremely sensitive to the geometry of the junction and that the classical and quantum mechanical results are qualitatively similar but quantitatively very different. [34] Spectroscopy of the energy levels and associated currents of infinitely deep [35–37] and finite [38] quantum wells in crossed

magnetic and electric fields was calculated, and a crucial role of the energy spectrum anticrossings in the jumps of the equilibrium Hall currents was described. Theoretical analysis revealed that the magnetic field applied to the straight quantum wire with symmetrically embedded quantum dots leads to the Fano resonances [39] on the conductance Fermi energy dependence. [40–43, 70] It was predicted that asymmetric Fano resonances occur also in the electronic conductance across a shallow quantum well in a high tilted magnetic field. [45]

The edge state is often used to describe that what is the quantum Hall effect, and it is a classical feature of the the electrons in a system applied magnetic filed move along the edge of the system. In the Ref. [46], the author discuss about the two regime of high and low magnetic field. The explanation is based on the differences in lateral extension of the magnetic quantum states at the Fermi level in a narrow channel (of width W). One has to distinguish between a high-filed and a low-field regime, determined by the relative magnitude of W and the cyclotron orbit diameter $2l_B$ (with $l_B \equiv (\hbar k_F/eB)^{1/2}$, k_F being the Fermi wavevector and B the strength of magnetic field). In the high-field regime $2l_B < W$, right- and left-moving electrons with Fermi energy are spatially separated in edge states [47–49] at the opposite boundaries. These current-carrying edge states can coexist with quantized cyclotron orbits in the bulk of the sample (Landau states)–when the Fermi level, as determined by the carrier concentration, coincides with a Landau level. Edge states correspond classically to electrons skipping along the boundary (Fig.1.1). The high-field regime has been discussed by Halperin [50] and MacDonald and co-workers, [35, 51] who have shown how a Hall voltage arises because of differences in the population of right- and left-moving edge states. In the low-field regime $2l_B > W$ relevant to the experiments of Roukes *et al.*, [52] Landau states which are unperturbed by the boundaries no longer exist at the Fermi level. Concurrently, some edge states begin to interact with the opposite boundary. Prange [53] has calculated the magnetic quantum states in thin-plate geometry. The differences in lateral extension of the states which follow from his calculation may be understood from the classical correspondence

(Fig.1.1). In addition to skipping orbits (corresponding to edge states) we now also have trajectories which traverse the channel. The corresponding "transversing states" (also know as hybrid magnetoelectric subbands) interact with both boundaries. Because of the presence of these traversing states the arguments of Refs.10 and 11 no longer apply, and anomalies in the Hall voltage can be expected to occur in the low-field regime.
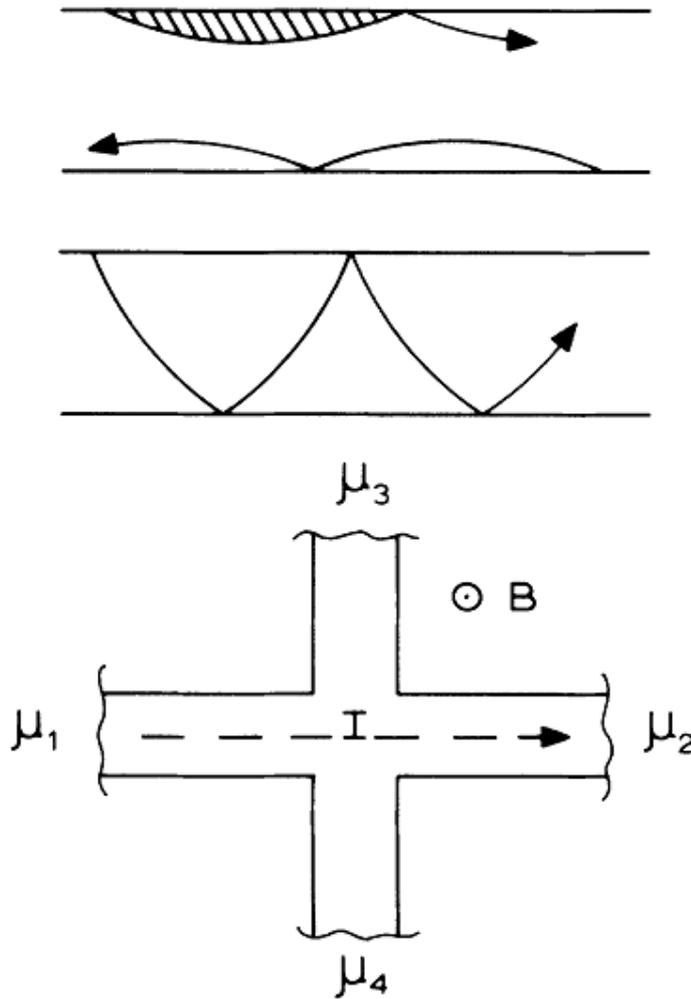
Figure 1.1: Top: Skipping orbits, corresponding to edge states. Center: Traversing trajectory, corresponding to a traversing state(hybird magnetroelectric subband). Bottom: Four-terminal conductor for Hall-resistance measurement. (C. W. J. Beenakker and H. van Houten, Phys. Rev. Lett. 60, 2406 (1988))

In this thesis, we want to discuss how the edge states happen as applying the magnetic field. The wavefunction and the direction of the current of the edge states should be match the classical feature. We use a simple system which is a narrow wire with a parabolic

confinement and a embedded δ-type barrier to understand how the edge states happen when the barrier is repulsive, and what is the differences between the resonance states come from the edge states and the quasi-bound states below each subband bottom.

To elaborate on this phenomenon and show its implication, the thesis is organized as follows. In the chapter 2, we introduce the background formalism, Landauer-Büttiker formalism, which is used in the calculating the transport problems. And we also describe the details of our system and the physical model in this chapter. In the next chapter 3, we solve this physical model in mode-matching (MM) approach, based on the Landauer-Büttiker formalism. And then we also solve this model in an approach of partial Fourier transformation of Lippmann-Schwinger (PFTLS) equation in chapter 4. In chapter 5, we compare the results of these two methods in chapter 3 and 4. Next, in chapter 7 and 6, we discuss the two cases of the attractive and repulsive δ-type potential barrier respectively and investigating the wavefunctions and the current density patterns that illustrate the electronic motion. And we will also discuss the two phenomena of resonance according to the edge states and the quasi-bound states. We draw the brief summaries and some discussions in chapter 8. And in the chapter 9, we have show some results of double and multiple barriers here. These results are still very interesting and we will analyze in the future.

Chapter 2

Introduction to Landauer-Büttiker formula and our physical model

In this chapter, we first introduce the Landauer-Büttiker formalism in Sec.2.1, and then we draw out our system of interest in this work in Sec.2.2. We also simplify the Hamiltonian to the dimensionless one and list the units we used in this work.

2.1 Landauer-Büttiker formalism

We adapt the Landauer-Büttiker approach to calculate the conductance across the source and drain.

In 1957, Landauer [54] proposed a novel point of view that transport should be viewed as a consequence of incident flux. Later in 1970 [55], he further proposed that the conductance of a one-dimensional(1-D) conductor sandwiched between two phase-randomizing resorvoirs is given by

$$G = \frac{2e^2}{h} \frac{T}{R}$$

where T and R are the transmission and reflection coefficients of the conductor treated as a single complex scattering center, and only one spin direction is included.

The formula was rediscovered in 1980 by Anderson et al [56] by employing it in a

rigorous formulation of the scaling theory of localization. Since then Landauer formula caught the attention of wilder community [57]. Nevertheless, another version of conductance $G = \frac{2e^2}{h}T$ was obtained by Economou and Soukoulis later in 1981 [58]. The answer was that they pertain to different physical quantities [59]

This started a long controversy on "which of the Landauer formula is correct?".

For the original Landauer formula, $G = \frac{I}{\mu_A - \mu_B}T$, where μ_A and μ_B are the chemical potentials on the left and the right side of the barrier. However, the conductance formula by Economou *et. al.* is $G_c = \frac{I}{\mu_1 - \mu_2}T$. Here, G_c is the conductance measured between the two outside reservoirs. The ambiguity of the two Landauer formulas was clarified by Imry in 1986 [63].

Apart from the controversy which is confusing before mid-80s, Landauer formula faced another practical difficulties as it is restricted in single channel one-dimensional case only.

However, the Multichannel Landauer formula were proposed by Büttiker on 1985 [60] and later in 1986 [61], he predicted a symmetry property in a four-probe experiment under a magnetic flux and was successfully observed by Benoit *et. al.* [62] Since the confirmation of the formula, it has been a concrete foundation for quantum transport theory. In short, Landauer's great insight that conduction in solids can be thought as a scattering problem, and Büttiker brilliant extension of the multichannel formula has become the key understanding of quantum transport in mesoscopic system. Hence, It is also now well known as Landauer-Büttiker formula.

Next, we try to derive the multichannel Landauer-Büttiker Formula starting from single channel case based on the framework of M. Büttiker *et. al.* [60].

Assume that there are two reservoir of electrochemical potential μ_1 and μ_2 respectively and the two end of 1D channel; and, there is a barrier in between the reservoirs.

If we add a small bias at the two reservoir, then the difference of electrochemical potential between the reservoir will be $\mu_1 - \mu_2 = \Delta\mu$. The transmission probability of an electron from reservoir 1 to reservoir 2 can be calculated by Quantum Mechanics as T. As both side of electrons from reservoir 1 to 2 or reservoir 2 to 1 cancel out each other,

only those transmitted electrons in between $\Delta\mu$ contribute to the current . In 1D, $J = I$.

Therefore the current. I can be written as

$$I = -2e\frac{dn}{dE}\left(\mu_1 - \mu_2\right)T\frac{\hbar k_F}{m}$$

Note that $\frac{dn}{dE}\left(\mu_1 - \mu_2\right)$ is the number of states per unit length that are injected from reservoir 1; the velocity is equal to $\hbar k_F/m$; and, the number 2 refers to spin factor. Besides, density of state per unit length in 1D is

$$\frac{dn}{dE} = \frac{dk}{2\pi/L}\frac{1}{\left(\hbar^2 k_F\right)/m} = \frac{m}{\hbar^2 k_F}\frac{1}{2\pi}$$

Therefore, $I = -\frac{2e}{h}\left(\mu_1 - \mu_2\right)T$. Moreover, the definition of conductance, $G = I/V$, and $\mu_1 - \mu_2$ is given by the voltage across V, so that $\mu_1 - \mu_2 = -eV$. As a result, we have

$$G = \frac{I}{V} = \frac{-2e/h\left(ev\right)T}{V} = \frac{2e^2}{h}T$$

For the $N \times N$ multichannel system, we have the incident channel as n, the transmission probability to m as T_{nm}, and the reflection probability to m as R_{nm}. Therefore, the total transmission probability, T_n from the n-th channel is $\sum_{m=1}^{N} T_{nm}$; and the total current, $I_{tot} = \sum_{n}^{N} I_n$, in which

$$I_n = -\frac{2e}{h}\left(\mu_1 - \mu_2\right)\sum_{m=1}^{N} T_{nm}$$

and,

$$I_{tot} = -\frac{2e}{h}\left(\mu_1 - \mu_2\right)\sum_{n}^{N}\sum_{m=1}^{N} T_{nm}$$

Subsequently, the conductance of $N \times N$ multichannel system would be:

$$G = \frac{2e^2}{h}\sum_{n}^{N}\sum_{m=1}^{N} T_{nm}$$

2.2 Our physical model and formulation

Before our work, there are several previous papers that had considered similar systems. The simplest channel confining potential, which is an infinite uniform 2D wire with hard wall, was considered in papers [66, 67, 69]. It is easier to extend the magnetic field to high magnetic field regime in the hard wall confinement. In the reference [67] of H. Tamura and T. Ando in 1991, a delta-profile potential impurity is considered, and there exist bound states with an energy larger than each landau-level energy for a repulsive scatterer, and a quasi-bound state relate to the attractive potential is also formed below each subband bottom. And in the other reference [66] of Gurvitz in 1995, he introduce analytically the quasibound states of local and non-local potentials. The state relate to the repulsive potential is not a bound one, it is rather a quasibound (resonance) state. And such a quasibound state can generate resonant transitions of carriers between the edges. As a result, repulsive impurities can produce direct interedge transitions inside the propagating modes (the inner-mode transitions), in contrast with attractive impurities, which generate interedge transitions via bound states in the evanescent modes (the inter-mode transitions).

Actually, for a wire, realistic narrow channel in split-gate devices can not be taken as uniform wires, but rather as a parabolic constructions in the propagating direction. The parabolic confining potential is used in the references [40, 68, 70, 71] with magnetic field. In the references [40, 70], the applied magnetic field is not very large and the resonance states above the subband relate to the repulsive is not generated. In the reference [68] of E.V. Sukhorukov *et. al.* in 1994, they consider a central short-range impurity in the wire with a higher magnetic field with approximate. They found that if the magnetic field is sufficiently strong bound states exist not only for attractive impurities but also for the repulsive ones. Bound states are found not only below any mode threshold in series, but also above. They showed that a series of N bound states exist above the N-th mode threshold.

We try to push our theoretical description of magnetoconduction in a narrow parabolic
confining potential which is more realistic to the high magnetic field regime. We will
investigate the transmission dip found at the threshold of subband for repulsive potential
and the two transmission dips found for the incident energy lies below a subband threshold.
And our approach can consider a general condition raging form low magnetic field to high
magnetic field.
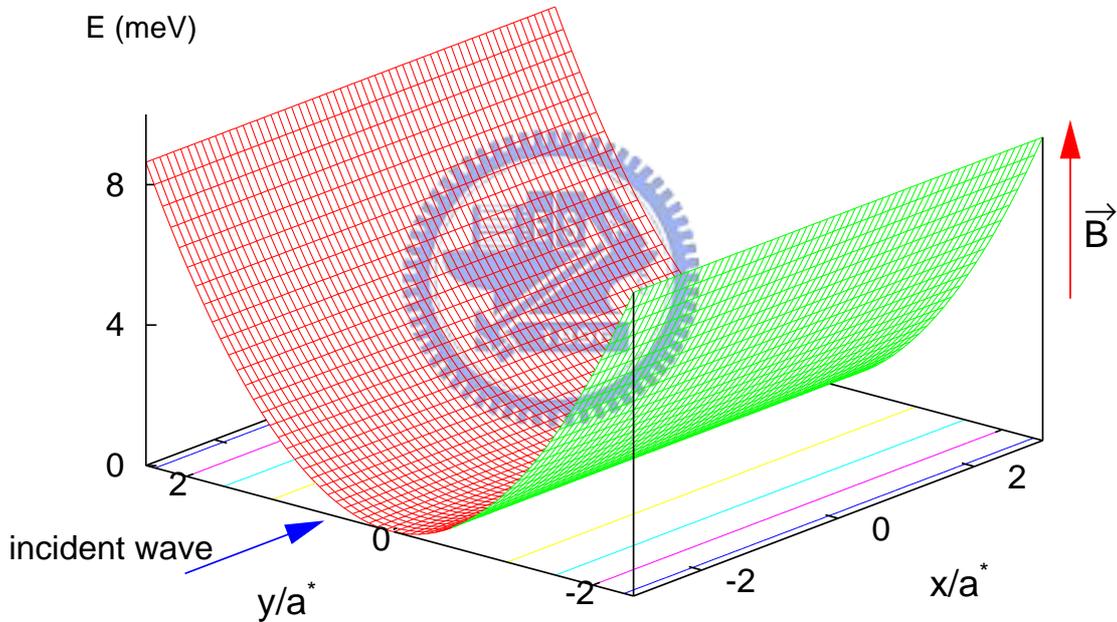
Figure 2.1: The figure of our system.

Our system of interest in this work is basically a quantum wire formed out of a 2DEG.
The propagation direction o the wire is x whereas the confinement potential that define
of quantum wire is given by $V_c(y)$. Of particular interest is the effect of a magnetic field,
pointing along z, on the transport characteristic in the presence of a transverse potential
barrier.

The confinement potential $V_c(y)$ is chosen to be parabolic namely

$$V_c(y) = \frac{1}{2}m^*\omega_y^2 y^2, \tag{2.1}$$

where m^* is the effective mass of an electron in media and ω_y is a potential parameter.

The unperturbed Hamiltonian H_0 of the electron in the constriction is given by

$$H_0 = \frac{\hbar^2}{2m^*}\left[\left(-i\nabla + \frac{e}{c\hbar}\mathbf{A}\right)^2 + \frac{1}{2}m^*\omega_y^2 y^2\right] \tag{2.2}$$

where $-e$ is the charge of the electron.

And in this work we focus on the scattering effect due to an impurity, which the potential of impurity is $V_d(x, y)$.

The total Hamiltonian:

$$H = \frac{\hbar^2}{2m}[-i\nabla + \frac{e}{c\hbar}\mathbf{A}(r)]^2 + V_c(y) + V_d(x, y) \tag{2.3}$$

$\mathbf{A}(\mathbf{r})$ is the vector potential

$$\mathbf{A}(r) = -By\hat{i} \rightarrow \mathbf{B}(\mathbf{r}) = \nabla \times \mathbf{A} = B\hat{k} \tag{2.4}$$

$V_c(y)$ is the confinement potential in the y-direction $V_c(y) = \frac{1}{2}m\omega_y^2 y^2$

$$H = \frac{\hbar^2}{2m}[-i\nabla - \frac{eB}{c\hbar}y\hat{i}]^2 + \frac{1}{2}m\omega_y^2 y^2 + V_d(x, y) \tag{2.5}$$

And then we choose some units to obtain the dimensionless expression of Hamiltonian

$$a^* = \frac{1}{k_F}, \; \varepsilon^* = \frac{\hbar^2 k_F^2}{2m^*}$$

and hence $\quad \omega_c^* = \frac{\hbar k_F^2}{m^*}, \; \omega_y^* = \frac{\hbar k_F^2}{m^*} = 2\frac{\varepsilon^*}{\hbar}, \; B^* = \frac{\hbar c}{e}k_F^2.$

Here $\omega_c = eB/m^*c$ is the cyclotron frequency, and $\omega_c = eB/m^*c = (e/m^*c)(\hbar ck_F^2/e)B =$

$(\hbar k_F^2/m^*)B = \omega_c^* B$, and $l_B = (\hbar c/eB)^{1/2}$ is the magnetic length.

In our numerical examples, the nano-channel(NC) is taken to be that in a high mobility $GaAs/Al_x Ga_{1-x} As$ with a typical electron density $n \sim 2.5 \times 10^{11}\,\mathrm{cm}^{-2}$, and $m^* = 0.067\,\mathrm{meV}$. Correspondingly, our choice of energy unit $E^* = \hbar^2 k_F^2/(2m^*) = 5,933\,\mathrm{meV}$, length unit $a^* = 1/k_F = 9.7937 \times 10^{-9} m = 97.937 \dot{A}$, angular frequency unit $\omega_c^* \hbar = \omega_y^* \hbar = \Omega^* \hbar = 2E^* = 11.866\mathrm{meV}$, and the magnetic field unit $B^* = 6.863\,\mathrm{Tesla}$. We also take $\omega_y = 0.5$ of which $\omega_y \omega_y^* \hbar = 5.933\,\mathrm{meV}$, such that the effective NC width is of the order of $10^2 \dot{A}$. In the following, in presenting the dependence of transmission on μ, it is more convenient to plot transmission(T) as a function of X instead, where $X = \mu/2\omega_y + \frac{1}{2}$. The integral value of X is the number of propagating channels. The conservation of current condition is better represented by the function $CSV(n)$ defined as $CSV(n) = log|1 - \sum_{n'}(|t_{n'n}|^2 + |r_{n'n}|^2)|$, where n is the incident channel and n' is the outgoing channel. We thus obtain the dimensionless Schrödinger equation

$$\Rightarrow \{-\nabla^2 + \Omega^2 y^2 + 2i\omega_c y \frac{\partial}{\partial x} + V_d(x,y)\}\psi(x,y) = E\psi(x,y) \qquad (2.6)$$

where $\Omega^2 = \omega_c^2 + \omega_y^2 = \omega_y^2 + B^2$

In this work, we consider now electron scattering from an barrier potential of the form

$$V_d(x,y) = V_0 V_s(y)\delta(x - x_0), \qquad (2.7)$$

where $V_s(y)$ is an arbitrary function of the coordinate y, but we use it to be a uniform function of the transversal coordinate y and equal to 1 for simplify. x_0 is the longitudinal position of the barrier, and the magnitude of V_0 sets the magnitude of the barrier potential, which may be repulsive ($V_0 > 0$) or attractive ($V_0 < 0$).

In Ch.3, we keep the scattering potential $V_d(x,y) = V_0 V_s(y)\delta(x - x_0)$ and $V_s(y)$ is still an arbitrary function of the coordinate y in the analytical calculation, and set $V_s(y) = 1$ in the numerical process for a simpler system.

Finally we can have the dimensionless Schrödinger equation of our physical model

$$\{-\nabla^2 + \Omega^2 y^2 + 2i\omega_c y \frac{\partial}{\partial x} + V_0 \delta(x - x_0)\}\psi(x, y) = E\psi(x, y) \tag{2.8}$$

Chapter 3

Mode-matching (MM) method

In this chapter, we use the mode-matching approach to solve our physical model. After the formalism, we find that the eigen-function of the wire with magnetic field is not a orthogonal and complete basis set .The propagating mode with real wave vector has a center shift on y-direction and the evanescent mode become a highly oscillating complex function. We choose another orthogonal basis set $\phi_n^o(y)$ to expend the eigen-function $\phi_n^{\pm}(y, k_n)$ which is the better one in our three choices. We also find out a special normalization constant for the evanescent modes which are complex functions. The normalization constant of propagating modes and evanescent modes are different and the normalization constant of evanescent modes depend on the center shift α_n.

3.1 Formalism

We first solve the unperturbed Hamiltonian in this section and obtain the eigen-function of the confinement potential.

In the previous Ch.2, we have obtained the dimensionless Schrödinger equation, Eq. (2.8)

$$\{-\nabla^2 + \Omega^2 y^2 + 2i\omega_c y \frac{\partial}{\partial x} + V_d(x, y)\}\psi(x, y) = E\psi(x, y) \tag{3.1}$$

Firstable, let's solve the wavefunction of unperturbed Hamiltonian:

$$\{-\nabla^2 + \Omega^2 y^2 + 2i\omega_c y \frac{\partial}{\partial x}\}\Psi(x,y) = E\Psi(x,y) \tag{3.2}$$

Because the asymptotic form of wavefunction at $x \to \pm\infty$ can be expanded as plane wave, we can assume the eigenfunction of this form

$$\Psi(x,y) \sim e^{\pm ikx}\phi^{\pm}(y) \tag{3.3}$$

where k is a wavevector.

Substituting Eq. (3.3) the above wavefunction into Eq. (3.2), we obtain

$$\Rightarrow \quad \left\{ \frac{\partial^2}{\partial y^2} - \Omega^2 (y \mp \frac{\omega_c k}{\Omega^2})^2 + \frac{\omega_c^2 k^2}{\Omega^2} - k^2 + E \right\} \phi^{\pm}(y) = 0 \tag{3.4}$$

$$\text{let } \alpha = \frac{\omega_c k}{\Omega^2}, \; u^{\pm} = y \mp \alpha,$$

which the superscript $\pm$ of u denotes the right (left) going wave,

and $K^2 = \frac{\omega_c^2 k^2}{\Omega^2} - k^2 + E = E - \frac{\omega_y^2}{\Omega^2}k^2$

$$\Rightarrow \quad \left\{ \frac{\partial^2}{\partial u^{\pm 2}} - \Omega^2 u^{\pm 2} + K^2 \right\} \phi^{\pm}(y) = 0$$

$$\text{let } u^{\pm\prime} = \sqrt{\Omega}u^{\pm},$$

$$\Rightarrow \quad \left\{ \frac{\partial^2}{\partial u^{\pm\prime 2}} - u^{\pm\prime 2} + \frac{K^2}{\Omega} \right\} \phi^{\pm}(y) = 0 \tag{3.5}$$

Based on the definition of Hermite function, we can obtain the discrete energy identity:

$$(2n+1)\Omega = \frac{\omega_c^2 k^2}{\Omega^2} - k^2 + E = E - \frac{\omega_y^2}{\Omega^2}k^2 \tag{3.6}$$

and $\phi_n(y) \propto e^{-u_n^{\pm\prime 2}/2}H_n(u_n^{\pm\prime}) = e^{-\frac{\Omega}{2}u_n^{\pm 2}}H_n(\sqrt{\Omega}u_n^{\pm})$ \hfill (3.7)

In Eq. (3.6), the energy is quantized, and then we change our variables to have the quantized physical quantities labeled by the subband index n:

$$k \to k_n, \alpha \to \alpha_n = \frac{\omega_c k_n}{\Omega^2}, u^\pm \to u_n^\pm = y \mp \alpha_n,$$
$$\phi^\pm(y) \to \phi_n^\pm(y, k_n) = N_n \times e^{-\Omega u_n^{\pm 2}/2} H_n(\sqrt{\Omega} u_n^\pm)$$

We can write down the total wavefunction:

$$\psi_n(x, y) = N_n \ e^{\pm i k_n x} e^{-\Omega(y \mp \alpha_n)^2/2} H_n(\sqrt{\Omega}(y \mp \alpha_n)) \tag{3.8}$$
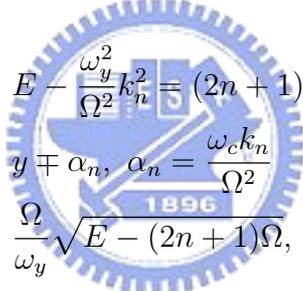
$$
\begin{aligned}
\varepsilon_n &= E - \frac{\omega_y^2}{\Omega^2} k_n^2 = (2n+1)\Omega, \\
u_n^\pm &= y \mp \alpha_n, \ \alpha_n = \frac{\omega_c k_n}{\Omega^2} \\
k_n &= \frac{\Omega}{\omega_y}\sqrt{E - (2n+1)\Omega}, \ \Omega^2 = \omega_y^2 + \omega_c^2.
\end{aligned}
$$

and $\phi_n^\pm(y, k_n)$ is the eigenfunction of this equation

$$\left\{ \frac{\partial^2}{\partial y^2} - \Omega^2 (y \mp \frac{\omega_c k_n}{\Omega^2})^2 + K^2 \right\} \phi_n^\pm(y, k_n) = 0 \tag{3.9}$$

which is a shifted harmonic oscillator of frequency Ω, The center of the transverse eigenfunction $\phi_n^\pm(y, k_n)$ is at $y = \pm \omega_c k_n/\Omega^2$. Hence the larger the momentum $\pm \hbar k_n$ along x-direction, the more the center of wave function is shifted, and $\phi_n^\pm(y, k_n)$ is not longer a complete set. The center shift of wavefunction may be real or pure imaginary because it depends on the momentum k_n along x-direction.

3.2 Normalization constant and evanescent mode

The eigen-function $\phi_n^\pm(y, k_n)$ have a shift constant $\alpha_n = \omega_c k_n/\Omega^2$ which have presented in the previous chapter. The shift constant and the wave vector become a pure imaginary number for the evanescent modes, and the eigen-function become a complex function. We have to redefine the normalization constant for both propagating modes and evanescent modes, the normalization constant of propagation constant is similar to the case without magnetic field; the normalization constant of evanescent modes is different and be a more smaller number to confine the evanescent modes. And we also compare the normalization constant of propagating modes and evanescent modes and find out the relation between them.

In this section, we will determine the normalization constant for both the wave vector k_n are real and pure imaginary of the eigen-function $\phi_n^\pm(y, k_n)$. We use N_n^s for the real k_n, and N_n for the pure imaginary one.

We first write down the normalization identity,

$$\int \phi_n^{\pm*}(y, k_n)\phi_n^\pm(y, k_n)\, dy = 1. \tag{3.10}$$

and then we discuss the two case of real and pure imaginary wave vector k_n

1) If k_n is real: $(\phi_n^{\pm*} = \phi_n^\pm)$

$$\int \phi_n^\pm(y, k_n)\phi_n^\pm(y, k_n)dy = 1,$$

$$N_n^{s2} \int_{-\infty}^{\infty} e^{-\Omega(y\mp\alpha_n)^2} H_n[\sqrt{\Omega}(y \mp \alpha_n)]dy = 1,$$

$$\text{let } \sqrt{\Omega}(y \mp \alpha_n) = x^\pm,$$

$$\Rightarrow \frac{N_n^{s2}}{\sqrt{\Omega}} \int_{-\infty}^{\infty} e^{-x^{\pm2}} H_n^2(x^\pm)dx^\pm = 1,$$

$$\text{and } \int e^{-x^2} H_n^2(x)dx = 2^n n!\sqrt{\pi},$$

$$\Rightarrow N_n^s = \left(2^n n! \sqrt{\frac{\pi}{\Omega}}\right)^{-1/2}.$$

2) If k_n is pure imaginary: substituting Eq. (3.8) into the normalization identity, Eq. (3.10), we have

$$N_n^2 \int_{-\infty}^{\infty} e^{-\frac{\Omega}{2}(y \mp \alpha_n^*)^2} H_n[\sqrt{\Omega}(y \mp \alpha_n^*)] e^{-\frac{\Omega}{2}(y \mp \alpha_n)^2} H_n[\sqrt{\Omega}(y \mp \alpha_n)] dy = 1$$

$$\text{let } x = \sqrt{\Omega} y, \ q_n = \sqrt{\Omega} \alpha_n$$

$$N_n^2 \int_{-\infty}^{\infty} e^{-\frac{1}{2}(x \mp q_n^*)^2 - \frac{1}{2}(x \mp q_n)^2} H_n[x \mp q_n^*] H_n[x \mp q_n] \frac{dx}{\sqrt{\Omega}} = 1$$

$$\text{where } a_n = \pm q_n^* + (\pm q_n), \ b_n = \frac{\pm q_n^* - (\pm q_n)}{2} = \frac{\sqrt{\Omega}}{2}(\pm \alpha_n^* - (\pm \alpha_n))$$

$$\Rightarrow \quad N_n^{-2} = \frac{e^{-b_n^2}}{\sqrt{\Omega}} \int_{-\infty}^{\infty} e^{-x^2} H_n[x - b_n] H_n[x + b_n] dx \qquad (3.11)$$

Using the Eq. (A.78), we have:

$$\int_{-\infty}^{\infty} e^{-x^2} H_m(x + a) H_n(x + b) dx$$

$$= \sum_{k=0}^{Min[m,n]} 2^{m+n-k} a^{m-k} b^{n-k} \frac{m! n! \sqrt{\pi}}{k!(m-k)!(n-k)!} \qquad (3.12)$$

$$= \sum_{k=0}^{Min[m,n]} 2^{m+n-k} a^{m-k} b^{n-k} \binom{n}{k}\binom{n}{k} k! \sqrt{\pi}$$

using Eq. (3.12) and Eq. (3.11), it is easy to obtain the normalization constant of the

following form

$$
\begin{aligned}
N_n^{-2} &= \sqrt{\frac{\pi}{\Omega}} e^{-b^2} \sum_{k=0}^{n} 2^{2n-k} (-b_n^2)^{n-k} \binom{n}{k} \binom{n}{k} k! \\
&= \sqrt{\frac{\pi}{\Omega}} e^{-b_n^2} \sum_{k=0}^{n} 2^{2n-k} (-b_n^2)^{n-k} \frac{n!^2}{k!\,(n-k)!^2} \\
&= N_n^{s-2} e^{\Omega \mathrm{Im}(\alpha_n)^2} \sum_{k=0}^{n} \frac{(2\Omega \mathrm{Im}(\alpha_n)^2)^k}{k!} \binom{n}{k}
\end{aligned}
\tag{3.13}
$$

$$
\begin{aligned}
\text{and} \quad b_n &= \frac{\pm q_n^* - (\pm q_n)}{2} = \frac{\sqrt{\Omega}}{2}(\pm \alpha_n^* - (\pm \alpha_n)) = \mp i \sqrt{\Omega} \mathrm{Im}(\alpha_n), \\
b_n^2 &= -\Omega \mathrm{Im}(\alpha_n)^2.
\end{aligned}
$$

$$
N_n = N_n^s \, e^{-\frac{\Omega}{2}\mathrm{Im}(\alpha_n)^2} \left[\sum_{k=0}^{n} \frac{(2\Omega \mathrm{Im}(\alpha_n)^2)^k}{k!} \binom{n}{k} \right]^{-1/2}
\tag{3.14}
$$

Define the normalization constant factor Λ_n for the evanescent modes

$$
\Lambda_n \equiv \left[\sum_{k=0}^{n} \frac{(2\Omega \mathrm{Im}(\alpha_n)^2)^k}{k!} \binom{n}{k} \right]^{-1/2}.
\tag{3.15}
$$

In the propagating modes and k_n is real, $e^{-\frac{\Omega}{2}\mathrm{Im}(\alpha_n)^2} \Lambda_n = 1$ and $N_n = N_n^s$. In the evanescent modes, $e^{-\frac{\Omega}{2}\mathrm{Im}(\alpha_n)^2} \Lambda_n$ is smaller than 1 and N_n is smaller than N_n^s,

In the case of zero magnetic field, $\phi_n^s(y)$ reduce to $\phi_n^o(y) = N_n^o e^{-\frac{\omega_y}{2}y^2} H_n(\sqrt{\omega_y}y)$, where $N_n^o = (2^n n! \sqrt{\frac{\pi}{\omega_y}})^{-1/2}$.

Correspondingly, we get

$$
\phi_n^s(y) = N_n^s e^{-\frac{\Omega}{2}y^2} H_n(\sqrt{\Omega}y)
\tag{3.16}
$$

$$
\phi_n^o(y) = N_n^o e^{-\frac{\omega_y}{2}y^2} H_n(\sqrt{\omega_y}y)
\tag{3.17}
$$

$$
\phi_n^{\pm}(y, k_n) = N_n^s \Lambda_n e^{-\frac{\Omega}{2}\mathrm{Im}(\alpha_n)^2} e^{-\frac{\Omega}{2}u_n^{\pm 2}} H_n(\sqrt{\Omega}u_n^{\pm})
\tag{3.18}
$$

3.3 Mode-matching approach

In this section, we use the mode-matching approach to solve the problem with a δ-type impurity barrier. We write down the formalism in a general way for three kinds of basis set to expand the eigen-function $\phi_n^{\pm}(y, k_n)$.

We consider an impurity or an external potential in a quantum wire, the system under investigation can be described by $H = H_0 + V_d(x, y)$, where

$$H_0 = -\nabla^2 + \Omega^2 y^2 + 2i\omega_c y \frac{\partial}{\partial x} \qquad (3.19)$$

is the unperturbed Hamiltonian, $V_d(x, y) = V_0 \delta(x) V_s(y)$ which is the scattering potential.

The incident wavefunction from left (L) lead is given by

$$\psi_{in}(x, y, k_l) = e^{ik_l x} \phi_l^+(y, k_l) \qquad (3.20)$$

The corresponding scattering wavefunction is of the form

$$\begin{cases} \psi(x < x_0, y, k_n) = e^{ik_l x} \phi_l^+(y, k_l) + \sum_{n'} r_{n'l}^+ e^{-ik_{n'} x} \phi_{n'}^-(y, k_{n'}) \\ \psi(x > x_0, y, k_n) = \sum_{n'} t_{n'l}^+ e^{ik_{n'} x} \phi_{n'}^+(y, k_{n'}) \end{cases}, \qquad (3.21)$$

where

$$\phi_n^{\pm}(y, k_n) = N_n e^{-\frac{\Omega}{2}(y \mp \alpha_n)^2} H_n \left[\sqrt{\Omega}(y \mp \alpha_n) \right]. \qquad (3.22)$$

In addition, we can expand the wavefunction $\phi_n^{\pm}(y, k_n)$ into several sets of basis like $\phi_n^{\pm}(y, k_n) = N_n \ e^{-\Omega(y \mp \alpha_n)^2/2} H_n[\sqrt{\Omega}(y \mp \alpha_n)]$, $\phi_n^s(y) = N_n^s e^{-\frac{\Omega}{2}y^2} H_n(\sqrt{\Omega}y)$, and $\phi_n^o(y) = N_n^o e^{-\frac{\omega_y}{2}y^2} H_n(\sqrt{\omega_y}y)$. And the wavefunction $\phi_n^{\pm}(y, k_n) = \sum_j \phi_j^{\pm}(y) C_{jn}^{(\pm)\pm}$, $\phi_n^{\pm}(y, k_n) = \sum_j \phi_j^s(y) C_{jn}^{(s)\pm}$, or $\phi_n^{\pm}(y, k_n) = \sum_j \phi_j^o(y) C_{jn}^{(o)\pm}$, where $C_{jn}^{(\pm)\pm} = \delta_{jn}$, $C_{jn}^{(s)\pm} = \int dy \, \phi_j^s(y) \phi_n^{\pm}(y, k_n)$, and $C_{jn}^{(o)\pm} = \int dy \, \phi_j^o(y) \phi_n^{\pm}(y, k_n)$ correspondingly. In mathematically, no matter what kind of complete set we used, the result should be the same. But according to the center shift of the propagating and evanescent modes, the results are different and we will discuss in

the Sec. 3.5.

In order to simplify the formalism, we use $\chi_n^{(\pm,s,o)}(y)$ to replace the functions $\phi_n^{\pm}(y, k_n)$, $\phi_n^s(y)$, and $\phi_n^o(y)$ correspondingly.

$$\phi_n^{\pm}(y, k_n) = \sum_j \chi_j^{(\pm,s,o)}(y) C_{jn}^{(\pm,s,o)\pm} \tag{3.23}$$

$$\text{or} \quad \phi_n^{\pm}(y, k_n) = \sum_j \chi_j(y) C_{jn}^{\pm} \tag{3.24}$$

And then we can rewrite Eq. (3.21) of the below form

$$\psi(x < x_0, y, k_n) = \sum_j e^{ik_l x} \chi_j(y) C_{jl}^+ + \sum_{n',j} e^{-ik_{n'} x} \chi_j(y) C_{jn'}^- r_{n'l}^+ \tag{3.25}$$

$$\psi(x > x_0, y, k_n) = \sum_{n',j} e^{ik_{n'} x} \chi_j(y) C_{jn'}^+ t_{n'l}^+ \tag{3.26}$$

The Schrödinger equation in the presence of $V_d(x, y)$ is given by

$$\left[-\frac{\partial^2}{\partial x^2} - \frac{\partial^2}{\partial y^2} + 2i\omega_c y \frac{\partial}{\partial x} + \Omega^2 y^2 + V_0 \delta(x - x_0) V_s(y) \right] \psi(x, y) = \psi(x, y) \tag{3.27}$$

The scattering should satisfy two boundary conditions, one requirement is that $\psi(x, y)$ has to be continuous at $x = x_i$ and the other one stems from integration of the Schrödinger equation across $x = x_i$.

The wavefunction is continuous at $x = 0$:

$$\psi|_{0^+} = \psi|_{0^-} \tag{3.28}$$

$$\Rightarrow \sum_j \chi_j(y) C_{jl}^+ + \sum_{n',j} \chi_j(y) C_{jn'}^- r_{n'l}^+ = \sum_{n',j} \chi_j(y) C_{jn'}^+ t_{n'l}^+ \tag{3.29}$$

By integrating the Schrödinger equation through $x = 0$, we get

$$\sum_{n',j} ik_{n'}\chi_j(y)C^+_{jn'}t^+_{n'l} - \sum_{j} ik_l\chi_j(y)C^+_{jl} + \sum_{n',j} ik_{n'}\chi_j(y)C^-_{jn'}r^+_{n'l} - V_0 V_s(y)\sum_{n',j}\chi_j(y)C^+_{jn'}t^+_{n'l} = 0$$

(3.30)

Multiply these two boundary conditions Eq. (3.29) and Eq. (3.30) by $\chi_{j'}(y)$ and then integrate over y, we obtain

$$C^+_{j'l} + \sum_{n'} C^-_{j'n'}r_{n'l} = \sum_{n'} C^+_{j'n'}t^+_{n'l},$$

(3.31)

$$\sum_{n'} ik_{n'}C^+_{j'n'}t^+_{n'l} - ik_l C^+_{j'l} + \sum_{n'} ik_{n'}C^-_{j'n'}r^+_{n'l} - V_0 \sum_{n',j} f_{\chi,j'j}C^+_{jn'}t^+_{n'l} = 0.$$

(3.32)

where we use the below conditions. For $\chi_n(y) = \phi^s_i(y)$ or $\chi_o(y) = \phi^o_i(y)$, we have

$$\int_{-\infty}^{\infty} dy\, \chi^{(s,o)*}_i(y)\chi^{(s,o)}_i(y) = \delta_{i,j}; \qquad \int_{-\infty}^{\infty} dy\, \chi^{(s,o)*}_i(y)V_s(y)\chi^{(s,o)}_i(y) = f^{(s,o)}_{\chi,ij}.$$

(3.33)

and for $\chi_n(y) = \phi^{\pm}_n(y, k_n)$, we have

$$\int_{-\infty}^{\infty} dy\, \chi^{\pm*}_i(y)\chi^{\pm}_i(y) = \int_{-\infty}^{\infty} dy\, \phi^{(\pm)\pm*}_i(y, k_n)\phi^{(\pm)\pm}_j(y, k_n)$$

(3.34)

$$\int_{-\infty}^{\infty} dy\, \chi^{(\pm)*}_i(y)V_s(y)\chi^{(\pm)}_i(y) = f^{(\pm)}_{\chi,ij}.$$

(3.35)

and we redefine the coefficient

$$C^{(\pm)\pm}_{ij} = \int dy\, \phi^{(\pm)\pm*}_i(y, k_n)\phi^{(\pm)\pm}_j(y, k_n).$$

(3.36)

In order to extend Eq. (3.31) and Eq. (3.32) to matrix form, we define that:

$$[t_{mn}^{\pm}]_{j \times l} \equiv \begin{bmatrix} t_{00}^{\pm} & \cdots & t_{0n}^{\pm} & \cdots & t_{0l}^{\pm} \\ \vdots & \ddots & \vdots & & \vdots \\ t_{m0}^{\pm} & \cdots & t_{mn}^{\pm} & \cdots & t_{ml}^{\pm} \\ \vdots & & \vdots & \ddots & \vdots \\ t_{j0}^{\pm} & \cdots & t_{jn}^{\pm} & \cdots & t_{jl}^{\pm} \end{bmatrix}_{j \times l} \quad ; \tag{3.37}$$

$$[r_{mn}^{\pm}]_{j \times l} \equiv \begin{bmatrix} r_{00}^{\pm} & \cdots & r_{0n}^{\pm} & \cdots & r_{0l}^{\pm} \\ \vdots & \ddots & \vdots & & \vdots \\ r_{m0}^{\pm} & \cdots & r_{mn}^{\pm} & \cdots & r_{ml}^{\pm} \\ \vdots & & \vdots & \ddots & \vdots \\ r_{j0}^{\pm} & \cdots & r_{jn}^{\pm} & \cdots & r_{jl}^{\pm} \end{bmatrix}_{j \times l} \quad . \tag{3.38}$$

$$[C_{mn}^{\pm}]_{j \times l} \equiv \begin{bmatrix} C_{00}^{\pm} & \cdots & C_{0n}^{\pm} & \cdots & C_{0l}^{\pm} \\ \vdots & \ddots & \vdots & & \vdots \\ C_{m0}^{\pm} & \cdots & C_{mn}^{\pm} & \cdots & C_{ml}^{\pm} \\ \vdots & & \vdots & \ddots & \vdots \\ C_{j0}^{\pm} & \cdots & C_{jn}^{\pm} & \cdots & C_{jl}^{\pm} \end{bmatrix}_{j \times l} \quad ; \tag{3.39}$$

$$[f_{\chi,mn}]_{j \times l} \equiv \begin{bmatrix} f_{\chi,00} & \cdots & f_{\chi,0n} & \cdots & f_{\chi,0l} \\ \vdots & \ddots & \vdots & & \vdots \\ f_{\chi,m0} & \cdots & f_{\chi,mn} & \cdots & f_{\chi,ml} \\ \vdots & & \vdots & \ddots & \vdots \\ f_{\chi,j0} & \cdots & f_{\chi,jn} & \cdots & f_{\chi,jl} \end{bmatrix}_{j \times l} \quad . \tag{3.40}$$

And then we can write down Eq. (3.31) and Eq. (3.32) in matrix form

$$[C_{mn}^+]_{j' \times l} + [C_{mn}^-]_{j' \times n'}[r_{mn}^+]_{n' \times l} = [C_{mn}^+]_{j' \times n'}[t_{mn}^+]_{n' \times l} \tag{3.41}$$

$$[C_{mn}^+]_{j' \times n'}[k_m \delta_{mn}]_{n' \times n'}[t_{mn}^+]_{n' \times l} - [C_{mn}^+]_{j' \times l}[k_m \delta_{mn}]_{l \times l}$$

$$+ [C_{mn}^-]_{j' \times n'}[k_m \delta_{mn}]_{n' \times n'}[r_{mn}^+]_{n' \times l} + iV_0[f_{\chi,mn}]_{j' \times j}[C_{mn}^+]_{j \times n'}[t_{mn}^+]_{n' \times l} = 0 \tag{3.42}$$

Let $j' = j = n' = l = N_c$, all the matrices become square matrixes, where N_c is the total number of subband we used in the numerical calculation

$$[C_{mn}^+] + [C_{mn}^-][r_{mn}^+] = [C_{mn}^+][t_{mn}^+] \tag{3.43}$$

$$[C_{mn}^+][k_m \delta_{mn}][t_{mn}^+] - [C_{mn}^+][k_m \delta_{mn}] + [C_{mn}^-][k_m \delta_{mn}][r_{mn}^+] + iV_0[f_{\chi,mn}][C_{mn}^+][t_{mn}^+] = 0 \tag{3.44}$$

And then, it is trivial to get the coefficient of $t_{mn}^\pm$ and $r_{mn}^\pm$ by the inverse.

$$\begin{bmatrix} [t_{mn}^\pm] \\ [r_{mn}^\pm] \end{bmatrix}_{2N_c \times N_c} \tag{3.45}$$

$$= \begin{bmatrix} [C_{mn}^\pm] & -[C_{mn}^\mp] \\ [C_{mn}^\pm][k_m \delta_{mn}] + iV_0[f_{\chi,mn}][C_{mn}^\pm] & [C_{mn}^\mp][k_m \delta_{mn}] \end{bmatrix}_{2N_c \times 2N_c}^{-1} \begin{bmatrix} [C_{mn}^\pm] \\ [C_{mn}^\pm][k_m \delta_{mn}] \end{bmatrix}_{2N_c \times N_c}$$

$\phi_n^\pm = N_n e^{-\frac{1}{2}\Omega(y \mp \alpha_n)^2} H_n\left[\sqrt{\Omega}(y \mp \alpha_n)\right]$ have a good physical meaning because it is the eigenfunction in the wire in parabolic confinement with magnetic field, but not a complete set in this space, and cause some mathematic problems. $\phi_n^s(y) = N_n^s e^{-\frac{1}{2}\Omega y^2} H_n\left[\sqrt{\Omega}y\right]$ is the ordinary unshifted harmonic oscillator with confinement frequency Ω. We use this basis to be the projecting basis $\chi_n(y)$, this is a complete set rather than $\phi_n^\pm$, and has the same oscillation frequency Ω. It has good character in calculation and better behavior in small magnetic, but still diverge in some cases we want to see. And then we use the eigenfunction $\phi_n^o(y) = N_n^o e^{-\frac{1}{2}\omega_y y^2} H_n\left[\sqrt{\omega_y}y\right]$ which is the eigenfunction in parabolical wire

without magnetic field. It is also a complete set, but stronger calculation the other basis, $\phi_n^s(y)$ and $\phi_n^{\pm}(y)$. This is the best basis in these three eigenfunctions, some problem had be solved and good conservation in most case with not very strong magnetic field.

In this section we choose $\phi_n^o(y)$ to be our projecting basis, but we still list all of the others calculation in appendix.

$$
\begin{aligned}
C_{mn}^{(o)\pm} &= \int dy\, \phi_m^o(y)\phi_n^{\pm}(y) \\[2mm]
&= \sqrt{\frac{2m!n!}{\eta}}\,(\omega_y\Omega)^{1/4} e^{\frac{1}{2}\eta(\frac{\Omega\alpha_n}{\eta})^2 - \frac{1}{2}\Omega\mathrm{Re}[\alpha_n]^2}\Lambda_n \\[2mm]
&\times \sum_{p=0}^{m}\sum_{q=0}^{n} \frac{\bar{H}_{m-p}\left[\pm\frac{\sqrt{2\omega_y}\Omega\alpha_n}{\eta}\right]}{2^p}\frac{\bar{H}_{n-q}\left[\mp\frac{\sqrt{2\Omega}\omega_y\alpha_n}{\eta}\right]}{2^q} \\[2mm]
&\times \begin{cases} \displaystyle\sum_{s}^{\frac{\mathrm{Min}[p,q]-1}{2}} f_{r1}(2s+1)\,f_{r2}(\frac{p-2s-1}{2})\,f_{r3}(\frac{q-2s-1}{2}) & ,\ m,n \text{ are both odd.} \\[4mm] \displaystyle\sum_{s}^{(\mathrm{Min}[p,q])/2} f_{r1}(2s)\,f_{r2}(\frac{p-2s}{2})\,f_{r3}(\frac{q-2s}{2}) & ,\ m,n \text{ are both even.} \\[4mm] 0 & ,\ m+n \text{ is odd.} \end{cases}
\end{aligned}
\tag{3.46}
$$

$$
\text{where } \bar{H}_n(x) \equiv \frac{H_n(x)}{2^n n!},\ \eta = \omega_y + \Omega,\ \alpha_n = \frac{\omega_c k_n}{\Omega^2} \tag{3.47}
$$

$$
\text{and} \qquad f_{r1}(n) = (\frac{8\sqrt{\omega_y\Omega}}{\eta})^n/n!, \tag{3.48}
$$

$$
f_{r2}(n) = (\frac{3\omega_y - \Omega}{\eta})^n/n!, \tag{3.49}
$$

$$
f_{r3}(n) = (\frac{3\Omega - \omega_y}{\eta})^n/n!. \tag{3.50}
$$

$$
\begin{aligned}
f^o_{\chi,mn} &= \int_{-\infty}^{\infty} \phi^{o*}_i(y) V_s(y) \phi^o_i(y) dy \\
&= \sqrt{\frac{m!n!}{2^m 2^n}} \sqrt{\frac{\omega_y}{\omega_y + \beta}} e^{-a^2} \sum_{\kappa=0}^{\text{Min}[m,n]} \frac{2^\kappa}{\kappa!} \frac{(\frac{\beta}{\omega_y+\beta})^{m-\kappa}}{(m-\kappa)!} \frac{(\frac{\beta}{\omega_y+\beta})^{n-\kappa}}{(n-\kappa)!} H_{m+n-\kappa}[a] \quad (3.51)
\end{aligned}
$$

$$
\text{where } a = \sqrt{\frac{\beta\omega_y}{\omega_y + \beta}} y_0. \quad (3.52)
$$

3.4 Current density and conservation condition

The current density in a system with magnetic field is different from the case without magnetic field. In this section, we use the Hamiltonian of our system and the continuous equation to get the form of current density in a magnetic field. And we also know that the net current is contributed from the propagating modes and wave vector k_n is real; the current density in the evanescent mode is not zero but does not contribute to the total net current.

We first write down our Hamiltonian and the continuous equation

$$
H = -\nabla^2 + 2i\omega_c y \frac{\partial}{\partial x} = -\frac{\partial^2}{\partial x^2} - \frac{\partial^2}{\partial y^2} + 2i\omega_c y \frac{\partial}{\partial x} \quad (3.53)
$$

$$
H^* = -\frac{\partial^2}{\partial x^2} - \frac{\partial^2}{\partial y^2} - 2i\omega_c y \frac{\partial}{\partial x} \quad (3.54)
$$

$$
\frac{\partial}{\partial t}\rho = i(H^*\psi^* H - \psi^* H\psi) = -\nabla \cdot \mathbf{j} \quad (3.55)
$$

$$
\begin{aligned}
&(-\frac{\partial^2}{\partial x^2}\psi^*)\psi + \psi^*\frac{\partial^2}{\partial x^2}\psi^* \\
&= -\frac{\partial}{\partial x}(\frac{\partial}{\partial x}\psi^* \cdot \psi) + \frac{\partial}{\partial x}\psi^*\frac{\partial}{\partial x}\psi + \frac{\partial}{\partial x}(\psi^*\frac{\partial}{\partial x}\psi) - \frac{\partial}{\partial x}\psi \cdot \psi \\
&= \frac{\partial}{\partial x}\{\psi^*\frac{\partial}{\partial x}\psi - \frac{\partial}{\partial x}\psi^* \cdot \psi\}
\end{aligned}
$$

$$(-2i\omega_c y\frac{\partial}{\partial x}\psi^*)\psi - \psi^*(2i\omega_c y\frac{\partial}{\partial x})\psi$$

$$= -2i\omega_c y\frac{\partial}{\partial x}(\psi^*\psi)$$

$$= \frac{\partial}{\partial x}(-2i\omega_c y\psi^*\psi)$$

$$\Rightarrow \frac{\partial}{\partial t}\rho = \frac{-1}{i}\frac{\partial}{\partial x}\{\psi^*\frac{\partial}{\partial x}\psi - \frac{\partial}{\partial x}\psi^* \cdot \psi - 2i\omega_c y\psi^*\psi\} - \frac{1}{i}\frac{\partial}{\partial y}\{\psi^*\frac{\partial}{\partial y}\psi - \frac{\partial}{\partial y}\psi^* \cdot \psi\}$$

$$= \frac{-1}{i}\frac{\partial}{\partial x}\{\psi^*(\frac{\partial}{\partial x} - i\omega_c y)\psi - c.c.\} - \frac{1}{i}\frac{\partial}{\partial y}\{\psi^*\frac{\partial}{\partial x}\psi - c.c.\} \qquad (3.56)$$

and then we can define the current density along x- and y-direction

$$j_x = \frac{1}{i}\{\psi^*\frac{\partial}{\partial x}\psi - \frac{\partial}{\partial x}\psi^* \cdot \psi - 2i\omega_c y\psi^*\psi\} \qquad (3.57)$$

$$j_y = \frac{1}{i}\{\psi^*\frac{\partial}{\partial y}\psi - \frac{\partial}{\partial y}\psi^* \cdot \psi\} \qquad (3.58)$$

The third term of Eq. (3.57), $-2i\omega_c y\psi^*\psi$, is caused from the applied magnetic field and the current density on x-direction is y-dependent in the coordinates.

3.4.1 Current conservation on the longitudinal direction

In this subsection, we investigate the conservation condition on the longitudinal direction, the applied magnetic field introduce a factor depend on the magnetic field to the conservation condition. But the form of conservation condition is same as the one without magnetic field.

The total wavefunctions on the left and right side of the scattering potential are given by

$$\begin{cases} \psi_L = e^{ik_l x}\phi_l^+(y) + \sum_{n'} e^{-ik_{n'} x}\phi_{n'}^-(y)r_{n'l} \\ \psi_L^* = e^{-ik_l x}\phi_l^{+*}(y) + \sum_{n'} e^{ik_{n'}^* x}\phi_{n'}^{-*}(y)r_{n'l}^* \end{cases} \text{and} \begin{cases} \psi_R = \sum_{n'} e^{ik_{n'} x}\phi_{n'}^-(y)t_{n'l} \\ \psi_R^* = \sum_{n'} e^{-ik_{n'}^* x}\phi_{n'}^{-*}(y)t_{n'l}^* \end{cases} \qquad (3.59)$$

where l is the incident state and k_l is a real number.

Substitute Eqs.(3.59) in to Eq. (3.57) and obtain

$$
k_l \phi_l^{+*}(y)\phi_l^+(y) - \sum_{n'} k_{n'} e^{-i(k_{n'}+k_l)x} \phi_l^{+*}(y)\phi_{n'}^-(y) r_{n'l}
$$

$$
+ \sum_{n'} k_l e^{i(k_{n'}^*+k_l)x} \phi_{n'}^{-*}(y)\phi_l^+(y) r_{n'l}^* - \sum_{n',n''} k_{n''} e^{i(k_{n'}^*-k_{n''})x} \phi_{n'}^{-*}(y)\phi_{n''}^-(y) r_{n'l}^* r_{n'l}
$$

$$
+ k_l \phi_l^{+*}(y)\phi_l^+(y) + \sum_{n'} k_l e^{-i(k_{n'}+k_l)x} \phi_l^{+*}(y)\phi_{n'}^-(y) r_{n'l}
$$

$$
- \sum_{n'} k_{n'}^* e^{i(k_{n'}+k_l)x} \phi_{n'}^{-*}(y)\phi_l^+(y) r_{n'l}^* - \sum_{n',n''} k_{n''}^* e^{i(k_{n'}^*+k_{n''})x} \phi_{n'}^{-*}(y)\phi_{n''}^-(y) r_{n'l}^* r_{n'l}
$$

$$
- 2\omega_c y \Big\{ \phi_l^{+*}(y)\phi_l^+(y) + \sum_{n'} k_{n'} e^{-i(k_{n'}+k_l)x} \phi_l^{+*}(y)\phi_{n'}^-(y) r_{n'l}
$$

$$
+ \sum_{n'} e^{i(k_{n'}+k_l)x} \phi_{n'}^{-*}(y)\phi_l^+(y) r_{n'l}^* + \sum_{n',n''} e^{i(k_{n'}-k_{n''})x} \phi_{n'}^{-*}(y)\phi_{n''}^-(y) r_{n'l}^* r_{n'l} \qquad (3.60)
$$

in the left side of impurity barrier, and

$$
\sum_{n',n''} k_{n''} e^{-i(k_{n'}^*-k_{n''})x} \phi_{n'}^{+*}(y)\phi_{n''}^+(y) t_{n'l}^* t_{n''l} + \sum_{n',n''} k_{n'} e^{-i(k_{n'}^*-k_{n''})x} \phi_{n'}^{+*}(y)\phi_{n''}^+(y) t_{n'l}^* t_{n''l}
$$

$$
- 2\omega_c y \sum_{n',n''} e^{-i(k_{n'}^*-k_{n''})x} \phi_{n'}^{+*}(y)\phi_{n''}^+(y) t_{n'l}^* t_{n''l} \qquad (3.61)
$$

in the right side.

And then integrate these two equations, Eq. (3.60) and Eq. (3.61), over x from $-\infty$ to ∞, and we find that some terms with imaginary k_n is vanish in this integration.

The left side should equal to the right side, and we have

$$
k_l \phi_l^{+*}(y)\phi_l^+(y) - \sum_{n'} k_{n'} \phi_{n'}^{-*}(y)\phi_{n'}^-(y)|r_{n'l}|^2 - \omega_c y \left\{ \phi_l^{+*}(y)\phi_l^+(y) + \sum_{n'} \phi_{n'}^{-*}(y)\phi_{n'}^-(y)|r_{n'l}|^2 \right\}
$$

$$
= \sum_{n'} k_{n'} \phi_{n'}^{+*}(y)\phi_{n'}^+(y)|t_{n'l}|^2 - \omega_c y \sum_{n'} \phi_{n'}^{+*}(y)\phi_{n'}^+(y)|t_{n'l}|^2 \qquad (3.62)
$$

where the summation sum over all propagation modes.

And then integrating over y, we also have the following two equation

$$\int \phi_n^\pm(y, k_n)^* \phi_n^\pm(y, k_n) dy = 1, \text{ which is the normalization condition.}$$

$$\int y\phi_n^\pm(y, k_n)^* \phi_n^\pm(y, k_n) dy = \pm\text{Re}[\alpha_n] = \frac{\pm\omega_c \text{Re}[k_n]}{\Omega^2} \tag{3.63}$$

where k_n is real and $\phi_n^\pm(y, k_n)$ a is real function and a orthogonal set.

Finally we have the conservation equation in the x-direction:

$$\Rightarrow \quad (1 - \frac{\omega_c^2}{\Omega^2})\left\{\sum_{n'} k_{n'}|t_{n'l}|^2 + \sum_{n'} k_{n'}|r_{n'l}|^2 - k_l\right\} = 0 \tag{3.64}$$

where summation sum over the propagating modes and the wave vector must be real.

3.5 Numerical results

In the Fig. 3.1, we plot the results of the transmission as a function of applied magnetic field to compare the numerical results of the three basis sets. There are three curves in both figures, which are the results using the different basis in order, $\phi_n^\pm(y, k_n)$, $\phi_n^s(y)$ and $\phi_n^o(y)$. Except changing the basis, we fix $N_c = 17$, incident energy is at $7\omega_y E^*$, and $V_0 = 1.0E^*$ in (a) and $V_0 = -1.0E^*$ in (b). The block dashed line is the transmission without any scattering potential in the wire.

The three curves in the both figures are the results by using the different basis in order. It is easily to see that the results (curves) of $\phi_n^\pm(y, k_n)$ and $\phi_n^s(y)$ exceed the permitted range (The transmission must below the black dashed line in the figures). And the third curve of projecting to the basis $\phi_n^o(y)$ is more reasonable, this curve all below the black dashed line.

Although the three curves look quite different, but all of them lie together on the same line in the range of low magnetic filed (below $B = 0.2$). This result show that the calculation in this chapter works in the low magnetic regime no matter what basis we used, and the selection of basis effect a lots in the high magnetic regime.
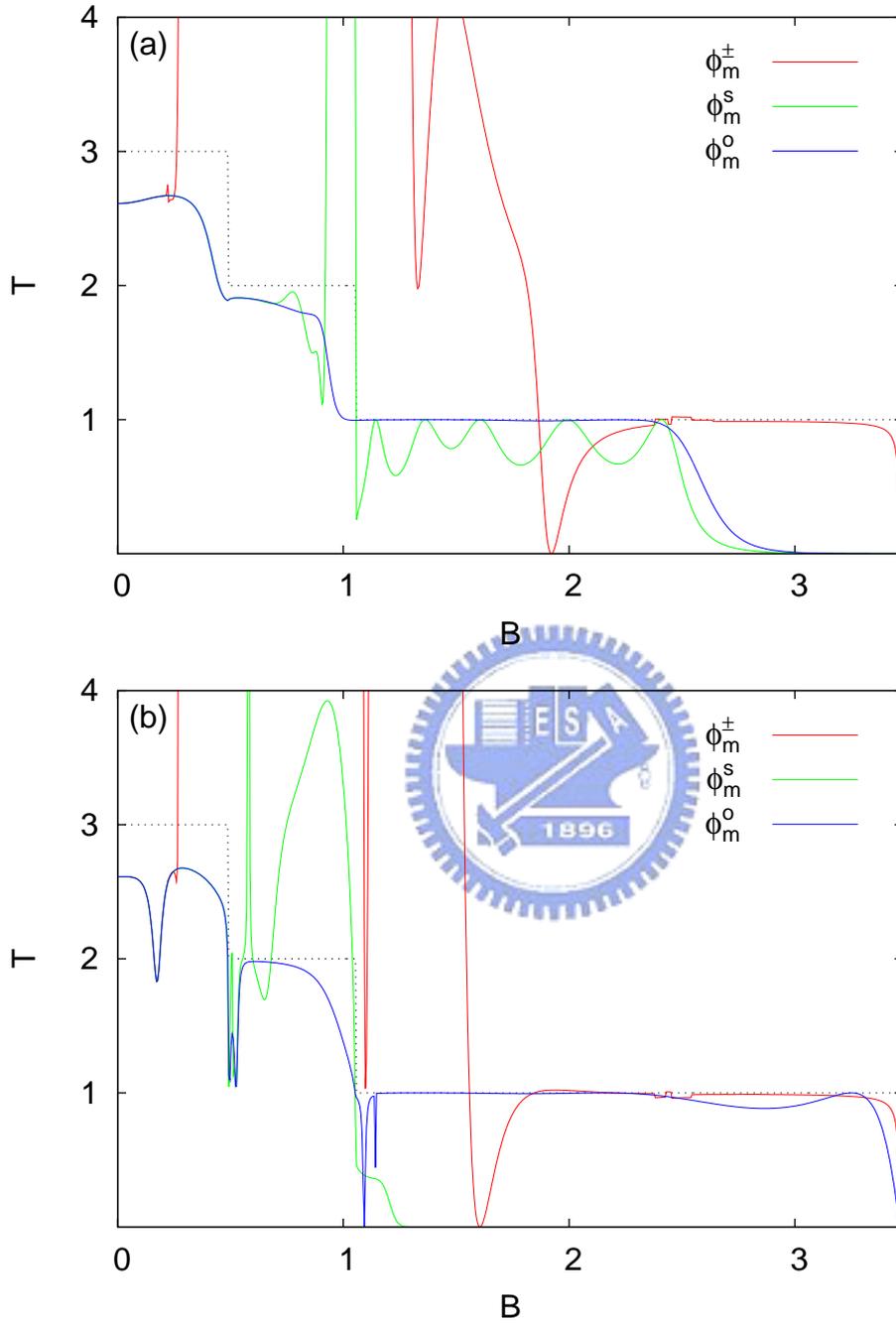
Figure 3.1: Compare the numerical results of three basis sets. The red line is the result projected to $\phi_m^{\pm}(y, k_m)$; the green one is projected to $\phi_m^s(y)$; and the blue one is projected to $\phi_m^o(y)$. The strength of the impurity barrier is repulsive with $1.0E^*$ in (a) and attractive with $-1.0E^*$ in (b).

Base on this comparison, we finally choose the basis set $\phi_n^o(y)$ to be our projecting basis in this work.

In the Fig. 3.2, we fix the incident energy at $7\omega_y E^*$ and plot the transmission as a
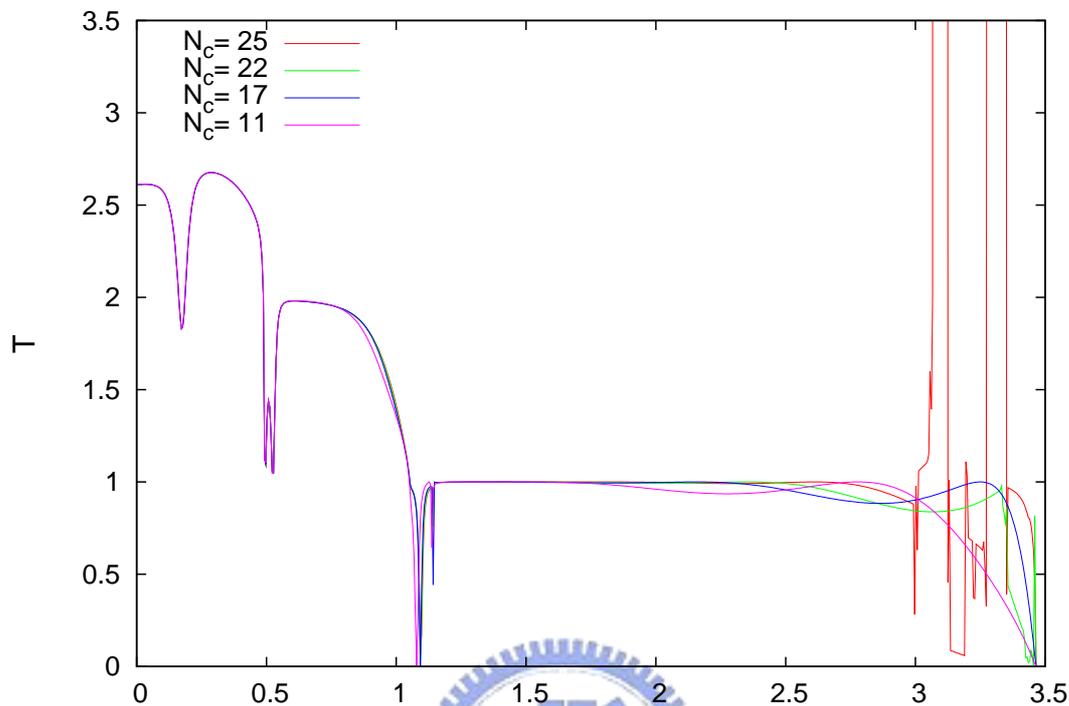
Figure 3.2:   Changing the number of subband N_c to check the saturation and the accuracy break down of the numerical calculation. We fix the incident energy at $E = 7\omega_y E^*$, the strength of the impurity barrier is $1.0E^*$.

function of B for various N_c to check the saturation and accuracy break down of numerical calculation. The strength of the attractive barrier in the wire is $V_0 = -1.0E^*$. Except the regime of high magnetic field, the more numbers of subbands we used in the calculation, the curves saturate form low magnetic field to more high magnetic field. But as long as we use too many of numbers of subbands, like 22 and 25 in the Fig. 3.2, the curves diverge when the magnetic field larger than $3.3B^*$ and $3.0B^*$, the more numbers of subbands we used in the calculation, the lower amplitude of magnetic field the curves diverge. This divergence is due to the accuracy in the computation is not enough. When the magnetic field is high, the structure of the matrix used to calculate the transmission and reflection will be difficult to find out its the inverse. It is easily diverged and need more accuracy to have the correct solution with less error. And the more elements of the matrix, the accuracy error will be enlarged. In the programs, we have already use the higher precision, quad-precision, than double precision to calculate the inverse of the matrixes, but in the

case of high magnetic field, it is not enough and still diverged, just like the curves in Fig. 3.2. This problem about the accuracy is the main problem if we want to have the saturate result in higher magnetic field, and we will discuss with this later.

In the Fig. 3.3, we plot the transmission as a function of incident energy for various numbers of subband form 26 to 30 to check the saturation the curves. The applied magnetic field is $1.0B^*$ and the strength of impurity barrier is repulsive with $1.0E^*$ in (a) and attractive with $-1.0E^*$ in (b). As the increasing of the numbers of subbands, the curves saturate form the lower incident energy to higher energy but slowly. In the Fig. 3.3, $B = 1.0B^*$, we find that the curves saturate below $X = 4$ when we use 30 subbands. In the range of $X > 4$, the curves is not really saturate as we magnify the figures. Consider 30 subbands as the most total number of subband we can used in the calculation remaining accuracy for the case of $B = 1.0B^*$. When the numbers of subbands is more than 30, in the case of $B = 1.0B^*$, the curve will diverge. And in the case of $B > 1.0B^*$, the curve diverge before saturate even if $X < 3.0$; on the contrary, the curves saturate and using fewer numbers of subbands than 30 if the amplitude of magnetic field is smaller than $B = 1.0B^*$.

3.6 Summary and discussions

In this chapter, we use the mode-matching approach to solve the magnetoconduction in the wire. The transverse eigen-function in the wire with magnetic field is written as $\phi_n^\pm(y, k_n)$, and the center of the eigen-function $\phi_n^\pm(y, k_n)$ is at $y = \pm\omega_c k_n/\Omega^2$. As the wave vector k_n is real, the center shift along the y-direction, the larger of $\omega_c k_n$, the more the center shift. As the wave vector k_n is pure imaginary, the center of $\phi_n^\pm(y, k_n)$ back to the center of the y-direction and become a complex function. There are two reason why we can not expand the eigen-function $\phi_n^\pm(y, k_n)$ well. One is according to the center shift of the eigen-function $\phi_n^\pm(y, k_n)$, it is quite different to expand the eigen-function which has two kind of shift. And another is that the eigen-function $\phi_n^\pm(y, k_n)$ is not an orthogonal
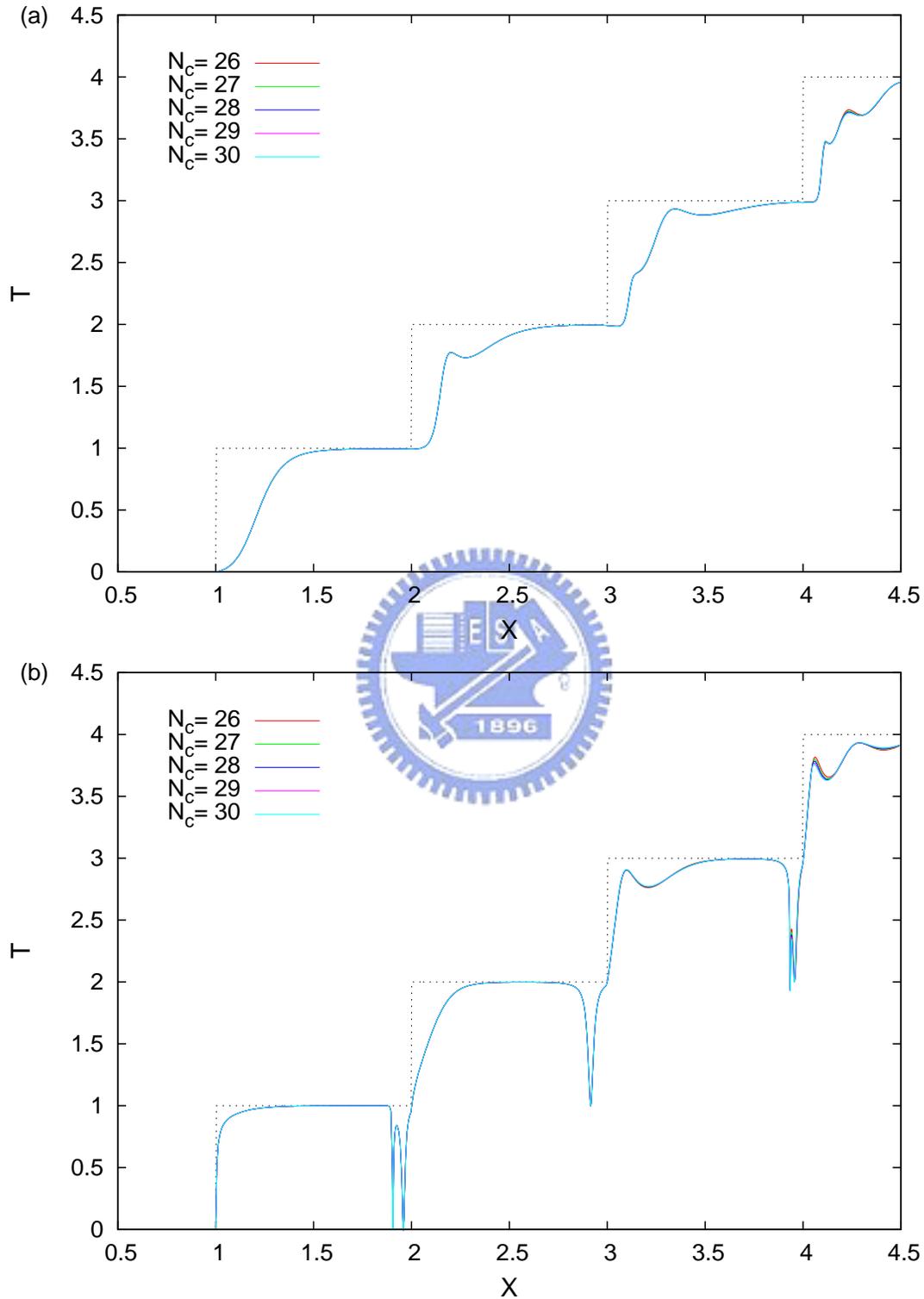
Figure 3.3: The saturation of transmission versus N_c from 26 to 30 for $B = 1.0$ and the strength of impurity barrier is repulsive with $1.0E^*$ in (a) and attractive with $-1.0E^*$ in (b).

basis and incomplete set, we have to expand the eigen-function to another basis which is orthonormal. And that is why the transmission and conservation are not reasonable as we project the eigen-function to itself. There are two choices to expand the eigen-function, one is $\phi_n^s(y)$ and the other is $\phi_n^o(y)$.

$\phi_n^s(y)$ is the eigen-function of a harmonic oscillation which the confinement is $\Omega^2 y^2$ on the y-direction. This kind of confinement, $\Omega^2 y^2$, depend on the strength of the magnetic field and more confined in the large magnetic field regime than the original confinement, $\omega_y^2 y^2$. This eigen-function $\phi_n^s(y)$ is more confined to the center more localized in the y-direction. And it may not cover the edge of the wire in a higher magnetic field where the edge state had generated. And then, the basis $\phi_n^o(y)$, which is the eigen-function in the wire without magnetic field. The covered range of this eigen-function $\phi_n^o(y)$ is more extensive in the y-direction then the eigen-function $\phi_n^s(y)$, and match to the original wire which have the real edge state.

And then we back to discuss the real eigen-function $\phi_n^\pm(y, k_n)$ in the wire. The character of this eigen-function is very different as the wave vector is real or pure imaginary. The center of the eigen-function shift and concentrate to the edge as the wave vector is real and the large kinetic energy and the magnetic field, the more shift. According to this phenomenon, it is better to choose the eigen-function $\phi_n^o(y)$ to be the projecting basis. But in the case of the wave vector is pure imaginary, the eigen-function become evanescent mode does not have the center shift and back to the center of the y-direction. Because the wavefunction is back to the center, it is better to use the eigen-function $\phi_n^s(y)$ to expand the evanescent modes in the center of y-direction, the eigen-function $\phi_n^s(y)$ is also more confined to the center.

The most problem is what character is more important in the higher strength of magnetic field, the difference is not very much in the low magnetic field. And find out the balance of the expansion between wave vector is real and pure imaginary(propagating modes and evanescent modes). And then we find that the eigen-function $\phi_n^o(y)$ is more balanced to expand both propagating modes and evanescent modes, and we use this basis

$\phi_n^o(y)$ to expand the eigen-function $\phi_n^{\pm}(y, k_n)$.

In the classical-like picture, the wavefunction shift and concentrate on the edge of the incident energy level when we apply a large magnetic field, and become the edge-state. This phenomenon of edge states is more important than the evanescent modes in the center of y-direction and need to be describe well. And that is the reason why eigen-function $\phi_n^o(y)$ is better than $\phi_n^s(y)$.

And we also care about the divergence of the inverse of the matrixes, and we spend lots of time to improve the accuracy of the calculation in program. And Finally we change most of codes of the programs and the subroutine which solve the inverse of a matrix to quad-precision, but already touch the limit of the numerical calculation. According to this situation, we develop another method to solve this system, the approach of partial Fourier transformation of Lippmann-Schwinger equation, and we will illustrate in next chapter.

Chapter 4

An approach of partial Fourier transformation of the Lippmann-Schwinger (PFTLS) equation

In CH.3, the numerical results can not saturate in the high magnetic field regime and diverge with the numerical accuracy when we use more numbers of subband in calculation. We think that is because the eigen-function $\phi_n^{\pm}(y, k_n)$ is not an orthogonal basis set and the shift properties of the propagating modes and the evanescent modes are different, it is hard to find a basis set which can describe the propagating modes and evanescent modes well at the same time. In the reference [66], the author use a Fourier transformation on x-direction of the Schrödinger equation, and the problem can be technically simplified when turn to the mixed, momentum-coordinate representation of the wavefunction. We will use a similar technic to solve our problem. Due to this technic, partial Fourier transformation, the evanescent modes are not a complex function and the basis set of $\phi_n^{\pm}(y, k)$ (where k is the integrating variable of Fourier transformation) become a orthogonal set. This method can avoid the complex evanescent modes we worried about in the previous chapter, and

this calculation can be extended to the high magnetic regime.

4.1 Formalism

In the beginning, we also consider the Schrödinger equation Eq. (2.8) and the electronic transport in a laterally confined system can be described $(x_0 = 0)$

$$\left\{ -\frac{\partial^2}{\partial x^2} - \frac{\partial^2}{\partial y^2} + \Omega^2 y^2 + 2i\omega_c y \frac{\partial}{\partial x} + V_0 \delta(x) V_s(y) \right\} \Psi(x, y) = E \, \Psi(x, y) \qquad (4.1)$$

Let $\Psi(x, y) = \sum_n \int \frac{dk}{2\pi} e^{ikx} \psi_{n,k} \phi_n(k, y)$ which we partially write the total wavefunction in coordinate space x to the momentum space k, it is easy to obtain

$$\sum_n \left\{ \int \frac{dk}{2\pi} k^2 e^{ikx} \psi_{n,k} \phi_n(k, y) - \frac{\partial^2}{\partial y^2} \int \frac{dk}{2\pi} e^{ikx} \psi_{n,k} \phi_n(k, y) \right.$$

$$+\Omega^2 y^2 \int \frac{dk}{2\pi} e^{ikx} \psi_{n,k} \phi_n(k, y) + 2\omega_c y \int \frac{dk}{2\pi} (-k) e^{ikx} \psi_{n,k} \phi_n(k, y)$$

$$\left. +V_0 V_s(y) \delta(x) \int \frac{dk}{2\pi} e^{ikx} \psi_{n,k} \phi_n(k, y) \right\} = E \sum_n \int \frac{dk}{2\pi} e^{ikx} \psi_{n,k} \phi_n(k, y) \qquad (4.2)$$

and we transform this above equation to momentum space

$$\int dx \, e^{-iqx} \int \frac{dk}{2\pi} k^2 e^{ikx} \psi_{n,k} \phi_n(k, y) = q^2 \psi_{n,q} \phi(q, y) \qquad (4.3)$$

$$\int dx \, e^{-iqx} \int \frac{dk}{2\pi} (-k) e^{ikx} \psi_{n,k} \phi_n(k, y) = -q \psi_{n,q} \phi(q, y) \qquad (4.4)$$

$$\int dx \, e^{-iqx} V_s(y) \delta(x) \int \frac{dk}{2\pi} e^{ikx} \psi_{n,k} \phi_n(k, y) = V_s(y) \int \frac{dk}{2\pi} \psi_{n,k} \phi_n(k, y) \qquad (4.5)$$

$$\sum_n \left\{ q^2 \psi_{n,q} \phi_n(q, y) - \frac{\partial^2}{\partial y^2} \psi_{n,q} \phi_n(q, y) + \Omega^2 y^2 \psi_{n,q} \phi_n(q, y) \right.$$

$$\left. -2\omega_c y q \psi_{n,q} \phi_n(q, y) + V_0 V_s(y) \int \frac{dk}{2\pi} \psi_{n,k} \phi_n(k, y) \right\} = E \sum_n \psi_{n,q} \phi_n(q, y) \quad (4.6)$$

And the eigen-function of the confinement on y-direction have these conditions

$$-\frac{\partial^2}{\partial y^2}\phi_n(q,y) + \Omega^2 y^2 \phi_n(q,y) - 2\omega_c yq\phi_n(q,y) = \epsilon'_n(q)\phi_n(q,y) \qquad (4.7)$$

$$\epsilon'_n(q) = \epsilon_n - \frac{\omega_c^2 q^2}{\Omega^2} = (2n+1)\Omega - \frac{\omega_c^2 q^2}{\Omega^2} \qquad (4.8)$$

$$\phi_n(q,y) = N_n e^{-\frac{\Omega}{2}(y-\frac{\omega_c q}{\Omega^2})^2} H_n(\sqrt{\Omega}(y - \frac{\omega_c q}{\Omega^2})) \qquad (4.9)$$

Since q is the Fourier transform variable and must be real, $\phi_n(q,y)$ is an orthogonal basis set and the normalization constant N_n of $\phi_n(q,y)$ should be equal to $N_n^s = (2^n n!\sqrt{\pi/\Omega})^{-1/2}$.

In order to simplify our model, we choose the potential $V_s(y)$ equal to 1 which is uniform on transverse direction. In the case of without magnetic field, the wavefunction and the impurity barrier are symmetry and the particles will not transit between different subbands. The effect of subband mixing must be caused by applying magnetic field in the case of a symmetry system on the transverse direction. And then multiply $\phi_m^*(q,y)$ to the above Eq. (4.6) and integrate over y

$$q^2\psi_{m,q} + \epsilon'_m\psi_{m,q} + \sum_n \int \frac{dk}{2\pi} v_{m,n}(q,k)\psi_{n,k} = E\psi_{m,q} \qquad (4.10)$$

$$\text{where } v_{m,n}(q,k) = V_0 \int dy\, \phi_m^*(q,y)V_s(y)\phi_n(k,y)$$

$$= V_0\, e^{-\frac{\alpha^2}{4}(q-k)^2} \sum_{p=0}^{\text{Min}[m,n]} \frac{[-\frac{\alpha}{\sqrt{2}}(q-k)]^{m-p}}{(m-p)!} \frac{[\frac{\alpha}{\sqrt{2}}(q-k)]^{n-p}}{(n-p)!} \frac{\sqrt{m!n!}}{p!} \qquad (4.11)$$

$$\Rightarrow \quad q^2\psi_{m,q} + (\epsilon_m - \frac{\omega_c^2 q^2}{\Omega^2})\psi_{m,q} + \sum_n \int \frac{dk}{2\pi} v_{m,n}(q,k)\psi_{n,k} = E\psi_{m,q} \qquad (4.12)$$

$$(E - \epsilon_m - \frac{\omega_y^2}{\Omega^2}q^2)(\psi_{m,q} - \psi_{m,q}^{(0)}) - \sum_n \int \frac{dk}{2\pi} v_{m,n}(q,k)\psi_{n,k} = 0 \qquad (4.13)$$

$$\text{where } \psi_{m,q}^{(0)} \text{ is the zero order perturbation of } \psi_{m,q}. \qquad (4.14)$$

or $\qquad [\frac{\Omega^2}{\omega_y^2}(E - \epsilon_m) - q^2](\psi_{m,q} - \psi_{m,q}^{(0)}) - \sum_n \int \frac{dk}{2\pi} \frac{\Omega_2}{\omega_y^2} v_{m,n}(q,k)\psi_{n,k} = 0 \qquad$ (4.15)

$$\text{let } K_m^2 = \frac{\Omega^2}{\omega_y^2}(E - \epsilon_m)$$

And then, we obtain

$$[K_m^2 - q^2 + i\delta](\psi_{m,q} - \psi_{m,q}^{(0)}) - \frac{\Omega^2}{\omega_y^2} \sum_n \int \frac{dk}{2\pi} v_{m,n}(q,k)\psi_{n,k} = 0 \qquad (4.16)$$

where Eq. (4.16) is a 1-D equation in momentum space.

In usually, Lippmann-Schwinger equation method or iteration is used to solve this kind of problem in momentum space, but we use the inverse Fourier transformation to transform the $\psi_{m,q}$ in Eq. (4.16) back to the coordinate space. We define

$$\begin{cases} \tilde{v}_{m,n}(x) & \equiv \int \frac{d(q-k)}{2\pi} e^{i(q-k)x} v_{m,n}(q-k) \\ \psi_m(x) & = \int \frac{dk}{2\pi} e^{ikx} \psi_{m,k} \end{cases} \qquad (4.17)$$

or

$$\begin{cases} v_{m,n}(q,k) & = \int dx \ e^{-i(q-k)x} \tilde{v}_{m,n}(x) \\ \psi_{m,k} & = \int dx \ e^{-ikx} \psi_m(x) \end{cases} \qquad (4.18)$$

Eq. (4.16) become

$$(K_m^2 - q^2 + i\delta)(\psi_{m,q} - \psi_{m,q}^{(0)}) - \frac{\Omega^2}{\omega_y^2} \sum_n \int \frac{dk}{2\pi} v_{m,n}(q,k)\psi_{n,k} = 0 \qquad (4.19)$$

$$(K_m^2 - q^2 + i\delta)(\int dx \ e^{-iqx}\psi_m(x) - \int dx \ e^{-iqx}\psi_m^{(0)}(x))$$
$$-\frac{\Omega^2}{\omega_y^2} \sum_n \int \frac{dk}{2\pi} \int dx \ e^{-i(q-k)x}\tilde{v}_{m,n}(x) \int dx \ e^{-ikx}\psi_n(x) = 0 \qquad (4.20)$$

$$(K_m^2 - q^2 + i\delta)\left(\int dx e^{-iqx}\psi_m(x) - \int dx e^{-iqx}\psi_m^{(0)}(x)\right)$$
$$-\frac{\Omega^2}{\omega_y^2}\sum_n \int dx\ e^{-iqx}\tilde{v}_{m,n}(x)\psi_n(x) = 0 \tag{4.21}$$

$$\Rightarrow \quad (K_m^2 + \frac{\partial^2}{\partial x^2} + i\delta)(\psi_m(x) - \psi_m^{(0)}(x)) - \frac{\Omega^2}{\omega_y^2}\sum_n \tilde{v}_{m,n}(x)\psi_n(x) = 0 \tag{4.22}$$

$$\text{or} \quad (K_m^2 + \frac{\partial^2}{\partial x^2})\psi_m(x) + \sum_n \frac{\Omega^2}{\omega_y^2}\tilde{v}_{m,n}(x)\psi_n(x) = 0 \tag{4.23}$$

where

$$\tilde{v}_{m,n}(x) = \int \frac{d(q-k)}{2\pi} e^{i(q-k)x} v_{m,n}(q-k) \tag{4.24}$$

$$= \frac{V_0\gamma}{\sqrt{\pi}} i^{n-m} e^{-\gamma^2 x^2} \sum_{p=0}^{\text{Min}[m,n]} \left\{ 2^{p-\frac{m+n}{2}} \frac{\sqrt{m!n!}}{p!(m-p)!(n-p)!} H_{m+n-2p}(\gamma x) \right\} \tag{4.25}$$

$$\text{with } \gamma = \frac{\Omega^{3/2}}{\omega_c}$$

And finally we obtain the Eq. (4.23) which is a 1-D equation in coordinate space with a finite-range potential barrier. According to the Fourier transformation, the physical model we considered in Sec. 2.2, which is a 2-D wire with a δ-type embedded impurity barrier in the longitudinal direction with magnetic field can be reduced to a 1-D system with a finite range potential barrier. Our original model have be simplified and we can use the scattering matrix method which we will introduce in next section to solve the finite range potential problem.

To utilize the scattering matrix approach, we divide the scattering potential $\tilde{v}_{mn}(x)$ into a series with distance δL in between, each of them is described by a δ-type potential

$$\tilde{v}_{mn}(x) = \sum_{i=1}^{N_L} \tilde{v}_{mn}^{sc}(x_i) \tag{4.26}$$

$$\tilde{v}_{mn}^{sc}(x_i) = v_{mn}(x_i)\delta(x - x_i)\delta L \tag{4.27}$$

The potential $\tilde{v}_{mn}(s)$ can thus be described if we divide the potential into sufficiently large number of pieces, N_L.

And then we can use the scattering matrix approach to obtain the wavefunction $\psi_n(x)$ and the transmission and reflection coefficients.

In the programs, we write the equation $\tilde{v}_{m,n}(x)$ as

$$
\begin{aligned}
\tilde{v}_{m,n}(x) &= \frac{V_0\gamma}{\sqrt{\pi}} i^{n-m} e^{-\gamma^2 x^2} \sum_{p=0}^{\text{Min}[m,n]} 2^{p-\frac{m+n}{2}} \frac{\sqrt{m!n!}}{p!(m-p)!(n-p)!} H_{m+n-2p}(\gamma x) \\
&= \frac{V_0\gamma}{\sqrt{\pi}} i^{n-m} \sqrt{\frac{m!n!}{2^m 2^n}} e^{-\gamma^2 x^2} \sum_{p=0}^{\text{Min}[m,n]} \frac{2^p}{p!} \frac{2^{m-p}}{(m-p)!} \frac{2^{n-p}}{(n-p)!} \frac{H_{m+n-2p}(\gamma x)}{2^{m+n-2p}} \quad (4.28)
\end{aligned}
$$

and we define that $f_1(n) = 2^n/n!$, $f_2(n) = \sqrt{n!/2^n}$, and $H_t(n) = H_n(\gamma x)/2^n$.

The explicit derivation of $v_{m,n}(q,k)$ and $\tilde{v}_{m,n}(x)$ are given as follows

$$
v_{m,n}(q,k) = V_0 \int dy \; \phi_m^*(q,y) V_s(y) \phi_n(k,y) \quad (4.29)
$$

$$
= V_0 N_m N_n \int dy \left\{ e^{-\frac{\Omega}{2}(y - \frac{\omega_c q}{\Omega^2})^2} H_m[\sqrt{\Omega}(y - \frac{\omega_c q}{\Omega^2})] \right.
$$

$$
\left. \times e^{-\frac{\Omega}{2}(y - \frac{\omega_c k}{\Omega^2})^2} H_n[\sqrt{\Omega}(y - \frac{\omega_c k}{\Omega^2})] \right\} \quad (4.30)
$$

let $t = \sqrt{\Omega} y$, $\gamma = \Omega^{3/2}/\omega_c$.

$$
= V_0 N_m N_n \int \frac{dt}{\sqrt{\Omega}} e^{-\frac{1}{2}(t-\frac{q}{\gamma})^2 - \frac{1}{2}(t-\frac{k}{\gamma})^2} H_m[(t - \frac{q}{\gamma})] H_n[(t - \frac{k}{\gamma})] \quad (4.31)
$$

$$
= \frac{V_0 N_m N_n}{\sqrt{\Omega}} e^{-[\frac{1}{2\gamma}(q-k)]^2} \int dk \; e^{-[t - \frac{1}{2\gamma}(q-k)]^2} H_m(t - \frac{q}{\gamma}) H_n(t - \frac{k}{\gamma}) \quad (4.32)
$$

and let $\quad u = t - \dfrac{1}{2\gamma}(q + k)$

$$t = u + \frac{q}{2\gamma} + \frac{k}{2\gamma}$$

$$t - \frac{q}{\gamma} = u - \frac{q}{2\gamma} + \frac{k}{2\gamma} = u - \frac{q - k}{2\gamma}$$

$$t - \frac{k}{\gamma} = u + \frac{q}{2\gamma} - \frac{k}{2\gamma} = u + \frac{q - k}{2\gamma}$$

and $\quad W = \dfrac{q - k}{2\gamma}$

$$\Rightarrow v_{m,n}(q,k) \;=\; \frac{V_0 N_m N_n}{\sqrt{\Omega}} e^{-W^2} \int du\, e^{-u^2} H_m(u - W) H_n(u + W) \tag{4.33}$$

$$\sim\; v_{m,n}(q - k) \tag{4.34}$$

$$\tilde{v}_{m,n}(x) \;=\; \int \frac{d(q - k)}{2\pi} e^{i(q-k)x} v_{m,n}(q,k) \tag{4.35}$$

$$\text{let } W = \frac{q - k}{2\gamma}$$

$$=\; \frac{\gamma}{\pi} \int dW\, e^{i2x\gamma W} \frac{V_0 N_m N_n}{\sqrt{\Omega}} e^{-W^2} \int du\; e^{-u^2} H_m(u - W) H_n(u + W) \tag{4.36}$$

$$\text{where } N_m N_n = 2^{-\frac{m+n}{2}} \sqrt{1/m!n!}\sqrt{\Omega/\pi}$$

and using Eq. (A.78).

$$=\; \frac{V_0 \gamma}{\pi} \sum_{p=0}^{\mathrm{Min}[m,n]} \left\{ 2^{\frac{m+n}{2}-p} \frac{\sqrt{m!n!}}{p!(m - p)!(m - p)!}(-1)^{m-p} \right.$$

$$\left. \times \int dW\, e^{i2x\gamma W - W^2} W^{m+n-2p} \right\} \tag{4.37}$$

Using this relation:

$$\int\limits_{-\infty}^{\infty} x^n e^{-\beta^2 x^2} e^{iax} dx = i^n \frac{\sqrt{\pi}}{(2\beta)^n} e^{\frac{-a^2}{4\beta^2}} H_n(a/2\beta) \tag{4.38}$$

$$
\begin{aligned}
\tilde{v}_{m,n}(x) &= V_0 \frac{\gamma}{\pi} \sum_{p=0}^{\text{Min}[m,n]} 2^{\frac{m+n}{2}-p} \frac{\sqrt{m!n!}}{p!(m-p)!(m-p)!} (-1)^{m-p} \\
&\quad \times i^{m+n-2p} \frac{\sqrt{\pi}}{2^{m+n-2p}} e^{-\gamma^2 x^2} H_{m+n-2p}(\gamma x) \qquad (4.39) \\
&= \frac{V_0 \gamma}{\sqrt{\pi}} i^{n-m} e^{-\gamma^2 x^2} \sum_{p=0}^{\text{Min}[m,n]} \frac{2^{p-\frac{m+n}{2}} \sqrt{m!n!}}{p!(m-p)!(n-p)!} H_{m+n-2p}(\gamma x) \qquad (4.40)
\end{aligned}
$$

where $\gamma = \Omega^{3/2}/\omega_c$.

4.2 Scattering matrix method

In the previous section, we have wrote down the scattering potential in pieces in Eq. (4.26) and Eq. (4.27), and in this section we introduce the scattering matrix method in a general way.

To utilize the scattering matrix approach, we divide the scattering potential into a series with distance δL in between, each of them is described by a δ-type potential

$$
V_{sc}(x_i, y) = \delta L \, V_0(x_i) V_s(y) \delta(x - x_i) \qquad (4.41)
$$

The potential V_d can thus be described by $V_d(x,y) = \sum_{i=1}^{N_L} V_{x_i,y}$ if we divide the potential into sufficiently large number of pieces.

For a right-going incident wave $\psi(x, y)$ from the nth mode of the left reservoir, the corresponding scattering wavefunction can be expressed in the form

$$
\begin{aligned}
\psi_n^{(i)}(x < x_i, y, k_n) &= e^{ik_n x}\phi_n^+(y, k_n) + \sum_{n'} e^{-ik_{n'}x}\phi_{n'}^-(y, k_n)r_{i,n'n}^+, \qquad (4.42) \\
\psi_n^{(i)}(x > x_i, y, k_n) &= \sum_{n'} e^{ik_{n'}x}\phi_{n'}^+(y, k_n)t_{i,n'n}^+. \qquad (4.43)
\end{aligned}
$$

where $\phi_n^\pm(y, k_n)$ is the unperturbed eigen-function in the wire.

Following similar procedure we can also obtain the reflection and transmission coeffi-

cients, $r^-_{i,n'n}$ and $t^-_{i,n'n}$ for the left-going incident wave.

Refer to the paper, PRB. 44 1792 (1991), H. Tamura and T. Ando, we can have a detailed description of scattering matrix method. Due to the transmission and reflection coefficient amplitudes, $t^{\pm}_{m,n}$ and $r^{\pm}_{m,n}$. The scattering matrix, or the S matrix, is defines as

$$S = \begin{pmatrix} r^+ & t^- \\ t^+ & r^- \end{pmatrix} \tag{4.44}$$

The current conservation law requires the unitarity of the S matrix as

$$\tilde{S}^\dagger \tilde{S} = \tilde{S}\tilde{S}^\dagger = 1 \tag{4.45}$$

where $\tilde{S}$ consists of $N_c \times N_c$ transmission matrices $t^{\pm}$ and the reflection matrices $r^{\pm}$, which contain the scattering amplitudes from N_c incoming conducting channels to N_c outgoing conducting channels.

The overall S matrix for the disordered region containing a certain number of impurities with δ-type potential can be obtained by decomposing it into single-impurity parts and free-propagating parts using a composition law. ref If we consider the two S matrices defined by

$$S_1 = \begin{pmatrix} r^+_1 & t^-_1 \\ t^+_1 & r^-_1 \end{pmatrix} \text{ and } S_2 = \begin{pmatrix} r^+_2 & t^-_2 \\ t^+_2 & r^-_2 \end{pmatrix} \tag{4.46}$$

then the composed S matrix $S_{12} \equiv S_1 \otimes S_2$ for S_1 and S_2 in series can be calculated as

$$\begin{pmatrix} B \\ C \end{pmatrix} = \begin{pmatrix} r^+_1 & t^-_1 \\ t^+_1 & r^-_1 \end{pmatrix} \begin{pmatrix} A \\ D \end{pmatrix} \text{ and } \begin{pmatrix} D \\ E \end{pmatrix} = \begin{pmatrix} r^+_2 & t^-_2 \\ t^+_2 & r^-_2 \end{pmatrix} \begin{pmatrix} C \\ F \end{pmatrix} \tag{4.47}$$

$$\Rightarrow \begin{cases} B = r^+_1 A + t^-_1 D \\ C = t^+_1 A + r^-_1 D \end{cases} \text{ and } \begin{cases} D = r^+_2 C + t^-_2 F \\ E = t^+_2 C + r^-_2 F \end{cases} \tag{4.48}$$

$$\begin{aligned} D &= r_2^+(t_1^+ A + r_1^- D) + t_2^- F = r_2^+ t_1^+ A + r_2^+ r_1^- D + t_2^- F \\ \Rightarrow D &= (1 - r_2^+ r_1^-)^{-1} r_2^+ t_1^+ A + (1 - r_2^+ r_1^-)^{-1} t_2^- F \end{aligned}$$ (4.49)

and

$$\begin{aligned} B &= r_1^+ A + t_1^- D \\ &= [r_1^+ + t_1^+(1 - r_2^+ r_1^-)^{-1} r_2^+ t_1^+] A + t_1^-(1 - r_2^+ r_1^-)^{-1} t_2^- F \end{aligned}$$ (4.50)

$$\begin{aligned} C &= t_1^+ A + r_1^- D = t_1^+ A + r_1^- r_2^+ C + r_1^- t_2^- F \\ \Rightarrow C &= (1 - r_1^- r_2^+)^{-1} t_1^+ A + (1 - r_1^- r_2^+)^{-1} r_1^- t_2^- F \end{aligned}$$ (4.51)

and

$$\begin{aligned} E &= t_2^+ C + r_2^- F \\ &= t_2^+(1 - r_1^- r_2^+)^{-1} t_1^+ A + [r_2^- + t_2^+(1 - r_1^- r_2^+)^{-1} r_1^- t_2^-] F \end{aligned}$$ (4.52)
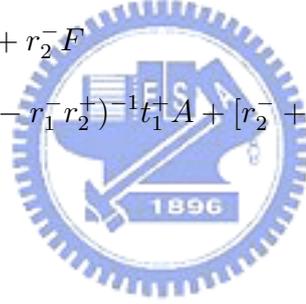
$$\begin{aligned} \begin{pmatrix} B \\ E \end{pmatrix} &= \begin{pmatrix} r_1^+ + t_1^+(1 - r_2^+ r_1^-)^{-1} r_2^+ t_1^+ & t_1^-(1 - r_2^+ r_1^-)^{-1} t_2^- \\ t_2^+(1 - r_1^- r_2^+)^{-1} t_1^+ & r_2^- + t_2^+(1 - r_1^- r_2^+)^{-1} r_1^- t_2^- \end{pmatrix} \begin{pmatrix} A \\ F \end{pmatrix} \\ &= \begin{pmatrix} r_{12}^+ & t_{12}^- \\ t_{12}^+ & r_{12}^- \end{pmatrix} \begin{pmatrix} A \\ F \end{pmatrix} \end{aligned}$$ (4.53)

$$\Rightarrow \begin{cases} t_{12}^+ = t_2^+(1 - r_1^- r_2^+)^{-1} t_1^+, \\ t_{12}^- = t_1^-(1 - r_2^+ r_1^-)^{-1} t_2^-, \\ r_{12}^+ = r_1^+ + t_1^- r_2^+(1 - r_1^- r_2^+)^{-1} t_1^+, \\ r_{12}^- = r_2^- + t_2^+ r_1^-(1 - r_2^+ r_1^-)^{-1} t_2^-. \end{cases}$$ (4.54)

Note that the composition law satisfies the associative law $(S_1 \otimes S_2) \otimes S_3 = S_1 \otimes (S_2 \otimes S_3)$, but does not satisfy the commutative law in general, i.e., $S_2 \otimes S_1 \neq S_1 \otimes S_2$. The overall

S matrix can be expressed as

$$S = S_1^{\text{free}} \otimes S_1^{\text{imp}} \otimes S_2^{\text{free}} \otimes \cdots \otimes S_{N_I}^{\text{imp}} \otimes S_{N_I+1}^{\text{free}} \qquad (4.55)$$

where N_I is the total number of impurities. It must be noted that this decomposition
method of the disordered region into parts by Eq. (4.55) cannot be applied to the system
containing impurities with the long-range potential.

4.3 Wavefunction and current density

We will write down the equations of wavefunction and the current density in the wire
with magnetic field in this section.

In the beginning, we have known that the total wavefunction could be written as the
below equation

$$\Psi(x,y) = \sum_n \int \frac{dk}{2\pi} e^{ikx} \psi_{n,k} \phi_n(k,y), \qquad (4.56)$$

where k is also the variable of the Fourier transformation here and must be a real number

$$\phi_n(k,y) = N_n^s e^{-\frac{\Omega}{2}(y - \frac{\omega_c}{\Omega^2}k)^2} H_n\left[\sqrt{\Omega}(y - \frac{\omega_c}{\Omega^2}k)\right] \qquad (4.57)$$

and then

$$\begin{aligned}
\Psi_n(x,y) &= \int \frac{dk}{2\pi}\, e^{ikx} \psi_{n,k} \phi_n(k,y) \\
&= \int dx' \tilde{\psi}_n(x') \int \frac{dk}{2\pi}\, e^{ik(x-x')} \phi_n(k,y)
\end{aligned} \qquad (4.58)$$

where
$$\int \frac{dk}{2\pi} e^{ik(x-x')} \phi_n(k,y)$$

$$= \int_{-\infty}^{\infty} \frac{dk}{2\pi} N_n^s e^{-\frac{\Omega}{2}(y-\frac{\omega_c}{\Omega^2}k)^2} H_n\left[\sqrt{\Omega}(y-\frac{\omega_c}{\Omega^2}k)\right] e^{ik(x-x')} \qquad , \text{let } u = \sqrt{\Omega}y - \frac{k}{\gamma}$$

$$= \frac{N_n^s}{2\pi}(-\gamma)\int_{\infty}^{-\infty} du\ e^{-\frac{u^2}{2}} H_n[u] e^{i\gamma(\sqrt{\Omega}y-u)(x-x')} \tag{4.59}$$

$$= \frac{N_n^s}{2\pi}\gamma e^{i\gamma\sqrt{\Omega}y(x-x')}\int_{-\infty}^{\infty} du\ e^{-\frac{u^2}{2}} H_n[u] e^{-i\gamma(x-x')u}$$

$$= \frac{N_n^s}{\sqrt{2\pi}}\gamma e^{i\gamma\sqrt{\Omega}y(x-x')}e^{-\frac{1}{2}\gamma^2(x-x')^2} H_n\left[\gamma(x'-x)\right] i^n \tag{4.60}$$

$$= \frac{N_n^s}{\sqrt{2\pi}}i^n\gamma e^{-\frac{1}{2}\Omega y^2}e^{\frac{1}{2}[i\gamma(x-x')+\sqrt{\Omega}y]^2} H_n\left[-\gamma(x-x')\right] \tag{4.61}$$

where we use the Eq.7.376 in the mathematic table [64], $\int dx\ e^{ixy}e^{-\frac{x^2}{2}} H_n(x) = \sqrt{2\pi}e^{-\frac{y^2}{2}} H_n(y)i^n$.

$$\Psi_n(x,y) = \int dx' \tilde{\psi}_n(x')\frac{N_n^s}{\sqrt{2\pi}}i^n\gamma e^{i\frac{\Omega^2}{\omega_c}y(x-x')}e^{-\frac{1}{2}[\gamma(x'-x)]^2} H_n\left[\gamma(x'-x)\right]$$

$$= \frac{N_n^s}{\sqrt{2\pi}}i^n\gamma e^{i\frac{\Omega^2}{\omega_c}yx}\int dx'\ \tilde{\psi}_n(x')e^{-i\gamma\sqrt{\Omega}yx'}e^{-\frac{1}{2}\gamma^2(x'-x)^2} H_n(\gamma(x'-x)) \tag{4.62}$$

$$= \frac{N_n^s}{\sqrt{2\pi}}i^n\gamma e^{-\frac{1}{2}\Omega y^2}\int dx'\ \tilde{\psi}_n(x')e^{\frac{1}{2}[i\gamma(x-x')+\sqrt{\Omega}y]^2} H_n(\gamma(x'-x)) \tag{4.63}$$

where $\tilde{\psi}_n(x)$ is exactly the solution of Eq. (4.23).

And we write this Eq. (4.63) in programs as:

$$\Psi_n(x,y) = \frac{N_n^s}{\sqrt{2\pi}}i^n\gamma e^{-\frac{1}{2}\Omega y^2}\int dx'\ \tilde{\psi}_n(x')e^{\frac{1}{2}[i\gamma(x-x')+\sqrt{\Omega}y]^2} H_n(\gamma(x'-x))$$

$$= (\frac{1}{\sqrt{2}})^{n+1}\frac{1}{\sqrt{n!}}\sqrt{\sqrt{\Omega}(\frac{1}{\sqrt{\pi}})^3}\ e^{-\frac{\Omega}{2}y^2}\gamma\ i^n$$

$$\times \sum_j \tilde{\psi}_n(x_j)(\Delta x)e^{\frac{1}{2}[i\gamma(x-x_j)+\sqrt{\Omega}y]^2} H_n(-\gamma(x-x_j)) \tag{4.64}$$

where Δx is the interval distance of x_{j+1} and x_j.

In the Sec. 3.4, we have the relation of the current density:

$$j_x = \frac{1}{i}\{\psi^*\frac{\partial}{\partial x}\psi - \frac{\partial}{\partial x}\psi^* \cdot \psi - 2i\omega_c y\psi^*\psi\} = \psi^*(\frac{\partial}{i\partial x} - \omega_c y)\psi + c.c. \tag{4.65}$$

$$j_y = \frac{1}{i}\{\psi^*\frac{\partial}{\partial y}\psi - \frac{\partial}{\partial y}\psi^* \cdot \psi\} = \psi^*\frac{\partial}{i\partial y}\psi + c.c. \tag{4.66}$$

$$
\begin{aligned}
\frac{\partial}{i\partial x}\Psi_n &= \frac{\partial}{i\partial x}\frac{N_n}{\sqrt{2\pi}}i^n\gamma e^{i\frac{\Omega^2}{\omega_c}yx} \\
&\quad \times \int dx'\ \tilde{\psi}_n(x')e^{-i\gamma\sqrt{\Omega}yx'}e^{-\frac{1}{2}\gamma^2(x'-x)^2}H_n(\gamma(x-x')) \\
&= \frac{N_n}{\sqrt{2\pi}}i^n\gamma e^{i\frac{\Omega^2}{\omega_c}yx}\int dx'\ \{\tilde{\psi}_n(x')e^{-i\gamma\sqrt{\Omega}yx'}e^{-\frac{1}{2}\gamma^2(x'-x)^2} \\
&\quad \times \frac{1}{i}\left[\begin{array}{l}\frac{i\Omega^2}{\omega_c}yH_n[\gamma(x'-x)] + \gamma^2(x'-x)H_n[\gamma(x'-x)] \\ -2\gamma^2(x'-x)H_n[\gamma(x'-x)] - H_{n+1}[\gamma(x'-x)]\end{array}\right]\} \\
&= \frac{N_n}{\sqrt{2\pi}}i^n\gamma e^{i\frac{\Omega^2}{\omega_c}yx}\int dx'\ \{\tilde{\psi}_n(x')e^{-i\gamma\sqrt{\Omega}yx'}e^{-\frac{1}{2}\gamma^2(x'-x)^2} \\
&\quad \times \left[\begin{array}{l}\frac{\Omega^2}{\omega_c}yH_n[\gamma(x'-x)] + i\gamma^2(x'-x)H_n[\gamma(x'-x)] \\ -i\gamma H_{n+1}[\gamma(x'-x)]\end{array}\right]\}
\end{aligned}
\tag{4.67}
$$

$$
\begin{aligned}
\frac{\partial}{i\partial y}\Psi_n &= \frac{N_n}{\sqrt{2\pi}}i^n\gamma e^{i\frac{\Omega^2}{\omega_c}yx} \\
&\quad \times \int dx'\ \tilde{\psi}_n(x')\sqrt{\Omega}\gamma(x-x')e^{-i\gamma\sqrt{\Omega}yx'}e^{-\frac{1}{2}\gamma^2(x'-x)^2}H_n(\gamma(x-x'))
\end{aligned}
\tag{4.68}
$$

where $\gamma = \Omega^{3/2}/\omega_c$.

And then we can substitute Eq. (4.67) and Eq. (4.68) into Eq. (4.65) and Eq. (4.66) and obtain the current density.

4.4 Numerical results

In the Fig. 4.1, we discuss the saturation versus N_c and plot the transmission as a function of B for various number of subband for the case of the barrier strength is repulsive with
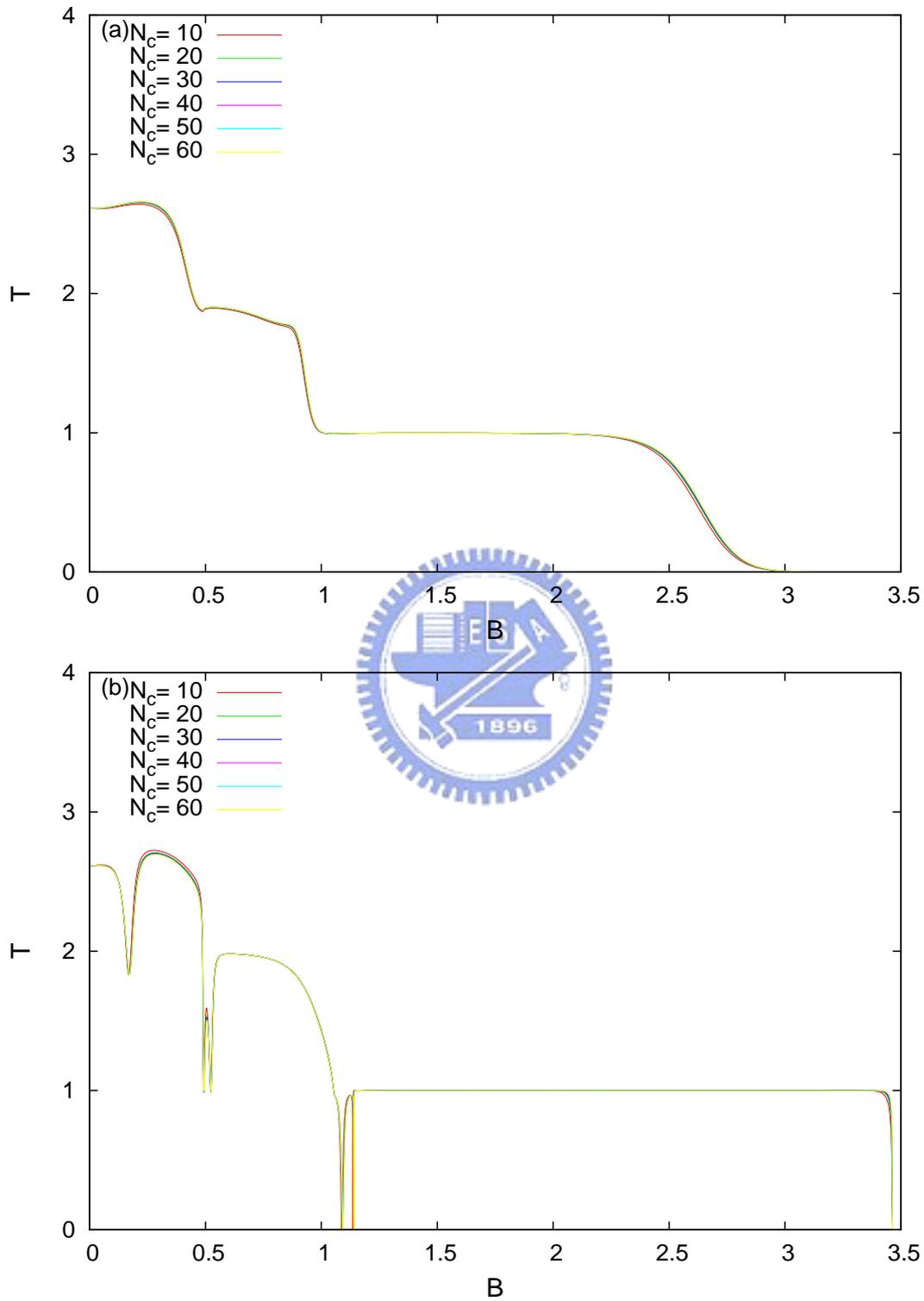
Figure 4.1: The saturation versus the numbers of subband N_c for a repulsive barrier with $1.0E^*$ in (a) and an attractive barrier with $-1.0E^*$ in (b). The incident energy is at $7\omega_y E^*$.

$1.0E^*$ in (a) and attractive $-1.0E^*$ in (b) We change the numbers of subbands used in the calculation for various of 10, 20, 30, 40, and 50. We can find that the curves had saturate for the larger numbers of subbands in both repulsive and attractive potential, and it is also conform to the conservation condition. Although it is saturate for the more subbands, but it saturate slowly and need much more subbands than the mode-matching approach.
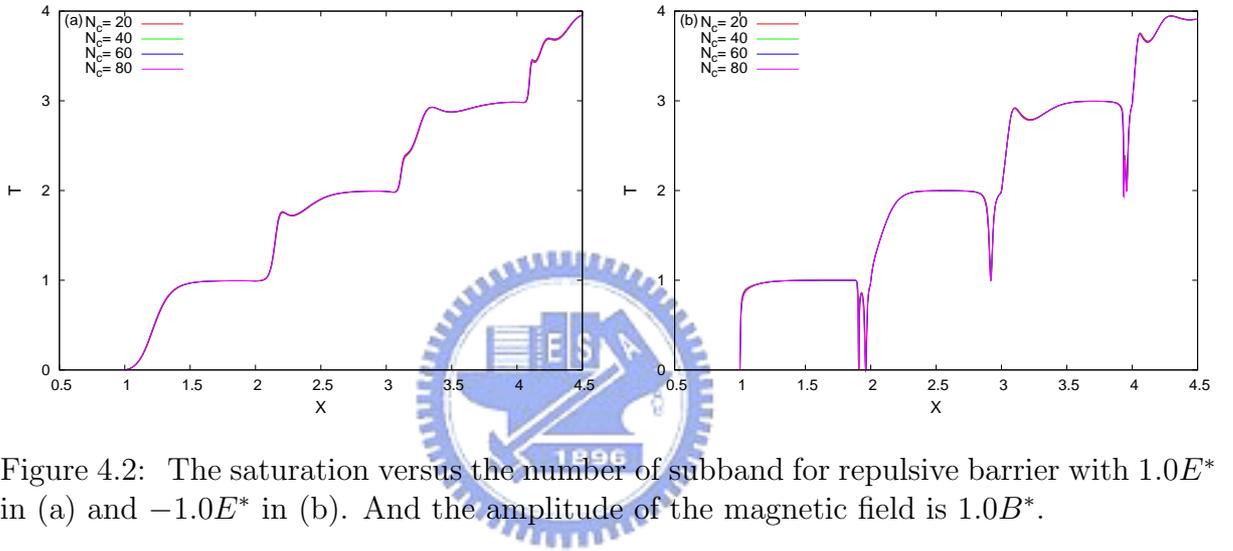
Figure 4.2: The saturation versus the number of subband for repulsive barrier with $1.0E^*$ in (a) and $-1.0E^*$ in (b). And the amplitude of the magnetic field is $1.0B^*$.
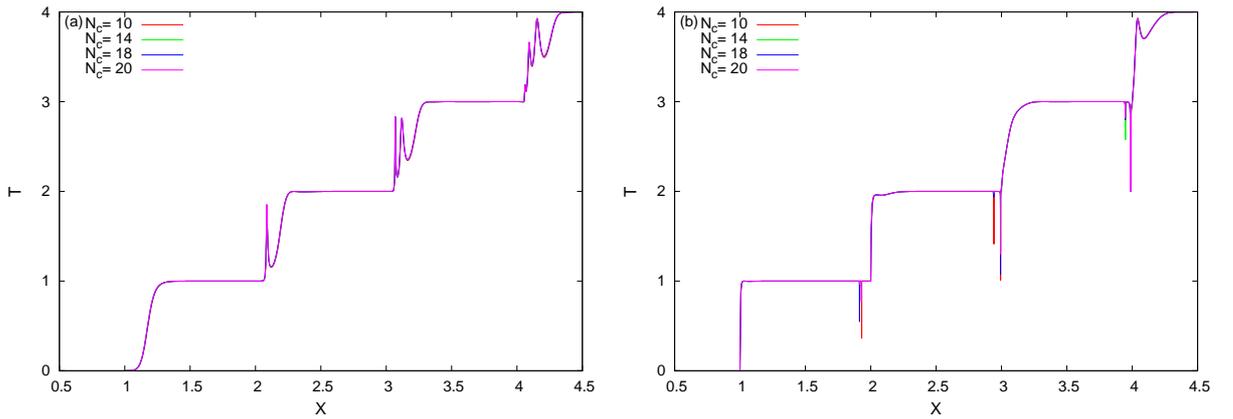
Figure 4.3: The saturation versus the number of subband for repulsive barrier with $1.0E^*$ in (a) and $-1.0E^*$ in (b). And the amplitude of the magnetic field is $2.0B^*$.

In Fig. 4.2 and Fig. 4.3, we find that the curves of transmission versus incident energy saturate and used fewer numbers of subbands in the higher strength of magnetic field. In the Fig. 4.2, the curves saturate with 80 subbands when $B = 1.0$, and in the Fig. 4.2, the

curves saturate with 20 subbands when $B = 2.0$ Because the subband level spacing will be wider as we increase the strength of the magnetic field, the overlap of each subbands and the transition of each subbands is smaller. And it need fewer subbands and can describe the interaction between subbands well.
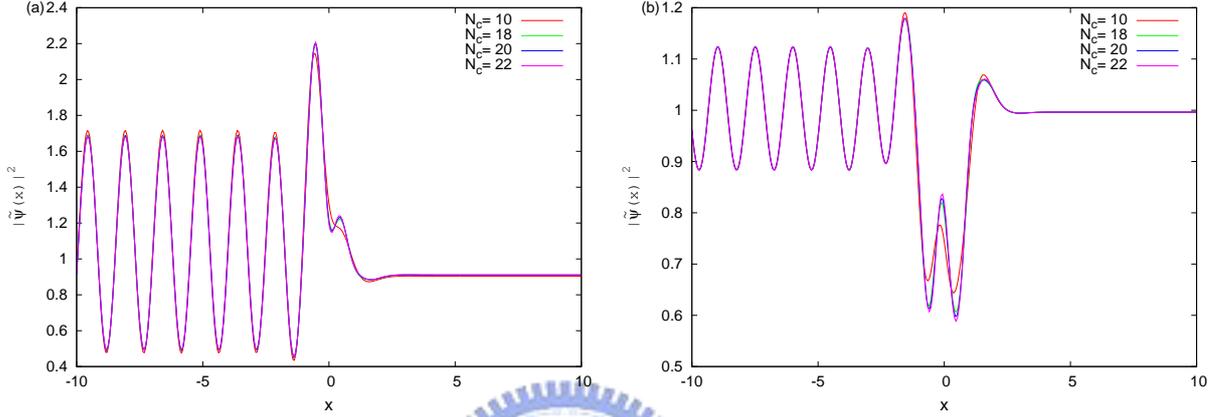
Figure 4.4: The probability density of $|\psi_n(x)|^2$ as a function of coordinate variable x for various N_c from 10 to 22, incident energy is $1.4\Omega E^*$ and the amplitude of magnetic field is 1.0. The barrier is repulsive in (a), and attractive in (b).

In the Fig. 4.4, we plot the magnitude square of wave function $\tilde{\psi}_n(x)$ which is the solution of Eq. (4.23) near $x = 0$ for various of numbers of subbands, 10, 18, 20, and 22. The incident energy is $X = 1.4$, the amplitude of the magnetic field is fixed to 1.0, and the barrier is (a) repulsive, $V_0 = 1.0E^*$, and (b) attractive, $V_0 = -1.0E^*$.

In the Fig. 4.4, we can find that the curves of wavefunctions does not really saturate yet even when we used 22 subbands in the case of $B = 1.0$, and the curves start to diverge when we increase the numbers of subbands to 23. And it not strange that the curves is not saturate because the transmission in the same parameter is not saturate either in Fig. 4.2, the strange thing is why the wavefunction diverge in this few subbands, we can have reasonable results in calculating the transmission with much more subbands. In the process of calculating the wavefunction $\tilde{\psi}_n(x)$, we use the scattering matrix method to obtain the wavefunction of each position on x-direction. We have to inverse the scattering matrix to obtain the coefficients here, and there is a problem about the accuracy of calculation. Of course we have to improve the precision and algorithm, but it is still a

limit of the numerical calculation.

We know that the wavefunction is more sensitive than the transmission and more hard to be saturate. In the Fig. 4.4, the curves are not saturate in quantity, but we believe that the character and profile will be almost saturate in qualitatively. According to this result, we use 20 subbands in our calculation and plot several figures of wavefunction in the case of small magnetic field which smaller than $B = 1.0B^*$. And investigate the physical insights about what happened in this system when we apply the magnetic field.
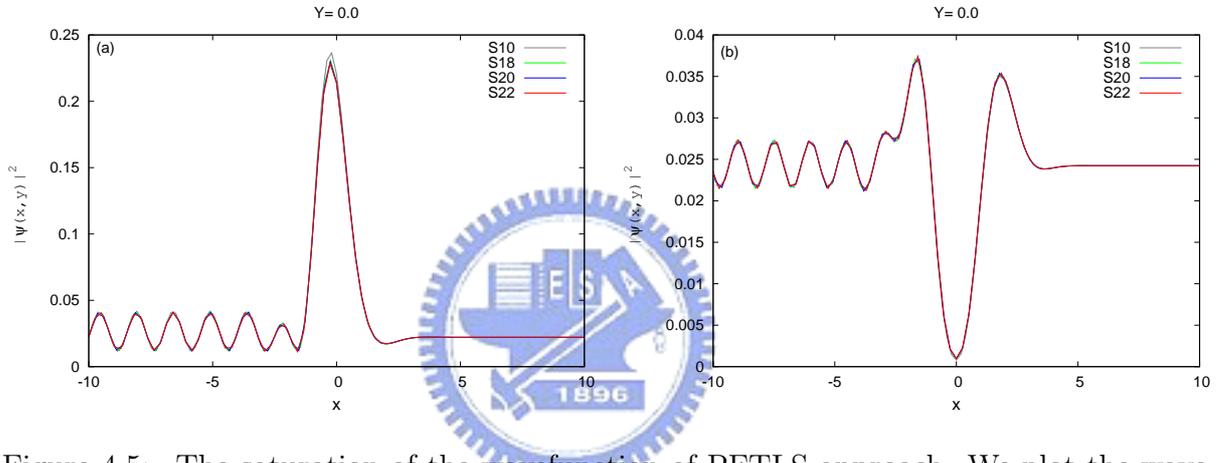
Figure 4.5: The saturation of the wavefunction of PFTLS approach. We plot the wavefunction of $-10 < x < 10$ and $x = 0$ for various numbers of subbands, 10, 18, 20, and 22, and the incident energy $X = 1.6$, the amplitude of magnetic field is 1.0, and the strength of the barrier is repulsive, 1.0 in (a), and attractive, -1.0 in (b).

In the Fig. 4.5, we plot the wavefunction of $-10 < x < 10$ and $y = 0$ by using the approach of PFTLS for various numbers of subbands, 10, 18, 20, and 22 in the case of incident energy $X = 1.6$, the amplitude of magnetic field is 1.0, and the strength of barrier is repulsive, 1.0 in (a) and attractive, -1.0 in (b). We can find that the wavefunction saturate down as we increase the numbers of subbands to 20 and 22, and in the others plotting of wavefunction by using the approach of PFTLS, we all use 20 subbands.

4.5 Summary

In Ch.3, we have discuss about the center shift of the eigen-function $\phi_n^{\pm}(y, k_n)$, the center of the eigen-function shift to the edge in the wire as the wave vector is real, and the

center is back to the center of the wire as the wave vector is pure imaginary. In other words, the eigen-function $\phi_n^{\pm}(y, k_n)$ is a propagating mode and a real function if the wave vector is real, and be an evanescent mode and a complex function if the wave vector is pure imaginary. Because the eigen-function $\phi_n^{\pm}(y, k_n)$ is not a orthonormal basis and a complete set as the wave vector k_n is a pure imaginary variable, we have to expand the eigen-function $\phi_n^{\pm}(y, k_n)$ to a orthonormal basis $\phi_n^o(y)$ which we have done in Ch.3.

In this chapter, we use the approach of partial Fourier transformation to transform the x coordinate to momentum space and keep the wave vector real and be the Fourier transformation variable. According to this method, the eigen-function $\phi_n^{\pm}(y, k_n)$ will be a orthonormal and complete basis. It is a good news to avert the expansion of eigen-function $\phi_n^{\pm}(y, k_n)$ to another, but what we have to pay is the more heavily numerical calculation and the δ-type barrier will become a finite range potential.

After we transform the original Hamiltonian to partial momentum space and then transform back to the coordinate space, the original two-dimensional problem which is a wire and embedded a δ-type barrier will become a quasi-one-dimensional problem. In some sense, it is earlier to be solved then a two-dimensional problem here and we use the scattering matrix method.

In the next chapter, we will discuss what is the same and what is different between these two approaches, MM and PFTLS, and which one is better in our case. And we have also compare the numerical results of these two approach, and make sure our calculation is correct and believable.

Chapter 5

Comparing the numerical results from the MM and PFTLS approaches

We compare the numerical results from the MM and PFTLS approaches in this chapter. We compare the curves of transmission ,the wavefunction and current density patterns, and find that the results of these two approaches are almost the same.

5.1 Transmission

In the Fig. 5.1, we plot the transmission versus the amplitude of magnetic field of the two approaches, MM and PFTLS. We fix the incident energy at $E = 7\omega_y E^*$ which $X = 3$ and the barrier strength is repulsive with $1.0E^*$ in (a) and attractive with $-1.0E^*$ in (b). We find that the curves in both approaches in Fig. 5.1(a) and (b) does not overlay together but they have more overlap when we increase the numbers of subbands. In the Ch. 3 and 4, we know that the two approaches have their own regime which can saturate easier and the unsuitable regime which can not saturate in the calculations, *e.q.* the approach of MM is more easier to saturate in the lower magnetic field regime and can't saturate in the
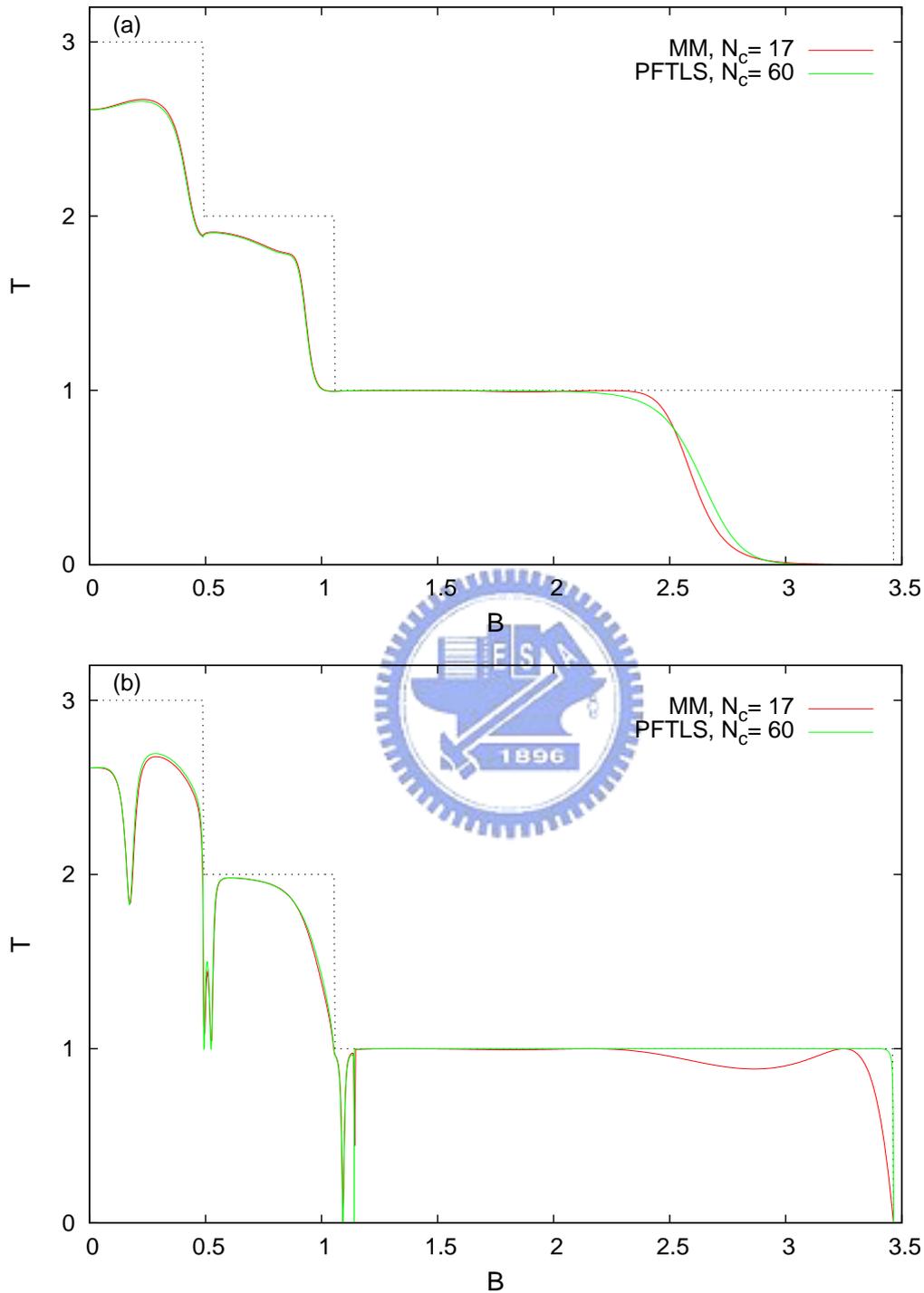
Figure 5.1: The transmission versus the amplitude of magnetic field of the two approaches, MM and PFTLS. we fix the incident energy at $7\omega_y E^*$ which $X = 3$ and the barrier strength is repulsive with $1.0E^*$ in (a) and attractive with $-1.0E^*$ in (b).

higher magnetic field regime which we had discussed in the Sec. 3.6; and the approach of

PFTLS is easier to saturate in the higher magnetic field regime and hard to saturate in

the lower magnetic field regime which we had also discussed in the Sec. 4.5. According
to the different of these two approaches, the curves in Fig. 5.1 of these two approaches
is reasonable that does not overlay together. But the the regime of lower magnetic field,
the curves should be closer as we increase the numbers of subbands which used in the
approach of PFTLS, and it does, $e.q.$ the curves of approach of MM are roughly saturate
below the amplitude of the magnetic field is $B = 1.0B^*$, and the curves of approach of
PFTLS are saturate above the amplitude of the magnetic field is $B = 1.0B^*$ by using
80 subbands. The curves should overlay together near the amplitude of magnetic field is
$B = 1.0B^*$ in the Fig. 5.1.

Besides the comparing of quantity, in qualitatively the character is the same in both
approaches which showed in the Fig. 5.1.

In the Fig. 5.2, we compare the curves of transmission versus incident energy of the
two approaches, MM and PFTLS. In this comparison, we fix the amplitude of magnetic
field to $B = 1.0B^*$ and the strength of barrier to $1.0E^*$ but repulsive in (a) and attractive
in (b). According to the discussion of the Fig. 3.3 and Fig. 4.2, we use 30 subbands for
the calculation of the approach of MM and the curve is saturate below $X = 4$, and use 80
subbands for the calculation of the approach of PFTLS and the curve is saturate. And we
find that the curves in Fig. 5.2 overlay together in the lower incident energy, $e.q.$ $X < 3$,
and within a little space between two curves above $X = 4$. And the two curves roughly
overlay together between $3 < X < 4$.

In Fig. 5.3, we enlarge the regime of $0.95 < X < 2.5$ and $1.8 < X < 2.01$ in Fig. 5.2,
and check how close of the curves of the two approaches. In the Fig. 5.3(a), it is still
hard to separate the difference of curves of the two approaches, MM and PFTLS. In the
Fig. 5.3(b), we find that the curves of 'MM, $N_c = 30$' and 'PFTLS, $N_c = 80$' does have
a little space between them and the spacing depend on the numbers of subbands used in
the calculation, the more numbers of subbands used, the less spacing between the two
approaches. According to this, we believe that the two approaches will be the same if we
can use "enough" subbands, but it is hard to do in the numerical calculation. And the
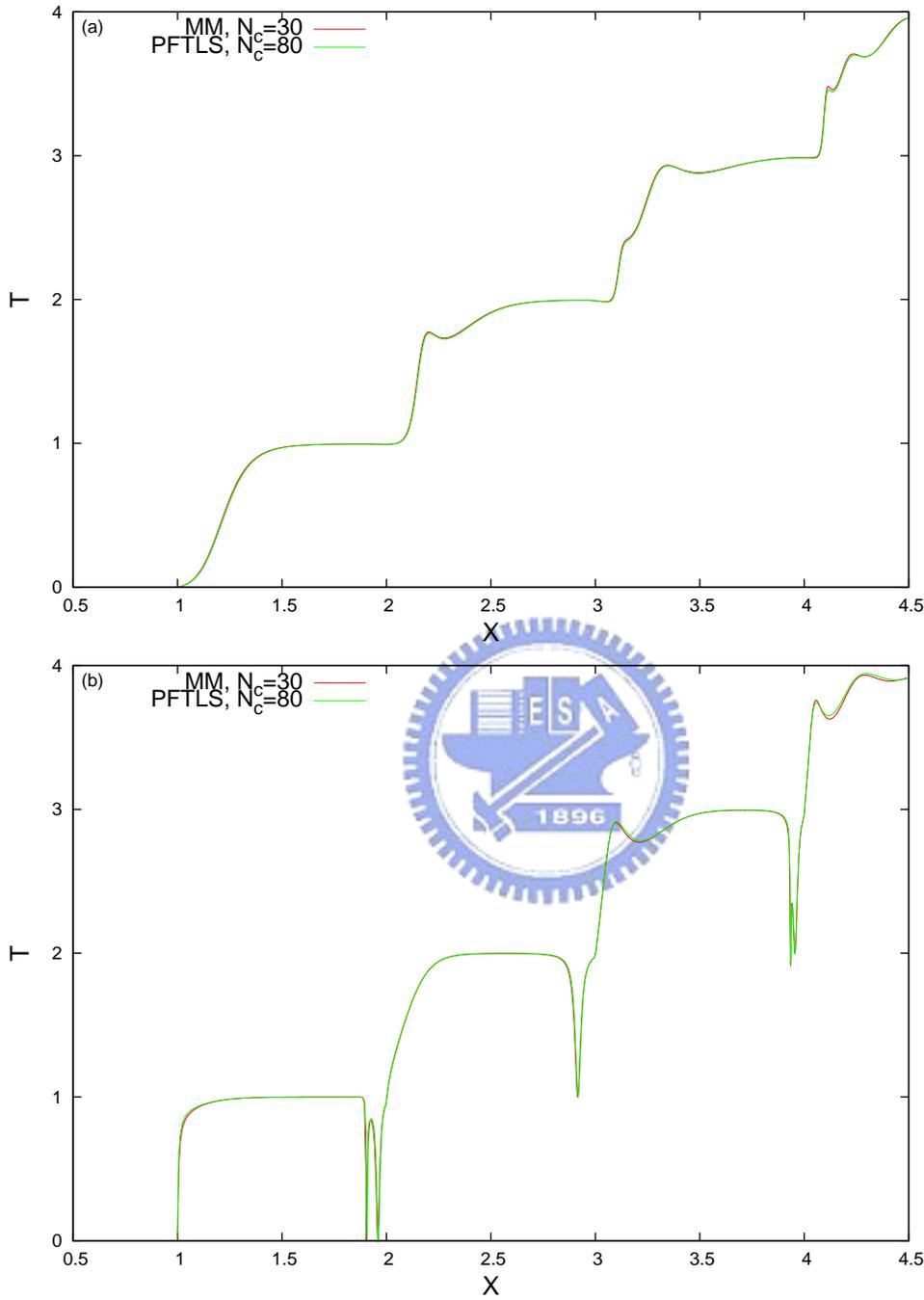
Figure 5.2: The transmission versus the incident energy X of the two approaches, MM and PFTLS. The magnetic field amplitude is $1.0B^*$ and the strength of the repulsive barrier is $V_0 = 1.0E^*$ in (a) and the attractive barrier is $V_0 = -1.0E^*$ in (b).

physical insight must had be saturate down in both approaches.
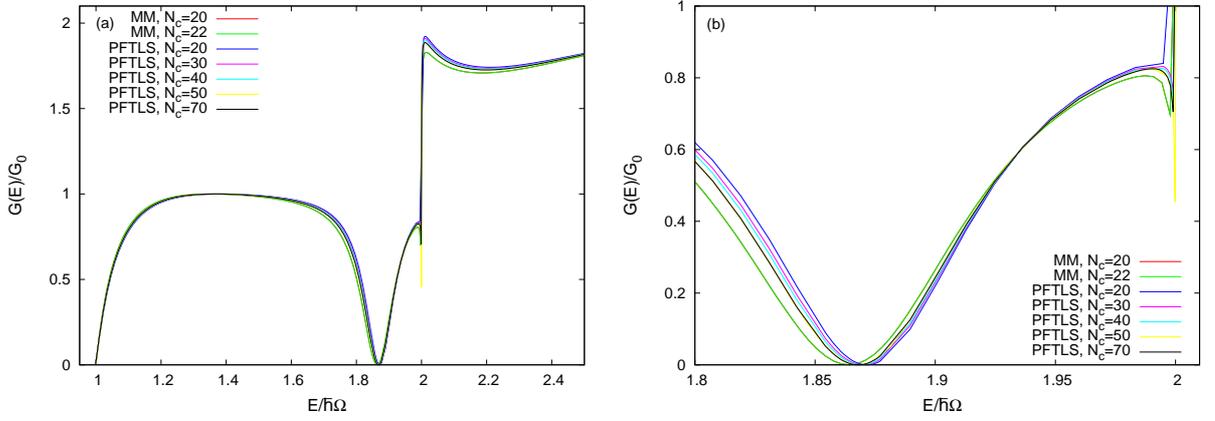
Figure 5.3: Comparing the saturation of the two approaches by plotting the transmission versus the incident energy, the magnetic field amplitude is $B = 0.5B^*$ and the strength of the impurity barrier is $V_0 = -1.0E^*$. And we enlarge one part of figure (a) from 1.8 to 2.01 in (b).
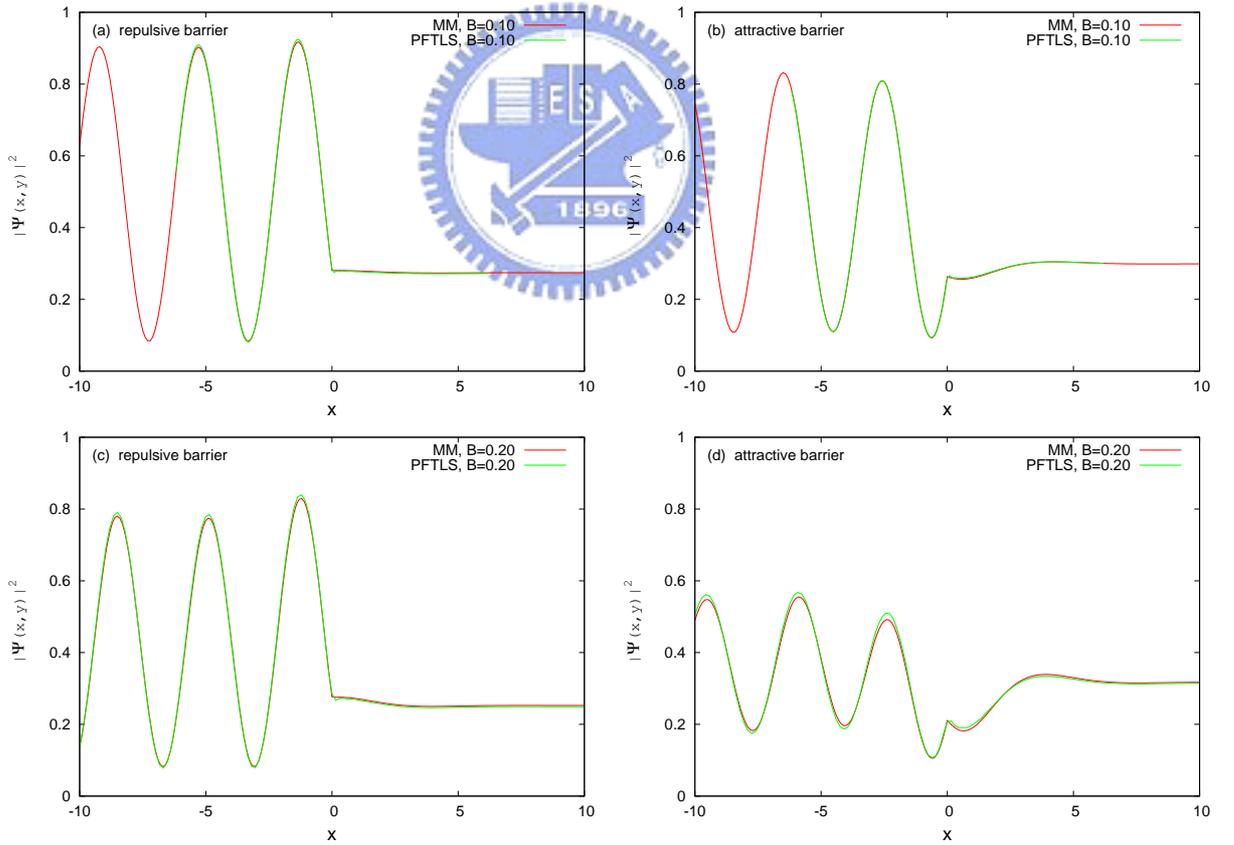
Figure 5.4: Compare the wavefunction of the two approaches, MM and PFTLS, for $-10 < x < 10$ and $y = 0$. The incident energy $X = 1.6$, and the strength of the barriers are repulsive and 1.0 in (a) and (c), attractive and -1.0 in (b) and (d), and the amplitude of the magnetic field are 0.1 in (a) and (b), 0.2 in (c) and (d).

5.2 Wavefunction and current pattern

In the Fig. 5.4, we plot the wavefunctions of $-10 < x < 10$ and $y = 0$ by using the two approaches in the case of incident energy $X = 1.6$, we also change the amplitude of magnetic field and strength of barrier, which the amplitude of magnetic field are 0.1 in figures (a) and (b) and 0.2 in figures (c) and (d), and the strength of barriers are repulsive, 1.0, in figures (a) and (c) and attractive, -1.0, in figures (b) and (d). And the used numbers of subbands are 50 in the approach of MM and 20 in the approach of PFTLS, which the wavefunction of MM and PFTLS are both saturate.

In the Fig. 5.4, we can find that the two curves of the two approaches are very close in each figure. In the case of $B = 0.1$ in figures (a) and (b), the two curves are almost overlap together, but $B = 0.2$, in figures (c) and (d), the two curves look similar but not overlap together. The spacing between the two curves become wider as the amplitude of magnetic field increase, because the transmission of the the approach of PFTLS is not saturate by using this few subbands in calculation, which we had also discussed about the Fig. 5.3 in the section 5.1. But in the case of $B = 0.1$, the amplitude of the magnetic field is too small, and the two approaches can both describe the system with magnetic field well.

In the Fig. 5.5, we plot the current density patterns in the wire with the implied magnetic field, $B = 0.15B^*$, and the incident energy $X = 1.9$, the strength of the barrier is 20 which is very strong the the total transmission is approach to zero. And the Fig. 5.5(a) is plotted by using the approach of MM and (b) use the approach of PFTLS. The two current density patterns of the two approaches look very similar. The direction of the current density patterns are almost the same but few place near $x = 0$. The current density of the place that the direction is different is very small and near the place which the current flow together, and it is very sensitive to the direction. But in the place of larger current, the current patterns are the same. Besides the direction of the current density patterns, the strength of the current density are also similar of these two figures
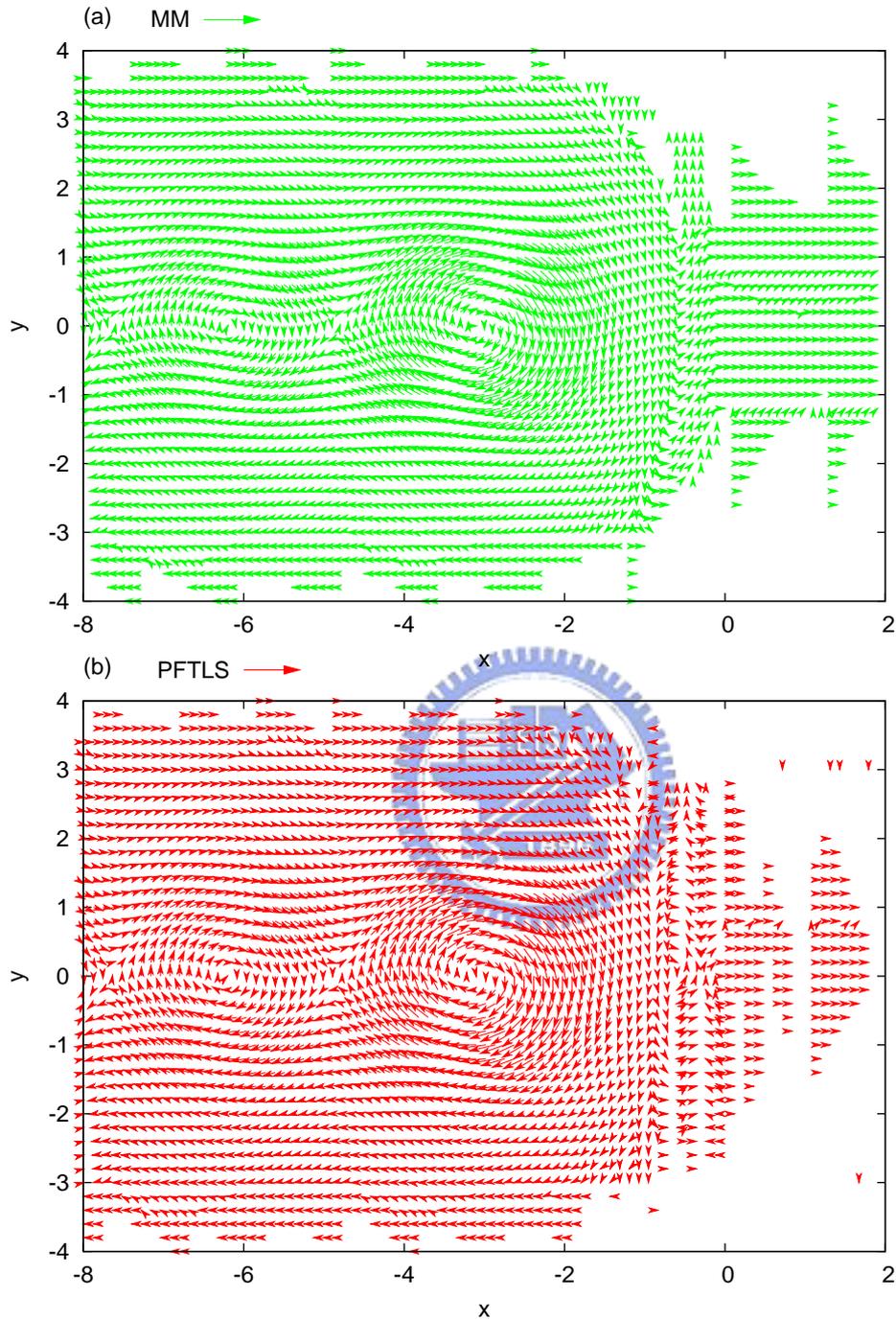
Figure 5.5: The current density in the wire with magnetic field, $B = 0.15B^*$, and the incident energy is $X = 1.9$ which is close to the subband bottom of second subband. And the strength of the barrier is repulsive, 20. (a) is the current density by using the approach of MM, and (b) use the approach of PFTLS.

in the Fig. 5.5.

5.3 Summary

In this chapter, we had compare about the numerical results of the two approaches, MM and PFTLS, and find that the results are very close in quantity and should be the same in qualitative. In the Sec. 5.1, the curves of the transmission versus incident energy are qualitatively the same, and the difference between the two kinds of curve is smaller as increasing the subband numbers. And in the Sec. 5.2, the wavefunction and the current density patterns are the same, but the quantities are different between these two approaches and it is because the transmission is not saturate in the approach of PFTLS by using 20 subbands. In the final, we can be sure that these two approaches have the same results in this calculation of this model, and each one has its suitable regime for approaching.

Chapter 6

Magnetoconduction in quantum channel with a repulsive barrier
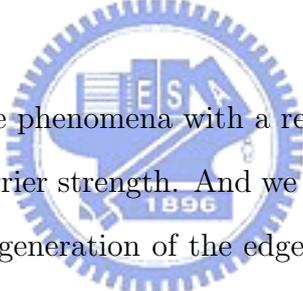
In this chapter, we discuss the phenomena with a repulsive barrier in the wire by tuning the magnetic field and the barrier strength. And we investigate the wavefunction and the current density patterns, the generation of the edge states and the edge state resonance above each subband bottom but the first subband.

6.1 Tuning of the magnetic field

In the Fig. 6.1 and Fig. 6.2 we plot the transmission of the first subband and second subband as a function of incident energy for various amplitudes of magnetic field from $0.0B^*$ to $2.0B^*$ and the strength of the repulsive had be fixed to 1.0. In these figures, we find that the curves of transmission has valley structures above each subband bottoms but the first one. In the Fig. 6.1, there is one valley above $X = 2$ for each curve, and in the range of the energy above $X = 3$, the curves have two valleys in the larger magnetic field, $e.g.$ $B > 1.2B^*$. And in the Fig. 6.2, in the range of the energy above $X = 2$, the curves have one valley when $B > 0.6B^*$; in the range of the energy above $X = 3$, each curve has one valley at least here and has two valley as $B > 1.6B^*$. The valley structure are

Figure 6.1: The transmission versus the incident energy and incident from the first subband for various amplitudes of the magnetic field form $0.0B^*$ to $2.0B^*$ and the strength of the repulsive barrier is $V_0 = 1.0E^*$. The dips structure happen above $X = 2$ and $X = 3$

the resonance of the edge states on the transverse direction near the barrier and we will discuss the valleys in detail in the section 6.3 with the wavefunction and current density patterns.

6.2   Tuning of the barrier strength

In the Fig. 6.3, the valley structures become stronger as increasing of the strength of the repulsive barrier, and we can see the two valleys above $X = 3$ become more clear when the strength of the magnetic field is larger. It is because the strength of the valleys depend on the amplitude of the overlap between the subbands and the impurity barrier, the more of the barrier potential, the larger of the valley profiles.
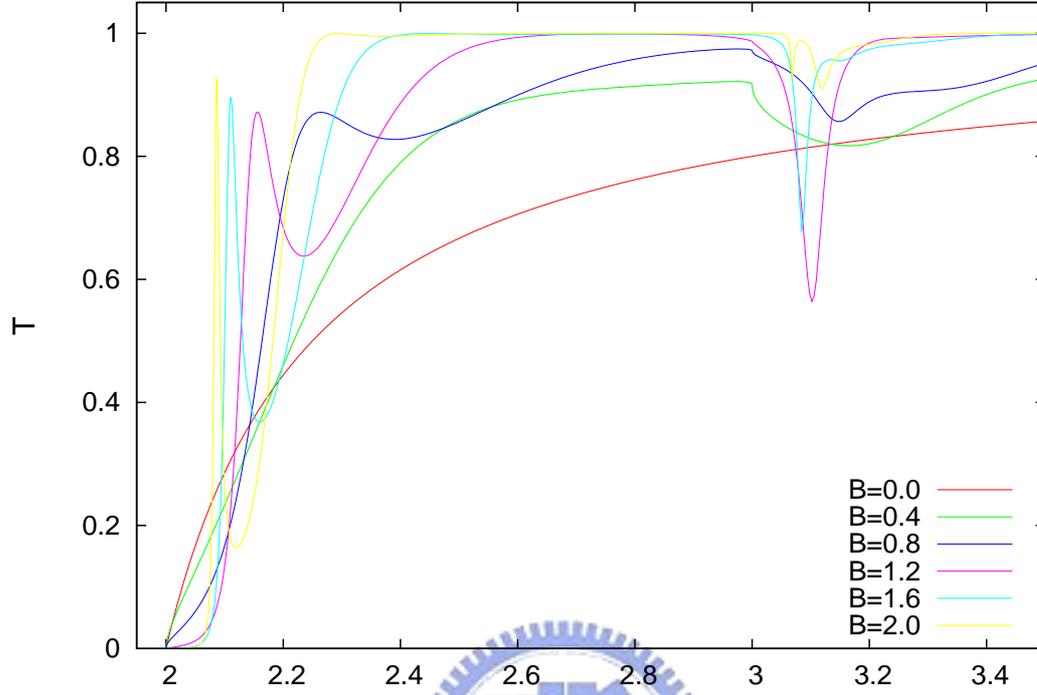
Figure 6.2: The transmission versus the incident energy and incident from the second subband for various amplitudes of the magnetic field form $0.0B^*$ to $2.0B^*$ and the strength of the repulsive barrier is $V_0 = 1.0E^*$. The valleys structures happen just above the integral X

6.3 Analyses of numerical results and physical interpretations

In the Fig. 6.4, we plot the total wavefunction and the current density patterns which we can see the edge states clearly in the wire of the repulsive barrier is 20, which is really strong and the transmission is almost zero, the amplitude of the magnetic field is $B = 1.0B^*$, and the incident energy is $X = 1.7$ and incident from the first subband. And the magnetic length is $1.0a^*$, and the cyclotron radius is $2.8a^*$ in this case. In the figure of the transport particle current density, the electrons are seen to describe the edge state current along the edge of the wire, the edge states is clearly generated in the Fig. 6.4; we are in the quantum Hall regime. The particle current density flow into the wire on the topside form the left side, and almost total reflect to the left on the underside of the
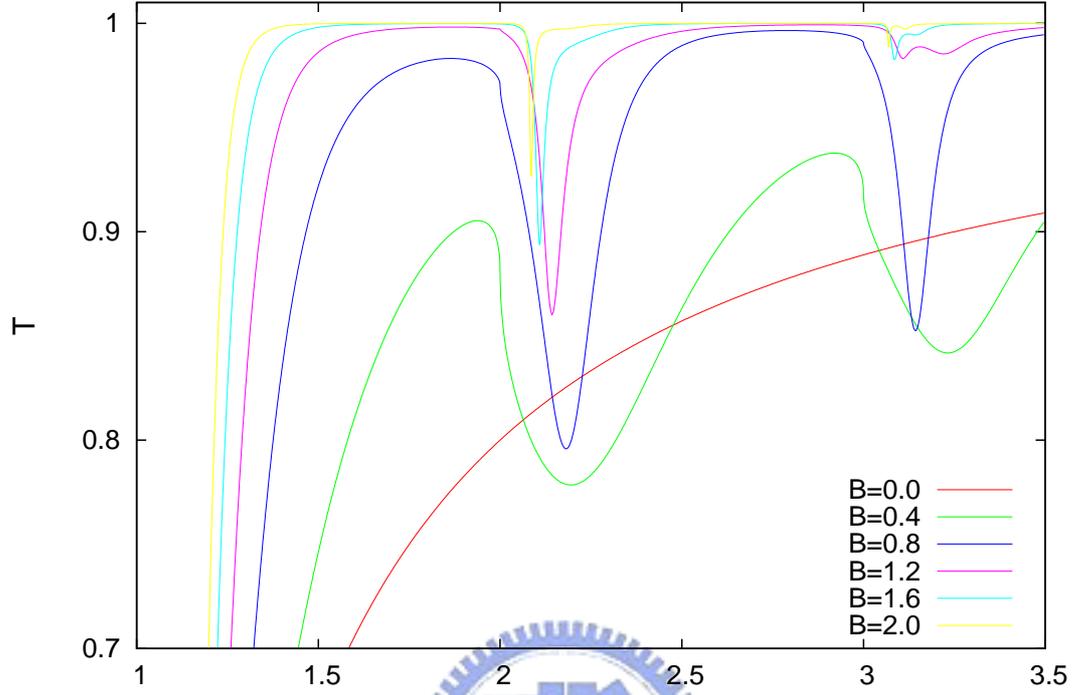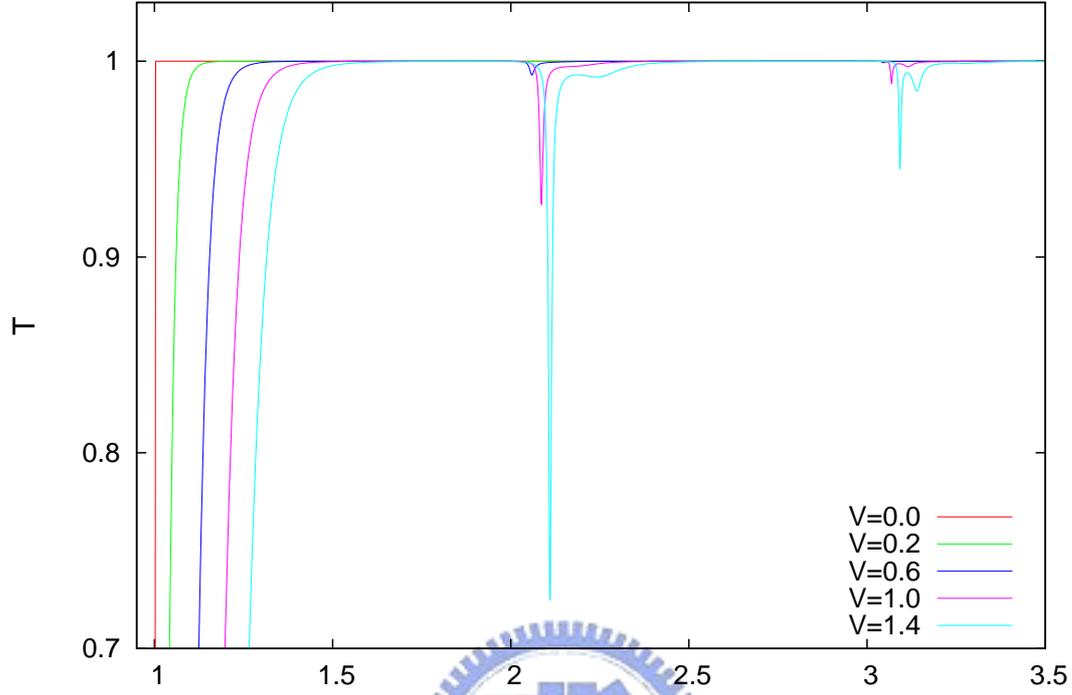
Figure 6.3:   The transmission versus the incident energy and incident from the first
subband for various strength of repulsive barrier from $0.0E^*$ to $1.4E^*$ and the amplitude
of the magnetic field is $2.0B^*$.

wire and before the barrier at $x = 0$. This phenomenon and the path of the edge state

is suitable to the classical picture that the charged particle move on the edge when it is

applied a large magnetic field.

In the Fig. 6.5, Fig. 6.6, and Fig. 6.7, we plot the wavefunction and the current density

patterns of the strength of repulsive barrier is $V_0 = 1.0E^*$, the amplitude of the magnetic

field is $0.5B^*$ and the magnetic length is $l_B = 1.41a^*$, the the incident wave come form

the first subband which the incident energy is $X = 1.8$, $X = 2.2$, and $X = 2.8$ in the

three figures in sequence. And the cyclotron radius are $r_c = 5.98a^*$, $r_c = 7.33a^*$ and

$r_c = 8.97a^*$ in the three figures. The small curve on the right of the top of each figure is

the transmission versus the incident energy and the wave incident from the first subband.

We want to find out the reason why there is a resonance valley near $X = 2.2$ in the

curve of transmission. In the Fig. 6.5, the edge state had generated and come from the left

to the right side in the upside of the wire, and the current has interference with the other
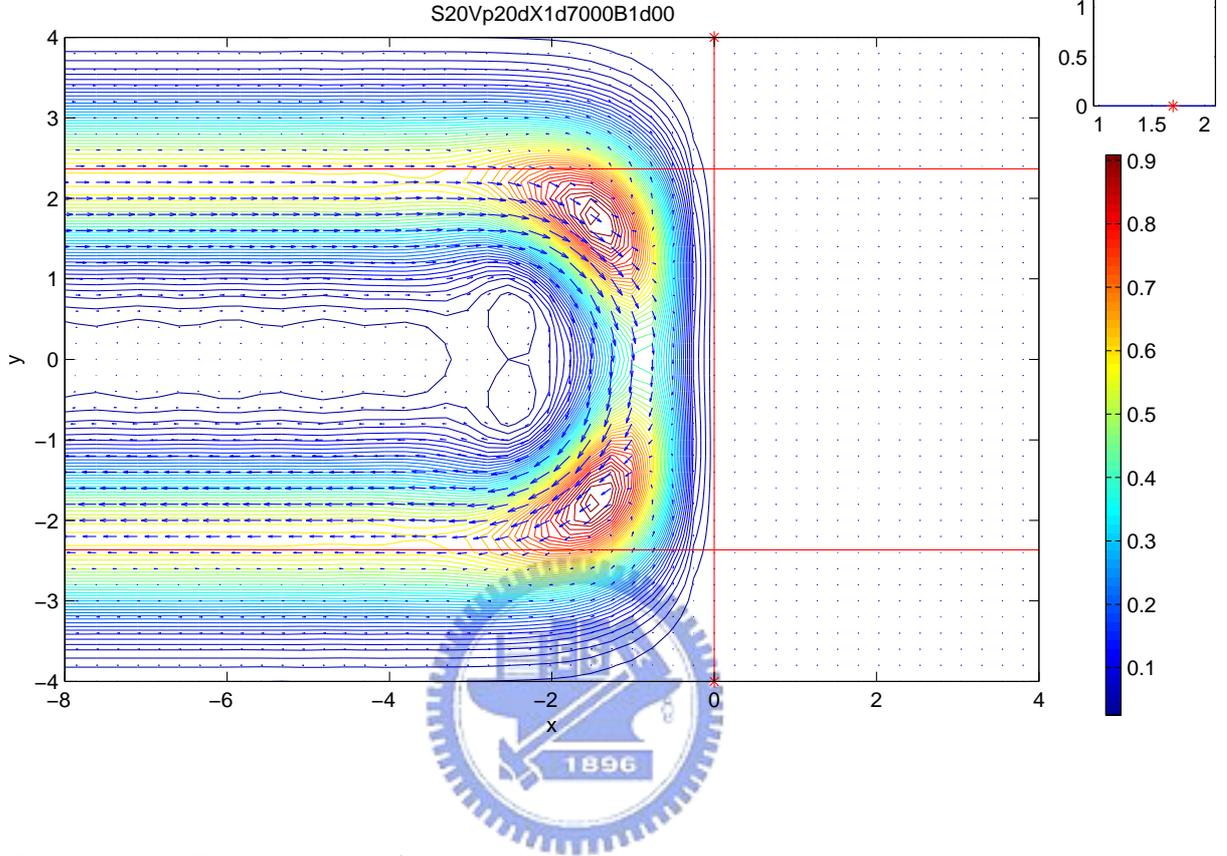
Figure 6.4: The total wavefunction and the current density patterns in the wire with a strong repulsive barrier $V_0 = 20E^*$, the amplitude of the magnetic field is $1.0B^*$, and the incident energy is $X = 1.7$ from the first subband.

edge state on the underside of the wire. We don't think the edge strongly interact with the evanescent modes because the amplitude of the evanescent mode is two order smaller then the propagating mode. In the Fig. 6.6, the incident energy is $X = 2.2$ and there is a valley on the transmission here. We can find that the propagating mode interact with the second propagating mode and have back scattering in both first and second propagating modes. And in the Fig. 6.7, the incident energy is $X = 2.8$ which is the highest one of these three figures. The first propagating mode had shift to the edge, and the center shift of the second propagating mode is also larger then the shift in Fig. 6.6. The interference of each propagating mode itself or between each other is small and have less back reflection.

We find that the resonance valley near $X = 2.2$ is a resonance with the propagating

66

Figure 6.5: Top: The total wavefunction and the current density patterns of the strength of the repulsive barrier is $V_0 = 1.0E^*$, the amplitude of magnetic field is $B = 0.5B^*$, and the incident energy is $X = 1.8$ from the first subband; Left of bottom: The wavefunction and the current density components of the first subband; Right of bottom: The wavefunction and the current density components of the second subband.

modes themselves but not have much interference with the evanescent modes because

we can see the amplitude of the evanescent mode is not very large. In order to have

Figure 6.6: Top: The total wavefunction and the current density patterns of the strength of the repulsive barrier is $V_0 = 1.0E^*$, the amplitude of magnetic field is $B = 0.5B^*$, and the incident energy is $X = 2.2$ from the first subband; Left of bottom: The wavefunction and the current density components of the first subband; Right of bottom: The wavefunction and the current density components of the second subband.

the resonance, the shifted wavefunction of propagating modes must have some overlap to

each other and then the resonance can have interference between each other. Due to the
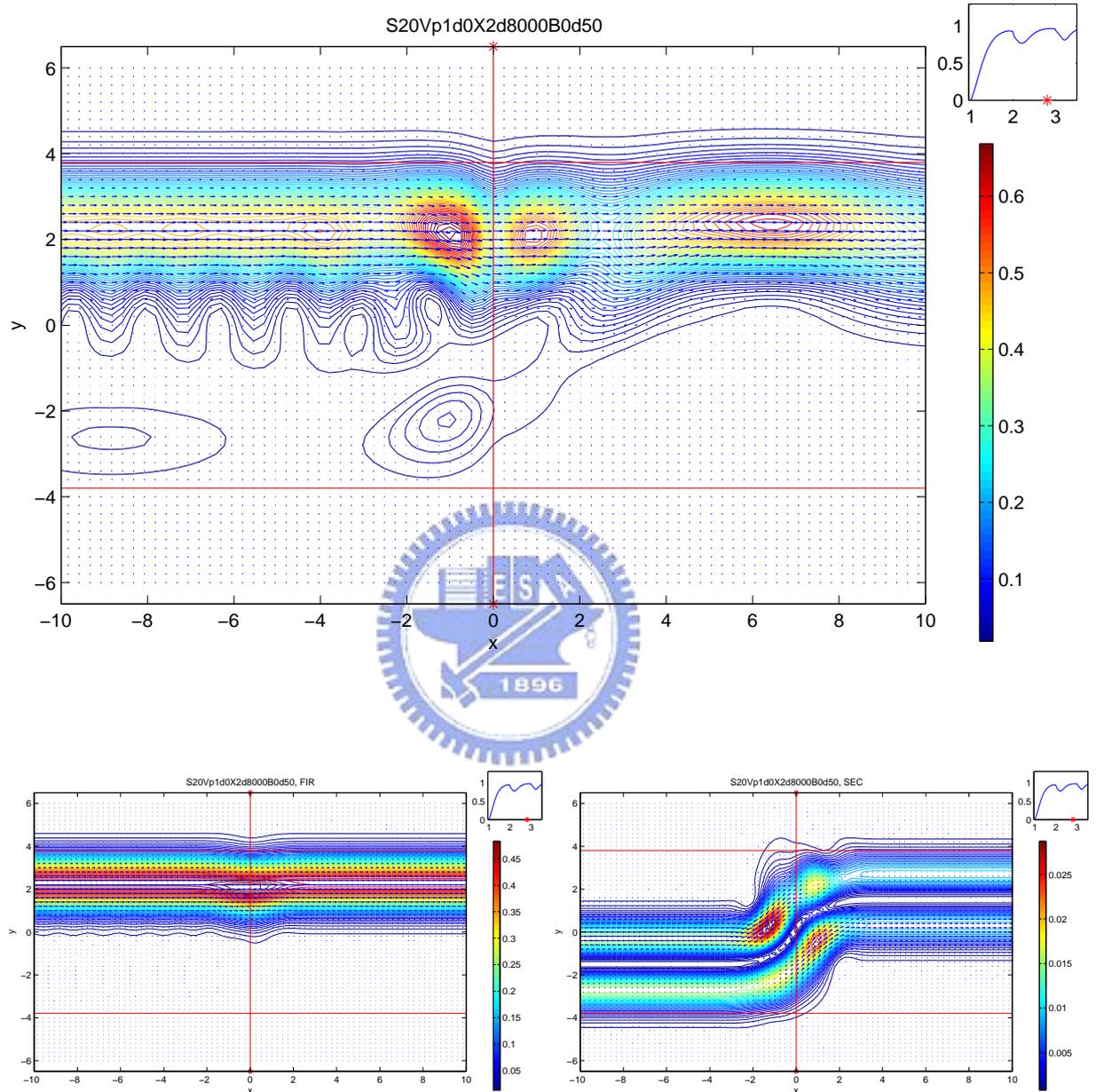
Figure 6.7: Top: The total wavefunction and the current density patterns of the strength
of the repulsive barrier is $V_0 = 1.0E^*$, the amplitude of magnetic field is $B = 0.5B^*$,
and the incident energy is $X = 2.8$ from the first subband; Left of bottom: The wave-
function and the current density components of the first subband; Right of bottom: The
wavefunction and the current density components of the second subband.

necessary overlap of each wavefunction, the resonance easier happen at the energy which

is a little large then each subband bottom.

This kind of resonance is very different with the resonance of the finite range potential. The resonance of the finite range potential is that one propagating mode has interference with itself and depend on the phase of the path difference, this kind of resonance could be a large one; but the edge state resonance is due to the interference of the propagating modes which are always not only one propagating mode, and the resonances are not a large one. And another specially character of the edge state resonance could be generated for a δ-type potential which is a localized potential on the longitudinal direction. That is never happened for a coordinate resonance without magnetic field.

And then we also plot the wavefunction and the current density patterns in Fig. 6.8 of the case of strength of repulsive barrier is $V_0 = 1.0E^*$ and the amplitude of magnetic field is 0.5, like the parameter of the three figures Fig. 6.5, Fig. 6.6, and Fig. 6.7. But change the incident energy and incident subband to the second propagating mode. In the Fig. 6.8, the incident energy is $X = 2.2$ and the cyclotron radius is $r_c = 2.99a^*$. The physical insight is similar to the above discuss, but in this figure we can easily see the particle current cycle and the diameter of the cycle is match to the magnetic length and the cyclotron radio (but the cyclotron radius is a radius) in order.

6.4 Summary

In this chapter, we find that the resonance valleys is according to the interference of the propagating modes themselves and not only one propagating mode. In order to have the resonance and the interference between different propagating modes, the shift wavefunction must have some overlap to each other and the impurity potential. Because our potential barrier is uniform of the transverse direction, the more strength of the impurity potential, the larger of the overlap. Sometimes, the wavefunction have not only one peak or one node, due to the overlap of the wavefunctions, they may have two or more valleys on the transmission. Besides, Due to the necessary overlap between each subbands, the resonance easier happen at the energy which is a little larger then each
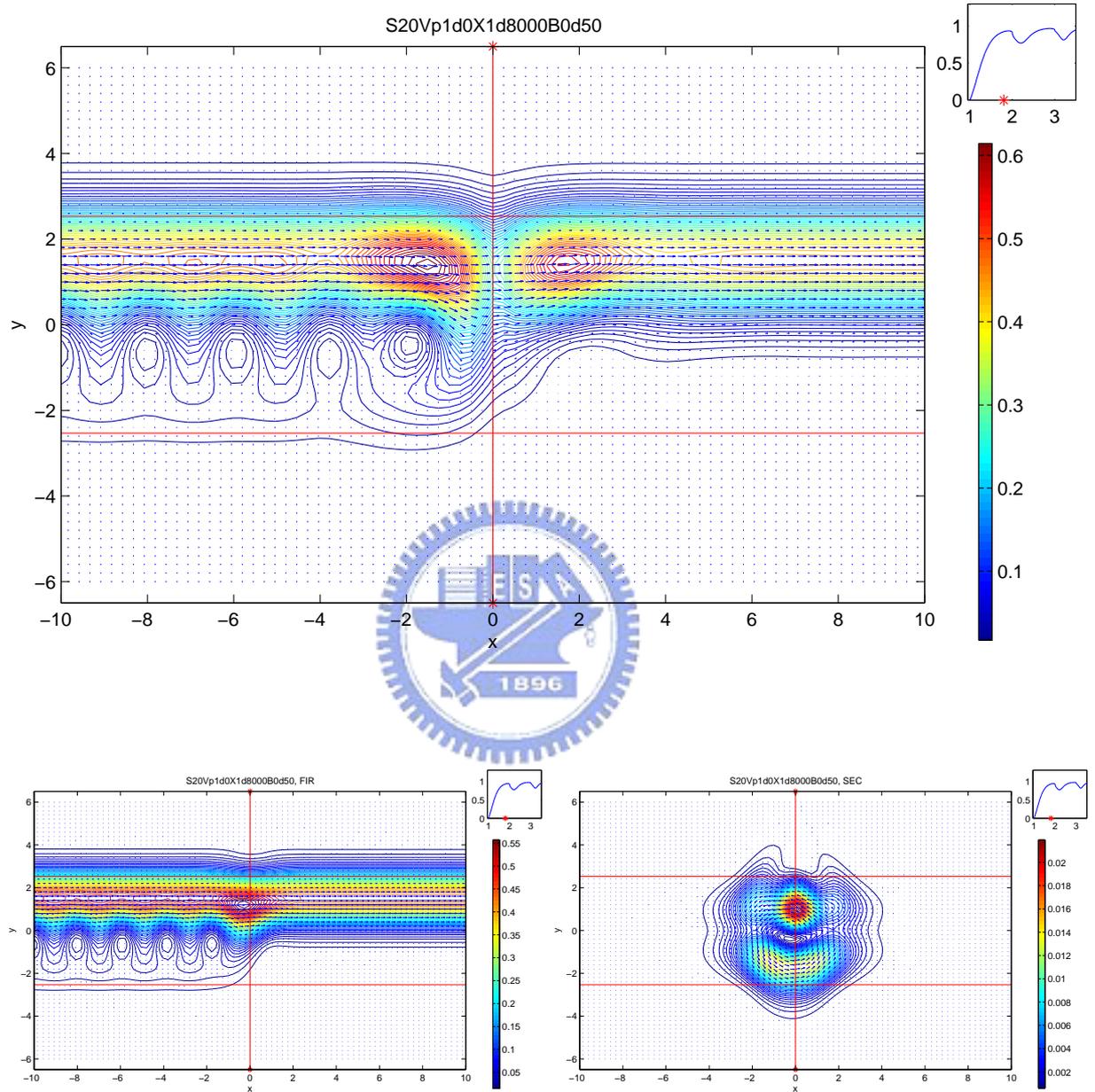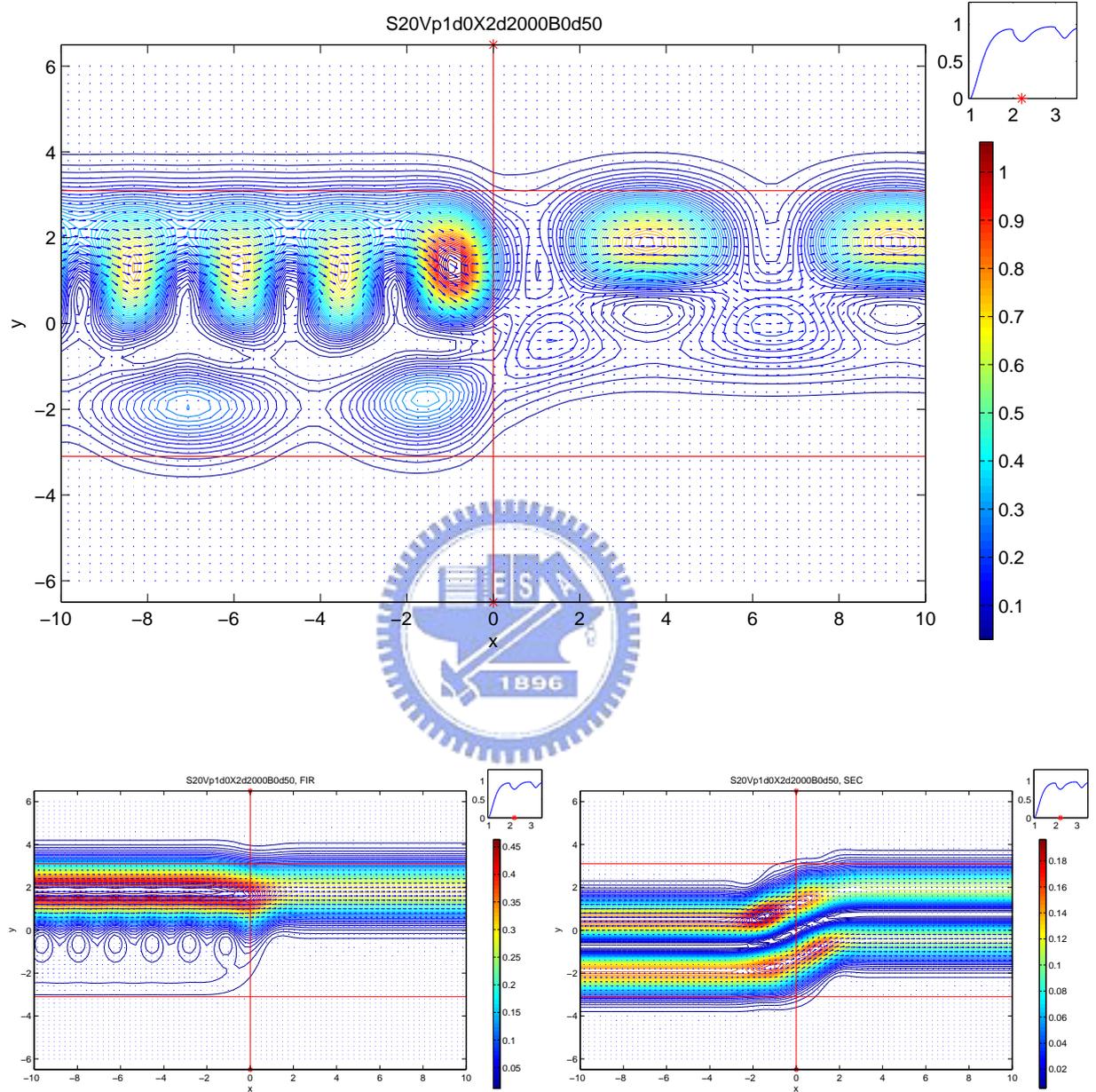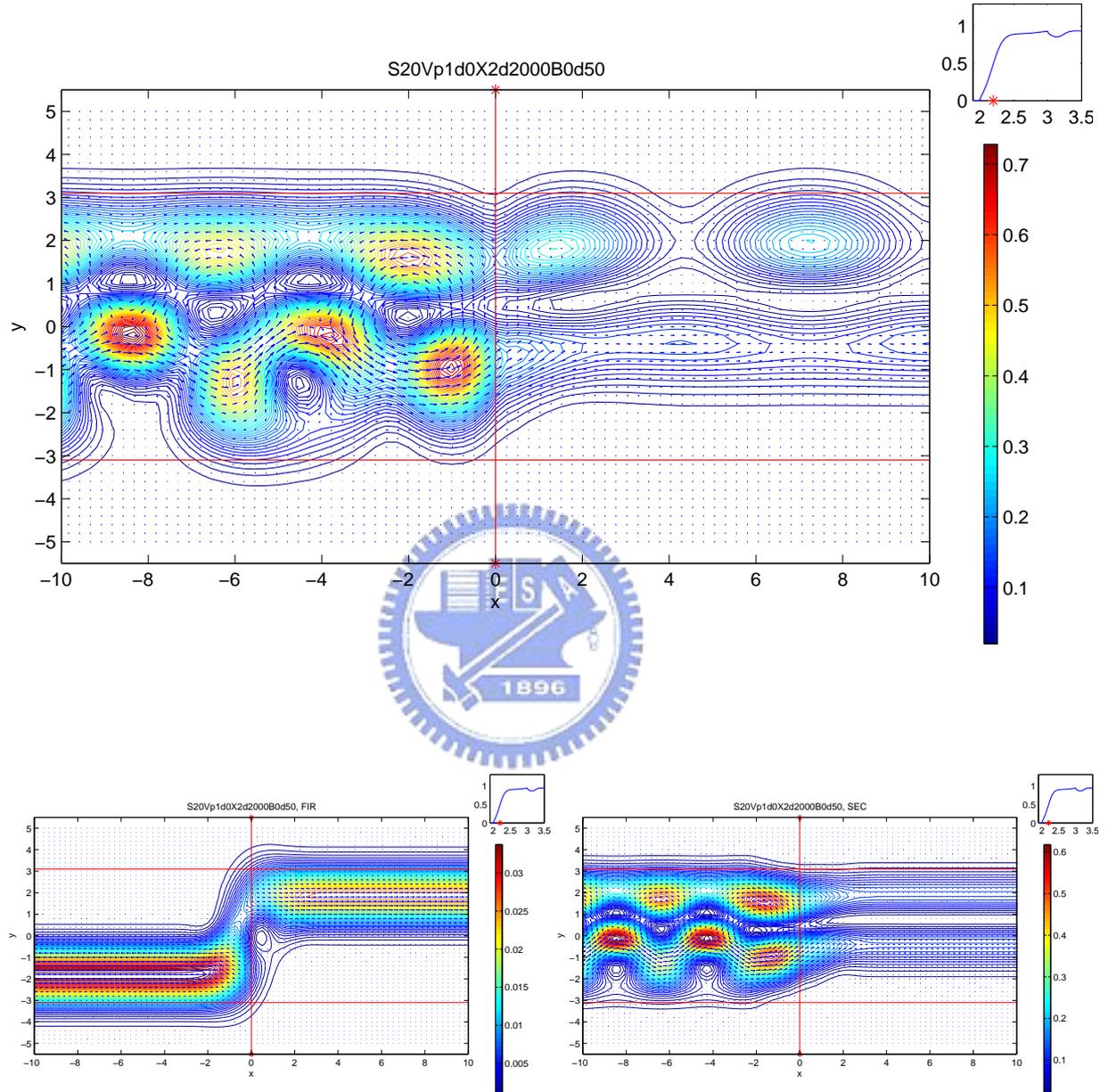
Figure 6.8:   Top: The total wavefunction and the current density patterns of the strength
of the repulsive barrier is 1.0, the amplitude of magnetic field is 0.5, and the incident energy
is $X = 2.2$ and incident from the second subband; Left of bottom: The wavefunction and
the current density components of the first subband; Right of bottom: The wavefunction
and the current density components of the second subband.

subband bottom. In other words, they should have a wavefunction with small kinetic

energy or small cyclotron radius to be the media to mix the propagating modes together.

This kind of resonance will not happen above the first subband bottom, because there is only one propagating mode here.

This kind of resonance is very different between the resonances due to the multiple scattering in a final range of potential. The resonance of the multiple scattering of a final range potential is that one propagating mode has interference with itself and depend on the phase difference of the multiple scattering and the position difference; this kind of resonance could be a large one. The edge state resonance is due to the interference or the overlap of different propagating modes and the impurity potential, the amplitude of the overlap are often small and the resonance will not be a large one.

And another specially character of the edge state resonance could be generated for a δ-type potential which is a localized potential on the longitudinal direction. The edge state resonance is a kind of resonance on the transverse direction, and differ with the resonance on the longitudinal direction without magnetic field. The physical insight is close to the classical picture, which the edge states mean the charged particle move along the edge and the potential barrier when it is applied a magnetic field. When the edge state move along the potential barrier, there are two boundaries which are the edge of the wire around the edge states, and the edge states can have the resonance between the edge of the wire on the transverse direction.

Chapter 7

Magnetoconduction in quantum channel with an attractive barrier

We discuss the phenomena with an attractive barrier in the wire by tuning the magnetic field and the barrier strength in this chapter. And we will investigate the effective strength of the impurity barrier with the applied magnetic field, the two quasi-bound states of the evanescent modes in pair caused from the complex property of eigen-function, and we also compare the magnetic length and the cyclotron radius with the classical width of the wire.

7.1 Tuning of the magnetic field

In the Fig. 7.1, we plot the transmission as a function of X for various B and fix $V_0 = -1.0E^*$. And in the Fig. 7.2, we change the amplitude of the applied magnetic field from $0.0B^*$ to $5.0B^*$ and mark the position in energy of the dip structures, and the strength of the impurity barrier is $-1.0E^*$ in (a) and $-1.4E^*$ in (b).

In the first curve of the Fig. 7.1(a), because the impurity barrier is uniform on the transverse direction, the system should be symmetry without magnetic field and could be reduced to a one dimension problem which $T \sim \frac{1}{1-2V_0/ik}$, and there are not subband

Figure 7.1: The transmission versus the incident for various amplitudes of magnetic field
from 0.0 to 2.0, and the strength of the impurity barrier is 1.0.

transition between each subbands.

As we apply the magnetic field to $B = 0.2B^*$, there is a fano profile happened suddenly at $X = 1.79$. And then we increase the amplitude of magnetic field to $0.4B^*$, the fano has a blue shift to the higher energy at $X = 1.85$. we can find that the first dips move to the higher energy when we increase the applied magnetic field till $B = 0.8B^*$(which is figured in the Fig. 7.2), and the fano become more and more sharp. As we increase the amplitude of magnetic field to $0.6B^*$, the second dip appear below the subband bottom of the second subband. The larger of the magnetic field, the second dips have red shift to the lower energy till $B > 2.8B^*$.

And then we trace out the relation of the energy of the first two dips and the amplitude of the applied magnetic field. In the Fig. 7.2, we and find that in the small magnetic field regime, the first dips move to the higher energy and the second dips move the the lower energy. As increasing the amplitude of magnetic field, the two dips mix together and the minimum of the transmission of the dips will not touch zero in the regime of the magnetic filed near $0.7B^*$; the Fano structures is gone in this regime. And in the high magnetic field regime, the third and the fourth dips appear below the bottom of second subband. As long as the magnetic field is large enough, the fifth and sixth dips or the 7-th and 8-th dips will be appear.

And in the Fig. 7.2, we find that the larger of the applied magnetic field, the smaller of the energy difference of the first two dips, and in the high magnetic field regime, the first two dip degenerate into together.

7.2 Tuning of the barrier strength

In the Fig. 7.3 and 7.4, we fix the amplitudes of the magnetic field of these two figures to $0.2B^*$ and $1.0B^*$, and plot the transmission as a function of X for various V_0 from $0.0E^*$ to $-1.4E^*$.

We find that the energy of the dip structures move to the lower energy as the strength
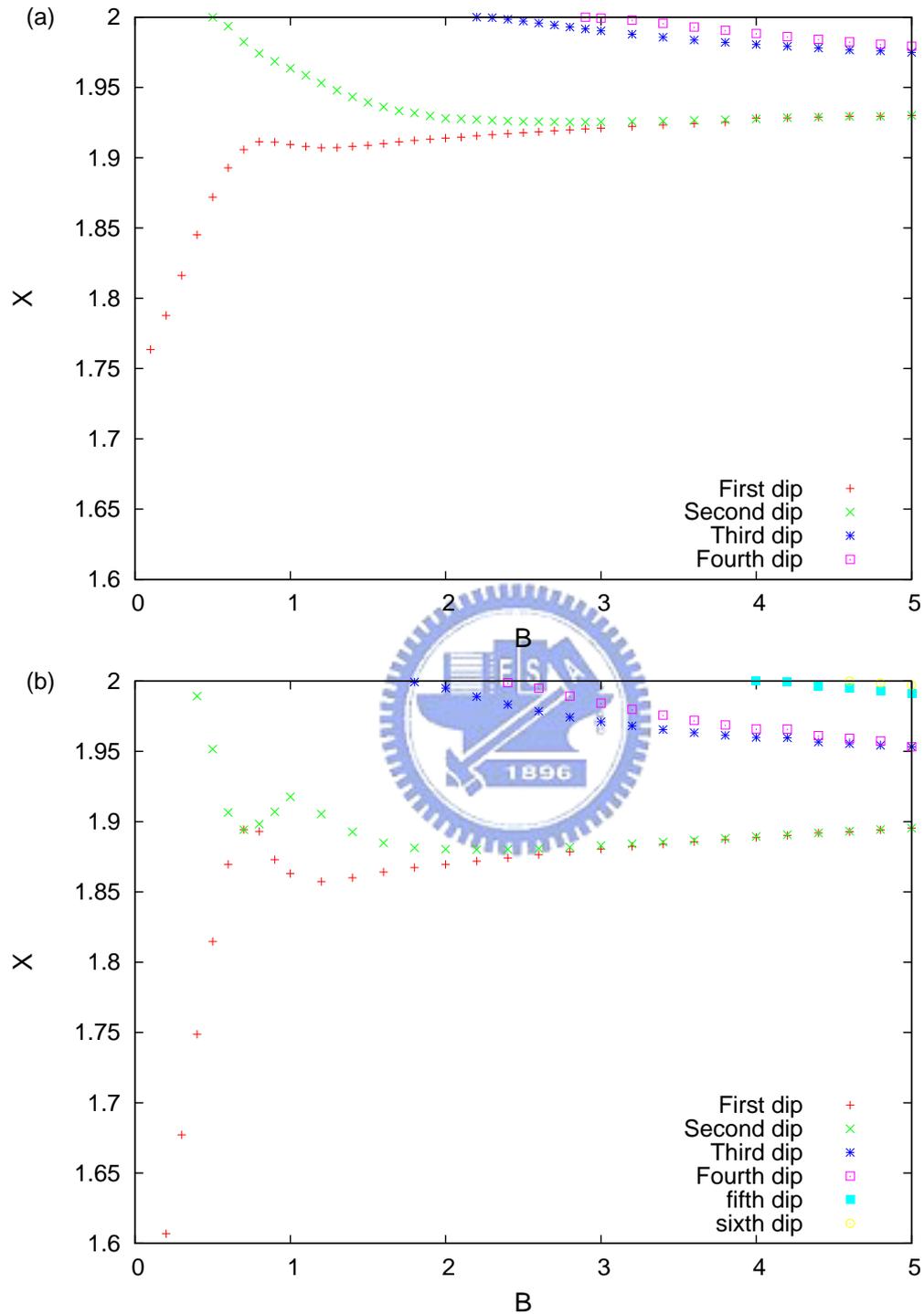
Figure 7.2: The position in energy X of the dip structure in the transmission curve versus
the amplitude of magnetic field; the strength of the impurity barrier is $1.0E^*$ in (a) and
$1.4E^*$ in (b).

of the attractive barrier become larger. In the Fig. 7.3, we find that the energy spacing

between one and the next data is getting larger when we increase the strength of the
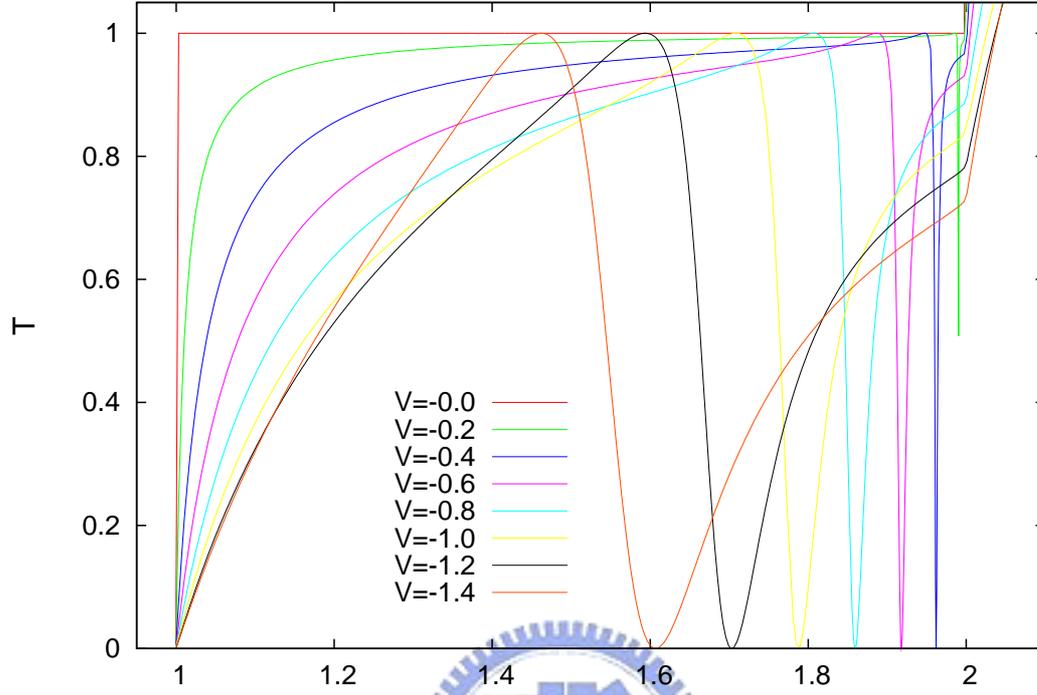
Figure 7.3: The transmission as a function of X for various strength of impurity barrier
from 0.0 to $-2.0E^*$. The magnetic field is $0.2B^*$.

impurity barrier, but in the Fig. 7.4, the difference of the energy spacing does not change
so obviously. The energy spacings or the position of the dips have fewer dependence in
the higher magnetic field regime.

In the regime of low magnetic field, the edge states are not generated and the wave-
function is spread in the center of the wire. The effective impurity potential should be
proportional to the impurity barrier in the wire below the Fermi energy. In the Fig. 7.5,
we define δE is the energy difference between the first dips and the subband bottom of
second mode, and we find that the slope of the curve approach to 0.5 as the magnetic
field approach to $0.0B^*$, which mean that the relation of the δE and the strength of the
impurity barrier is $V_0 \propto \sqrt{\delta E}$ or $\delta E \propto V_0^2$ in the small magnetic field regime. In the
regime of high magnetic field, the edge states are generated and shift to the edge of the
wire. In this situation, the transport of the two dimensional problem can be reduced to a
one dimensional like problem, and the electrons moving in the wire only see the barrier in
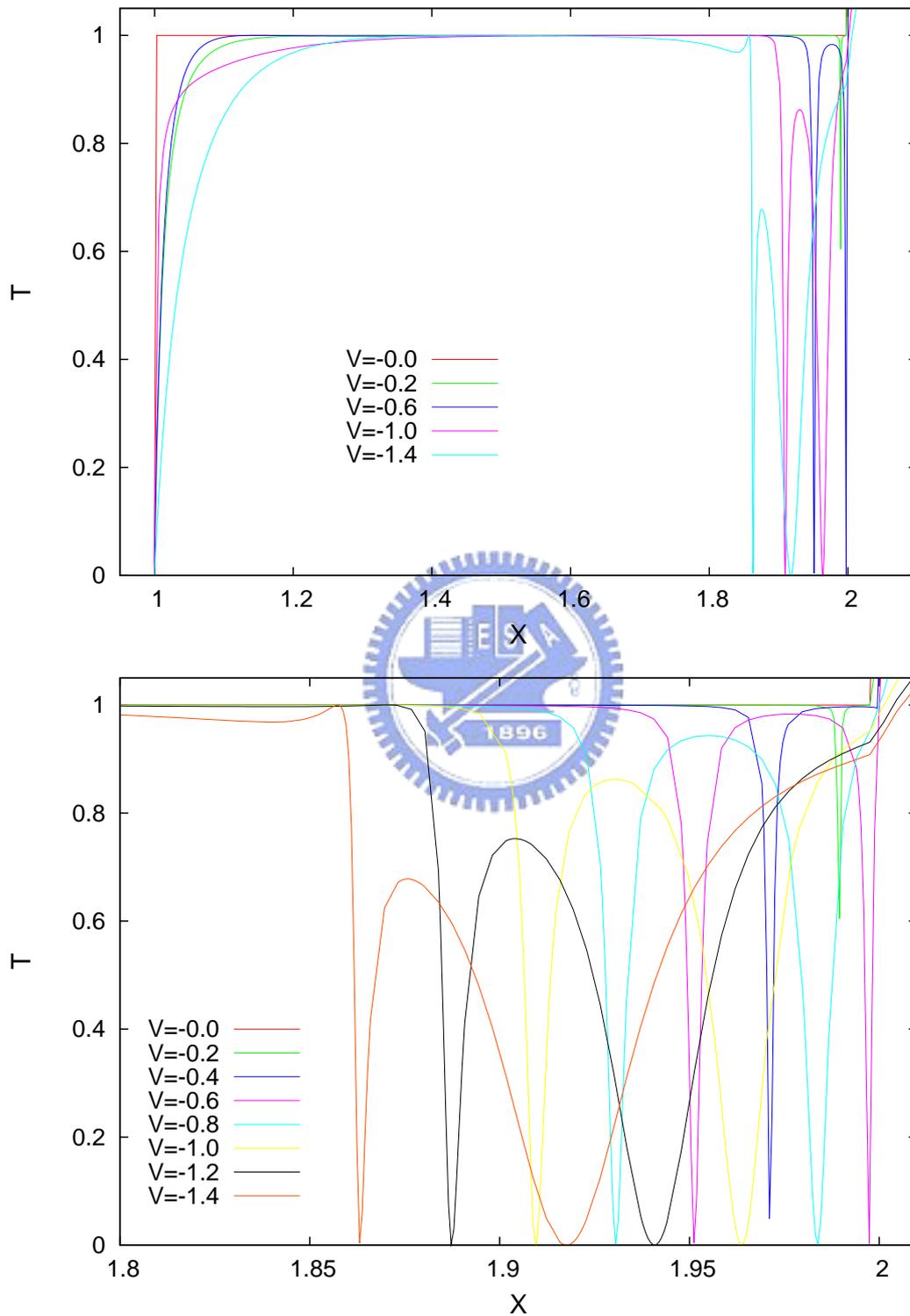
Figure 7.4: The transmission as a function of X for various strength of impurity barrier from 0.0 to $-2.0E^*$. The magnetic field is $1.0B^*$. Plotting Fig(a) again of energy range at 1.7 to 2.1 in Fig(b).
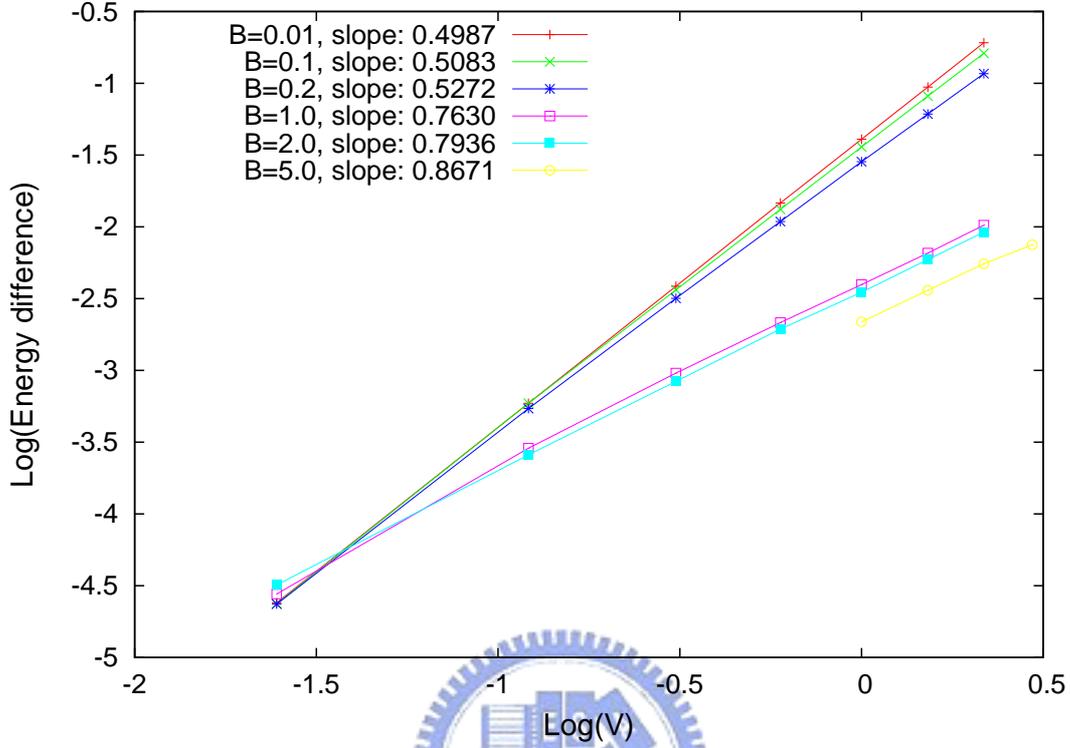
Figure 7.5: The relation of the position of the first dips with V_0.

the edge regime which is a small area. And the effective impurity potential is no longer the barrier in the wire and below the fermi energy, but the part of the edge regime, the effective strength of the effective impurity potential will be proportional to the strength of the impurity barrier more linearly.

7.3 Analyses of numerical results and physical interpretations

In the Figs.7.6 - 7.10, we plot the wavefunction and the current density patterns of the first two dips for $V_0 = 1.4E^*$ and the amplitude of the magnetic field is $0.4B^*$, $0.7B^*$, and $1.0B^*$ correspondingly, which the first two dips have mixed together at $B = 0.7B^*$.

We first determine the generation of the edge states depend on the amplitude of the magnetic field. In the Fig. 7.6 and 7.7, the applied magnetic fields are both $0.4B^*$ and the magnetic length is $l_B = 1.58a^*$ and the cyclotron radius are 7.23 and 8.31 in the two
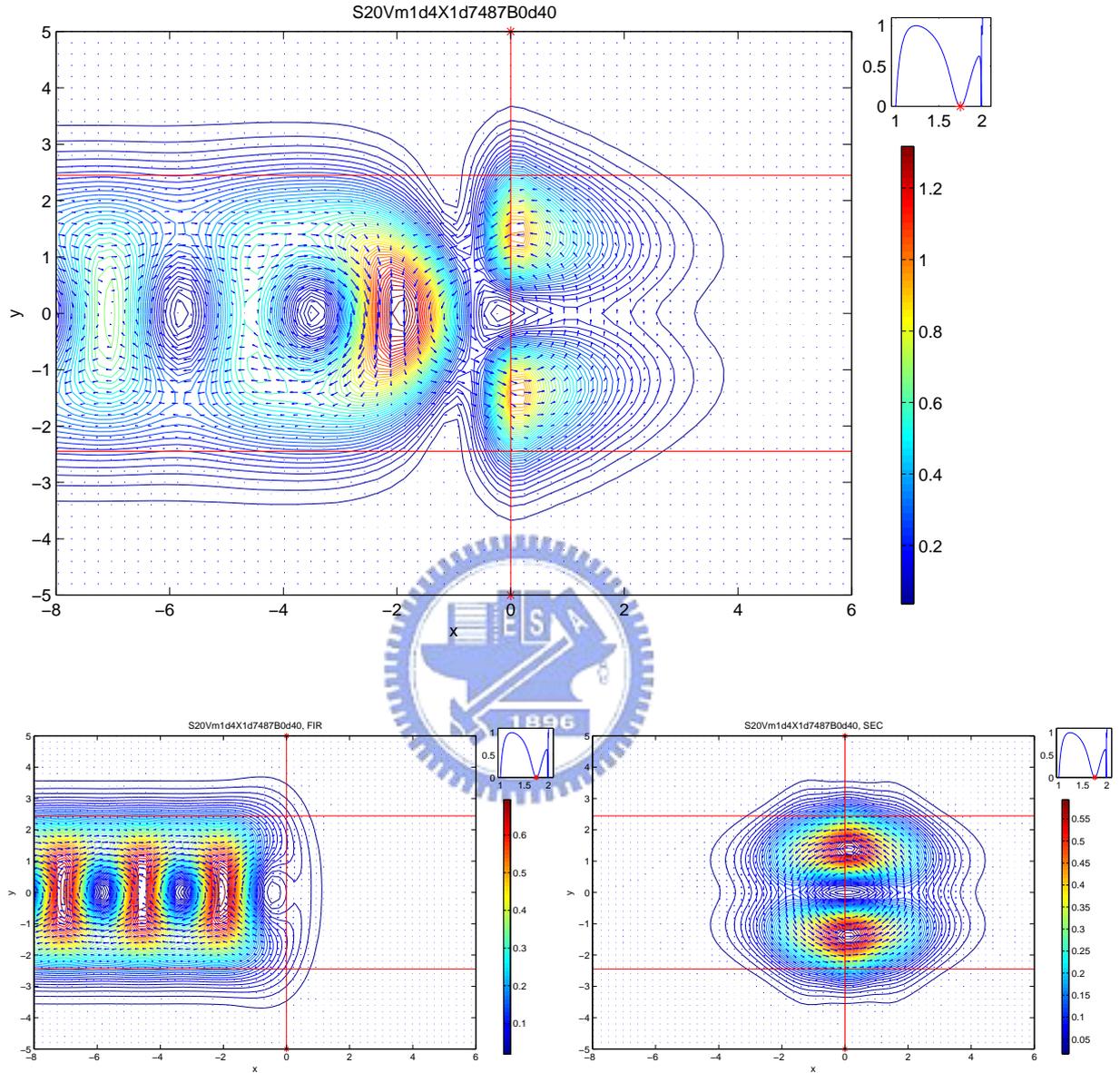
Figure 7.6: The wavefunction and the current density patterns at the first dip with $B = 0.4$, Top: the total wavefunction and current density patterns in the wire; Left of bottom: the contribution of the propagating mode; Right of bottom: the contribution of the evanescent mode.

figures. The cyclotron are both larger then the classical width of the wire, which are $r_c = 4.89a^*$ and $r_c = 5.62a^*$. And we can also see the figures, the interference between the upside and downside edge states is still viewable in the center part of the wire, and the edge states are not clearly generated. And in the Fig. 7.8, the amplitude of the applied
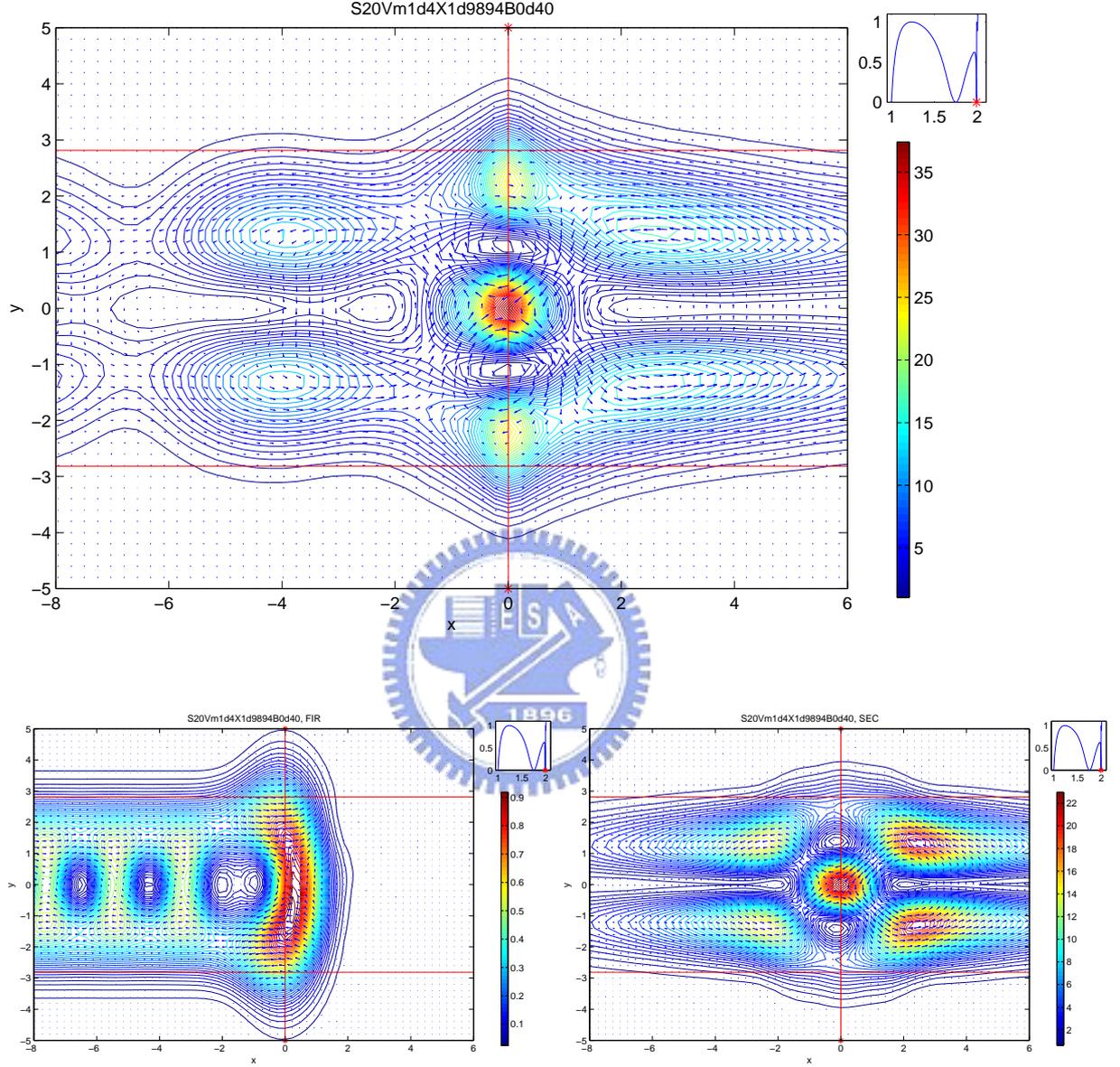
Figure 7.7: The wavefunction and the current density patterns at the second dip with $B = 0.4$, Top: the total wavefunction and current density patterns in the wire; Left of bottom: the contribution of the propagating mode; Right of bottom: the contribution of the evanescent mode.

magnetic field is $0.7B^*$ and the magnetic length is $l_B = 1.20a^*$. The cyclotron radius is $r_c = 4.52a^*$ in this figure and the classical width of the wire is $5.34a^*$. The length scales of cyclotron radius and classical width are more comparable and a little smaller then the case of $B = 0.4B^*$, and we can also see the figure and find that the interference is less
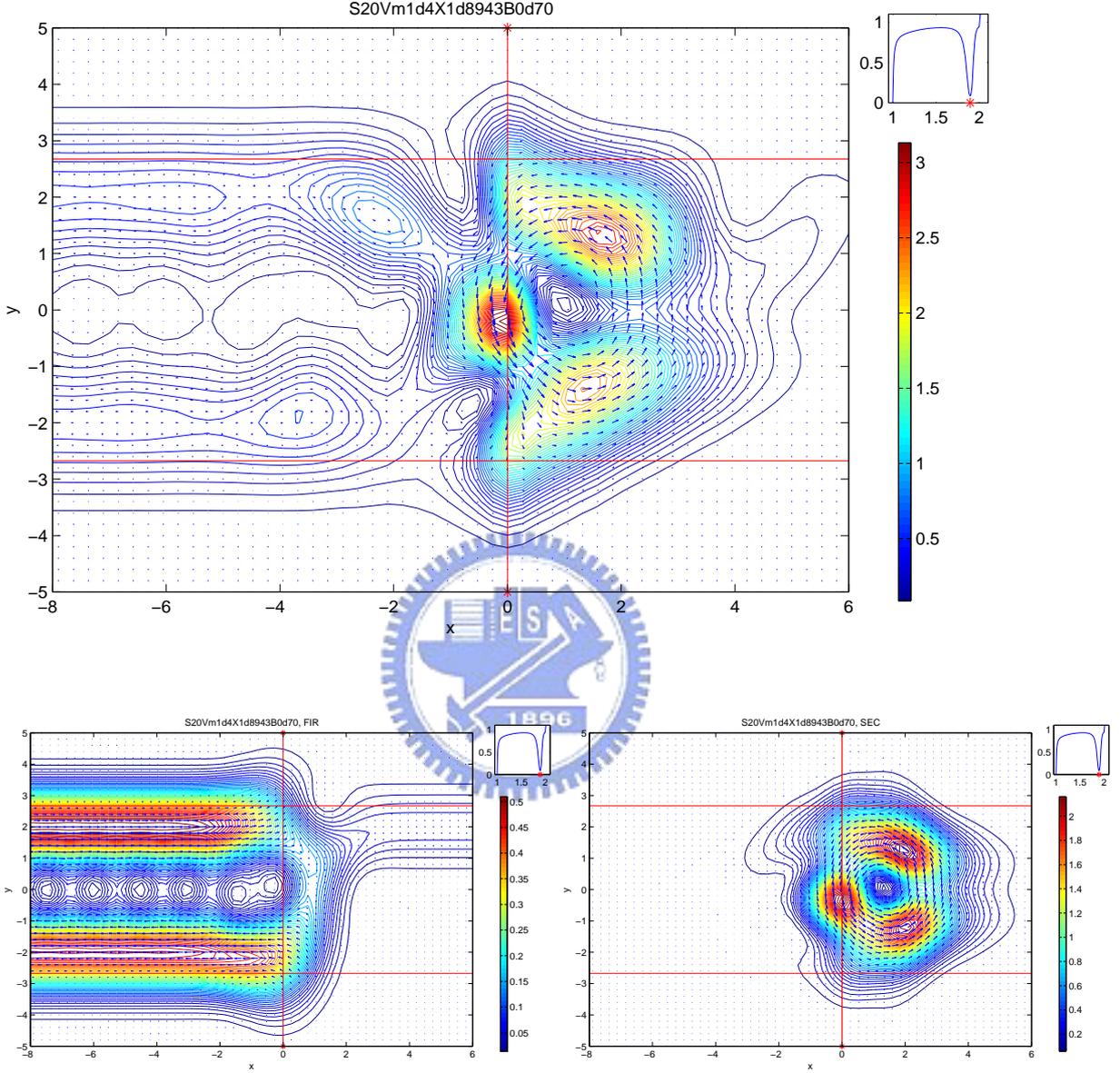
Figure 7.8: The wavefunction and the current density patterns at the dip structure with $B = 0.7$, Top: the total wavefunction and current density patterns in the wire; Left of bottom: the contribution of the propagating mode; Right of bottom: the contribution of the evanescent mode.

in the center part of the wire. The edge states are roughly generated in this magnetic field regime. In the Fig. 7.9 and 7.10, the amplitude of the magnetic field is $B = 1.0B^*$ and the magnetic field is $1.0B^*$ in these two figures. The cyclotron radius are $3.1a^*$ and $3.2a^*$ and the classical width of the wire are $5.26a^*$ and $5.42a^*$, and it is allowed to have
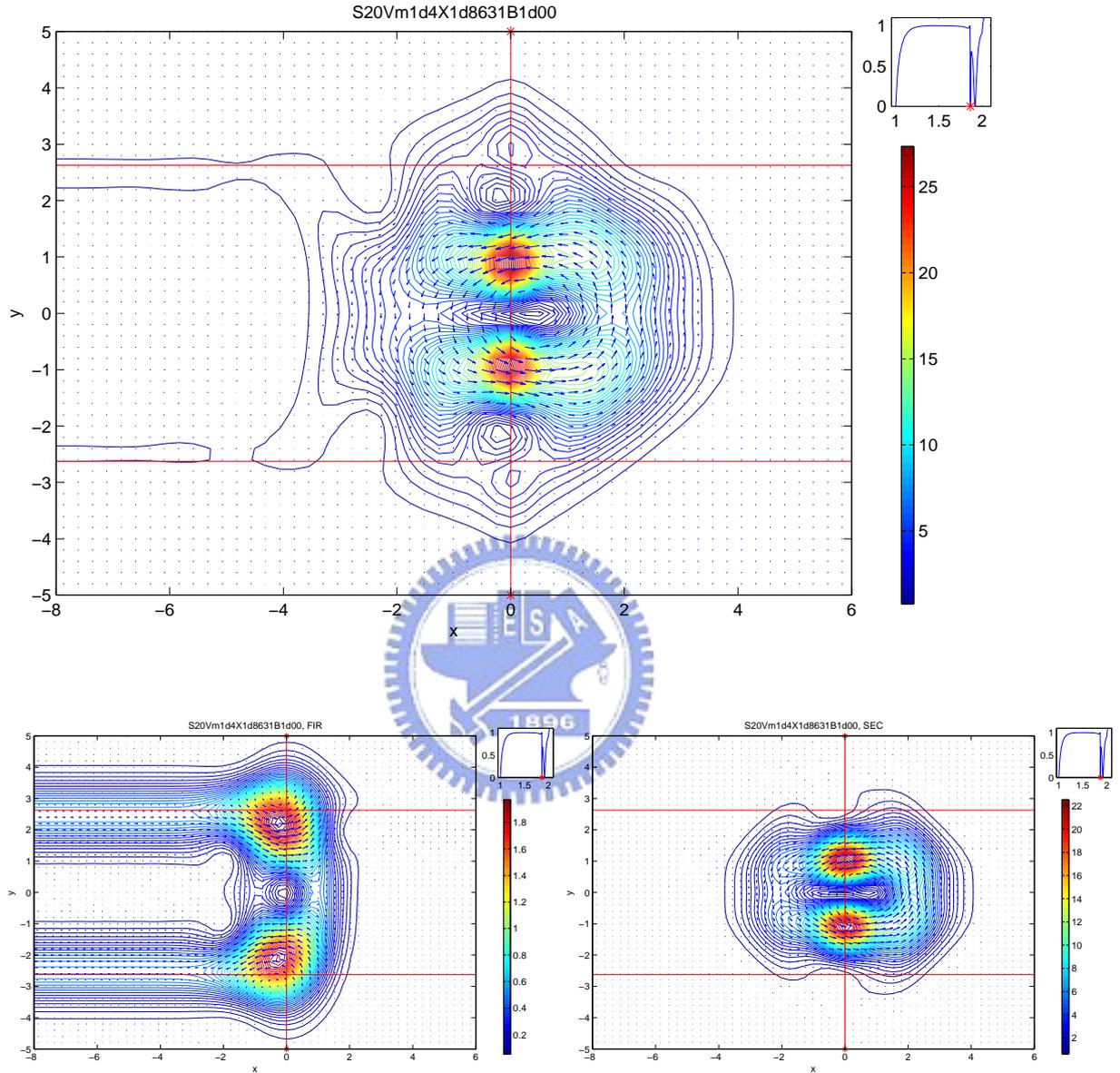
Figure 7.9: The wavefunction and the current density patterns at the first dip with $B = 1.0$, Top: the total wavefunction and current density patterns in the wire; Left of bottom: the contribution of the propagating mode; Right of bottom: the contribution of the evanescent mode.

the skipping orbit current in the wire. The cyclotron radius are smaller then the classical width and we can also see the figures, the amplitude of the interference of the edge states in the center part of the wire is very small and the edge state had been already generated. Due to the comparison, we know that we can compare the cyclotron radius and the width
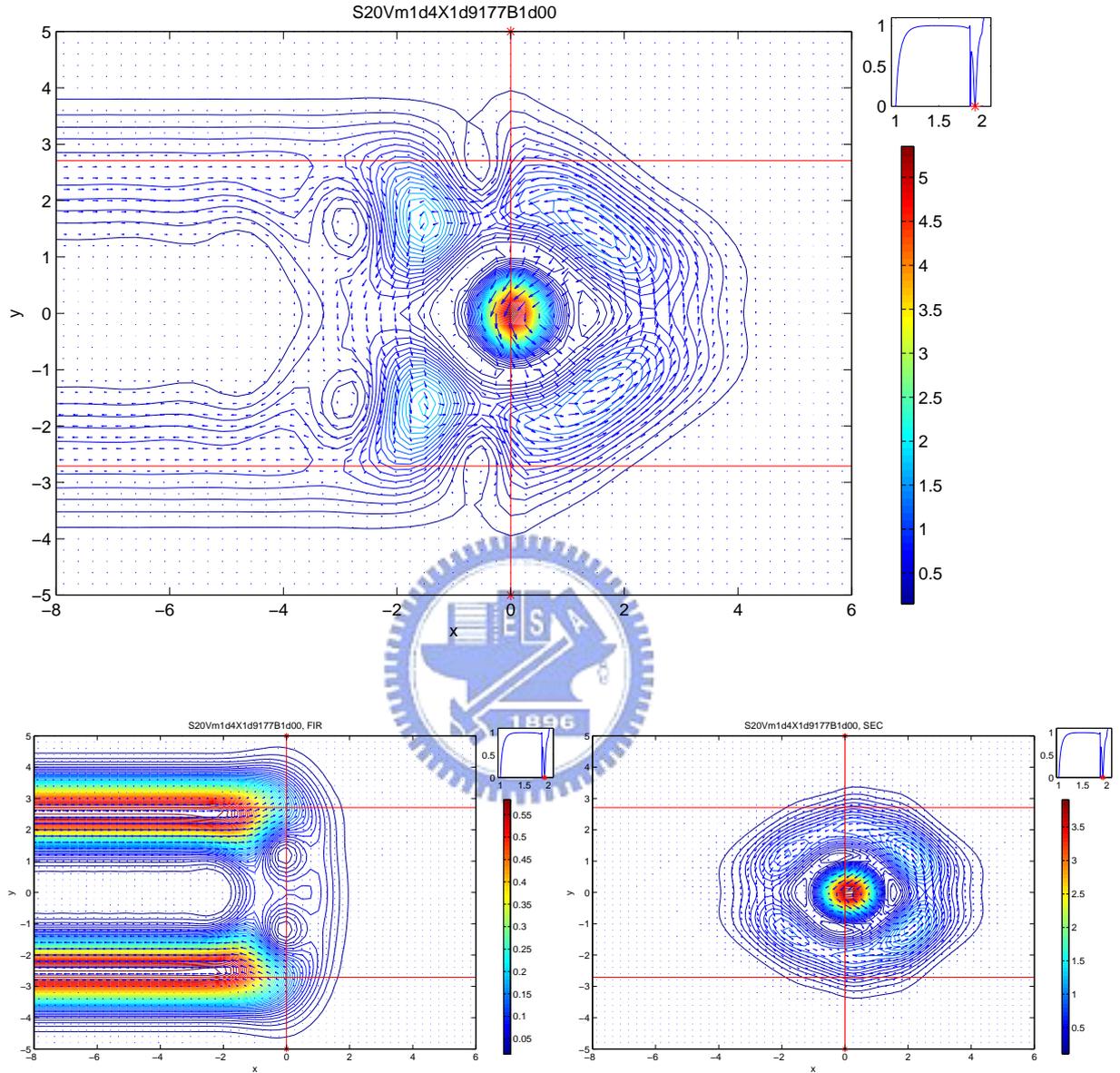
Figure 7.10: The wavefunction and the current density patterns at the second dip with
$B = 1.0$, Top: the total wavefunction and current density patterns in the wire; Left of
bottom: the contribution of the propagating mode; Right of bottom: the contribution of
the evanescent mode.

of the wire to know does the edge states are generated or not, although it is not really

correct and roughly.

In the system with magnetic field, we have two length scales about magnetic interaction

scale, magnetic length and cyclotron radius. Cyclotron radius is more classical-like then

the magnetic length and is better to describe the circular motion due to the Lorenz force. And we can also use the scale, cyclotron radius, to separate the edge states and the traversing states in the Fig. 1.1.

The amplitude of the wavefunction in the Fig. 7.7 is much larger then the other figures, the maximum value is at the center of the x- and y-direction and about 37. The next largest one is the Fig. 7.9, the maximum value is about 27. And the dip structures are also very sharp for these two figures, the wavefunction and the particle are highly attracted in the evanescent mode and be a strong bounding state.

And then we look for the current density patterns. The applied magnetic field in the system is perpendicular to the 2DEG wire and parallel to the $+\hat{z}$ direction. The current density is the particle current and according to the applied magnetic field, the current flow to right on the upside of the wire and flow to left on the downside as the edge states had generated. And we can also find the current density patterns of the bound states move vortically and anticlockwise in substance. Some small structure of the current density pattern between two edge states have opposite current density patterns, that are the interference of the two main edge state current.

In the Fig. 7.2(b), we can find that the point curve of first dips and the second dips have overlap near $B = 7B^*$, and compare to the Fig. 7.2(a), the original properties and reasons of these two dips should be different. In the five figures, Figs.7.6-7.10, the Fig. 7.6, 7.8, and 7.9 are the wavefunctions and the current density patterns of the first dips for various magnetic fields, and the Fig. 7.7, 7.8, and 7.10 are the second dips. Fig. 7.8 is a mixing point and we can look for the other four figures first, it is easy to compare the wavefunction and the figures of the evanescent mode to find that the wavefunction and the current density patterns are very different between the first dips and the second dips. For $x = 0$, we can find that there are even peaks on y-direction in the figures of first dips, and there are odd peaks for the second dips.

In order to discuss this phenomenon, we recall the equation 4.63

$$\Psi_n(x,y) = \frac{i^n N_n^s \gamma}{\sqrt{2\pi}} e^{i\frac{\Omega^2}{\omega_c}yx} \int dx' \; \tilde{\psi}_n(x') e^{-i\gamma\sqrt{\Omega}yx'} e^{-\frac{1}{2}\gamma^2(x'-x)^2} H_n(\gamma(x'-x)) \tag{7.1}$$

for $x = 0$, we can rewrite Eq. (7.1)

$$\Psi_n(0,y) = \frac{i^n N_n^s \gamma}{\sqrt{2\pi}} \int dx \; \tilde{\psi}_n(x) e^{-i\gamma\sqrt{\Omega}yx} e^{-\frac{1}{2}\gamma^2 x^2} H_n(\gamma x) \tag{7.2}$$

$$= \int dx \, \tilde{\psi}_n(x) \, \tilde{\phi}_n(x,y) \tag{7.3}$$

where we define $\tilde{\phi}_n(x,y) = \frac{i^n N_n^s \gamma}{\sqrt{2\pi}} e^{-i\gamma\sqrt{\Omega}yx} e^{-\frac{1}{2}\gamma^2 x^2} H_n(\gamma x)$.

For the evanescent mode ($n = 1$), $\tilde{\phi}_1(x,y) = (\pi\Omega)^{-1/4}\gamma^2 x e^{-\frac{\gamma^2 x^2}{2}} \{\sin(\gamma\sqrt{\Omega}xy) + i\cos(\gamma\sqrt{\Omega}xy)\}$. The real part of $\tilde{\phi}_1(x,y)$ is odd on the y-direction and even on the x-direction; the imaginary part of $\tilde{\phi}_1(x,y)$ is even on the y-direction and odd on the x-direction. And then we compare to the results of the wavefunction patterns, the real part of the $\tilde{\phi}_1(x,y)$ should be eliminated or be very small in the integration of Eq. (7.3) for the first dips; and similar, the imaginary part of $\tilde{\phi}_1(x,y)$ should be eliminated or be very small in the integration for the second. Due to this property, the function $\tilde{\psi}_1(x)$ have a phase shift or phase difference between the two dips.

Extending the above discussion, we know the wavefunction have a phase shift between the first dips and the second dips, and these two bound states are according to the real part and imaginary part of the wavefunction on y-direction, $\phi_n^{\pm}(k_n, y)$.

The real part and imaginary part are both part of the function $\tilde{\phi}_n(x,y)$ and have the same eigen-energy, and depend on the magnetic field. As we fix the magnetic field and incident into the wire from one state, there are two kinds of overlap coupling to the evanescent mode for the impurity barrier, one couple to the real part of the evanescent mode and the other one couple to the imaginary mode. The effective amplitude must be different due to the even and odd property of the evanescent mode. When we incident from the first propagating mode and applied a magnetic field, the wavefunction shift to

the edge on both $\pm y$-direction and symmetry for the plus or minus wave vector, it has larger overlap with the real part of the evanescent mode which is even. That is why the evanescent mode of the first dips is even in the figures. And the overlap depend on the wavefunction between incident mode and other modes, the overlap with the even (real) part will not always be the larger one and be first dip.

7.4   Summary

In this chapter, we have discussed the magnetoconduction in the wire with a attractive barrier, and there are more than one dip structure as we apply the magnetic field. The dips structure move with the amplitude of the applied magnetic field; in the small magnetic field regime, the fist dips structures have the blue shift,and the second one move to the lower energy; and in the high magnetic field regime, the first two dips structures degenerate together.

When we change the strength of the impurity barrier, the dips structures move to the lower energy as the impurity barrier become more attractive. In the small magnetic field regime, the energy shift of the dips structure move like a quasi-2D system and the $\delta E \propto V_0^2$; and in the high magnetic field, the edge states had generated and the current density patterns move like a quasi-1D system and the energy shift of the dips structure proportion to the strength of the impurity barrier more linearly.

And we have also discussed the wavefunction and current density patterns of the first two dips structures and investigate the reason the the two dips. The profiles of the bound states in the first and second dips is due to the real and imaginary part of the evanescent mode and the overlap of the propagating mode and the evanescent mode. The impurity barrier is different for the real part and the imaginary part, and the amplitude of the overlap between wavefunction and impurity barrier correspond to the position of the two dips. And that is why the position curves in the Fig. 7.2 has mixed together or cross over. And we can also know that the wavefunction has a phase shift between these two dips,

the wavefunction may be even at the energy of the first dips and changed to odd at the
second, or be contrary.

Furthermore, we have also discussed the two length scales, magnetic length and the
cyclotron radius. Cyclotron radius is more classical-like then the magnetic length and
is better to describe the circular motion due to the Lorenz force; the edge states is a
classical-like phenomenon. And we can also use the scale, cyclotron radius, to separate
the edge states and the traversing states in the Fig. 1.1.

Chapter 8

Concluding remarks

In this thesis, we have investigated how the edge states happen and the other phenomena in the wire as applying the magnetic field. We solve the physical model in two approaches and compare the results to have a believing feature about the physical phenomena. And we also using the wavefunction and the current density patterns to investigate the edge states and the other properties in detail. In the introduction, we know that the classical-like picture of the edge states had be used for a long time and it is quite reasonable to discuss most of the experiments, and we also compare our results to the classical-like picture and have a explanation in quantum mechanic.

In the beginning of this work, we have used the mode-matching approach to solve the physical model, but the conservation is not good enough in the high magnetic field regime and we can not plot the wavefunction and the current density patterns which the edge states had built up. Without the figures of wavefunction and current density density pattern, it is hard to make sure what kinds of structures were caused by the edge. And then we use the approach of partial Fourier transformation of Lippmann-Schwinger equation. This approach is better in the high magnetic field regime and the plotting of the wavefunction and the current density patterns is stable to show the patterns of edge states. And we also compare the results of these two approaches. In the regime of low magnetic field, the results of two approach are almost the same; this is a independent

check of the calculation.

And then, the first thing is separating the two kinds of states in the wire as we apply the magnetic field, the edge states and the traversing states which is showed in the Fig. 1.1. We can compare the cyclotron radius and the classical width of the wire for a given Fermi energy, as long as the cyclotron radius smaller then the width of wire, the electrons can have a circular motion along one edge without touch another edge on the other side; and the edge states had built up. The applied magnetic field in the system is perpendicular to the 2DEG wire and parallel to the $+\hat{z}$-direction. The current density is the particle current and according to the applied magnetic field, the current flow to right on the upside of the wire and flow to left on the downside as the edge states had generated. And we can also find the current density patterns of the bound states move vortically and anticlockwise in substance. Some small structure of the current density pattern between two edge states have opposite current density patterns, that are the interference of the two main edge state current.

When a repulsive impurity barrier is embedded, the edge state resonance will be generated. The edge state resonance is due to the interference of different subbands, especially the propagating mode, and be easily happened in the range of small kinetic energy, like the beginning of each subbands. And the edge state resonance can be introduced for a δ-type embedded impurity barrier, which is a local potential in the longitudinal direction.

As we embed an attractive impurity barrier, the quasi-bound states will be generated, and there are not only one quasi-bound state but two or more as the applied magnetic field is large. In usually, the quasi-bound states generated in pair, and one is caused from the real part of evanescent mode and the other is caused from the imaginary part. Due to this property of the dips, we know the wavefunction has phase shift as increase the incident energy or the magnetic field, and it is corresponding to the position of the edge state, the path of the edge states are different when the kinetic energy and the magnetic field are changed, and the difference of the path may introduce the phase shift.

The position of the dips also move as we change the strength of the impurity barrier.

In the case of attractive barrier, in the small magnetic field regime, the shift of the quasi-bound state energy proportion to the square of the strength of the impurity barrier, $\delta E \propto V_0^2$; and in the high magnetic field regime and the edge state had generated, the energy shift of the quasi-bound state move more linearly to the strength of impurity barrier.

Chapter 9

Possible future works

We have a basic model of a δ-type impurity barrier in a wire with magnetic field. It is easy to extend form this model to a final range potential in the longitudinal direction by using the scattering matrix method in the future. For example, we already have some numerical results of double barriers or multiple barriers in the wire with magnetic field.

9.1 Double and multiple barriers

We plot few figures for the case of double barriers and multiple barriers and there are some interesting structures. In the Fig. 9.1 and Fig. 9.2, they are the results of double δ-type barrier and we had also change the amplitude of magnetic field or the distance between the two barrier to find out some properties in the figures. It does has some special fano or dip structure which didn't happen in the discussion of one impurity barrier. And we think that the fano and dips structures may be caused from the dot-like pattern between the two barriers.

We first focus on the repulsive barriers in the Fig. 9.1(a) and Fig. 9.2(a). In the case of without the magnetic field, we know that the two impurity barriers can introduce the resonance states on the longitudinal direction between them, and the propagating mode can have interaction to the resonance states and introduce the resonance valleys, but not

fano structures. After applying the magnetic field, the resonance valleys are still there. The current density patterns start to have the circular motions, and in some situation of the cyclotron radius match the size of the dot, the current density can have circular motions resonance. This kind of circular motions resonance is a bound state and grab electrons in the dot. That may be the most possible reason to have the Fano or dip structures in the figures.

In the figures of attractive barriers, Fig. 9.1(b) and 9.2(b), there may be similar structures of circular motion resonance, but there are too many structures in the figures and need more time for further discussion in the near future.

And in the Fig. 9.3, we plot the result of multiple δ-type barriers, which is 25 slice in the wire. we can find that there are more band gaps as we increase the magnetic field. We know that the periodic potential barrier can introduce some band gaps in transmission, but we still don't know why the magnetic field move the position of the band gaps and also generate some extra band gaps.

Also, it might be interesting to discuss these structures and figure out the transport phenomena such as the Fano and dip structures in the conductance.
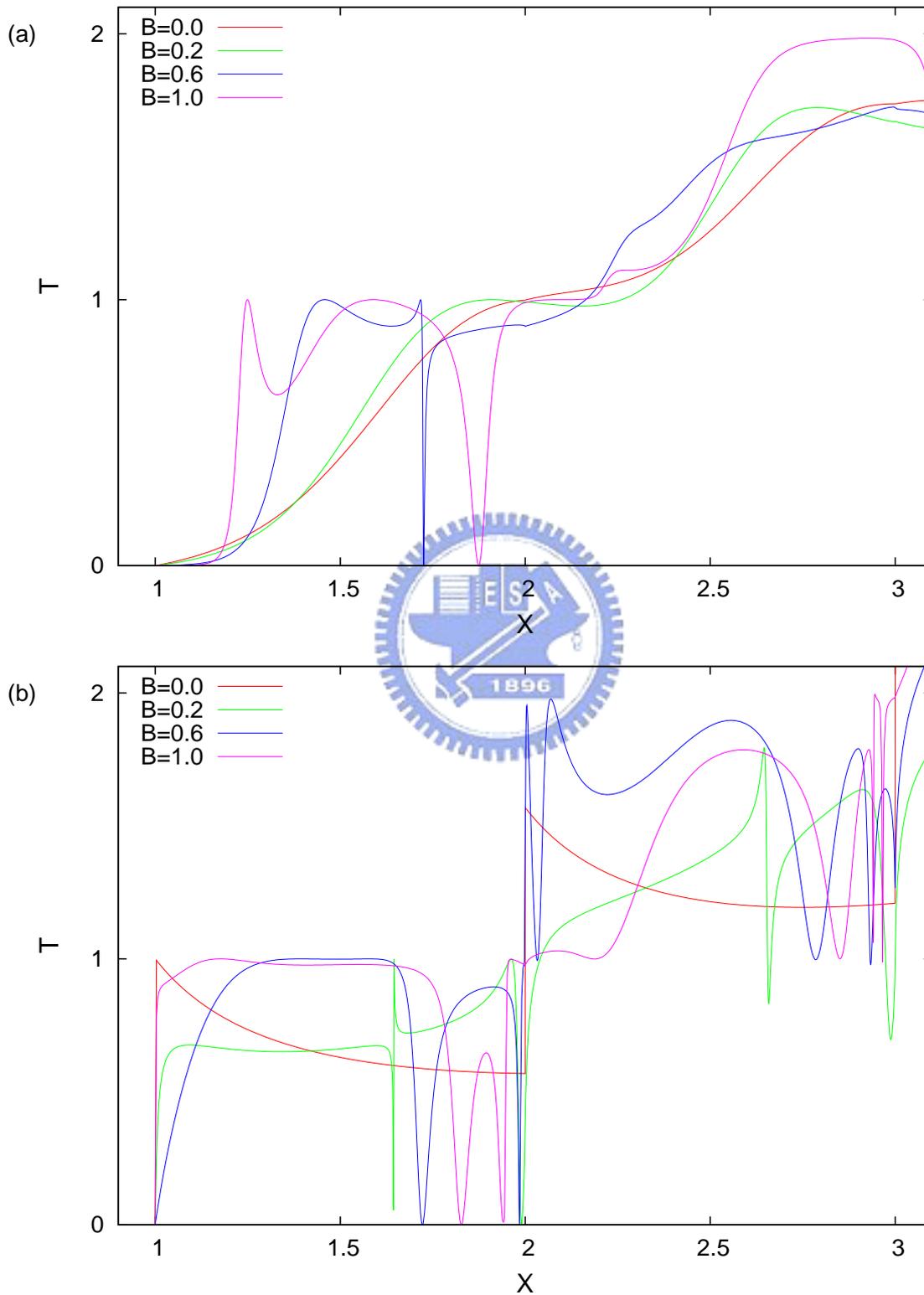
Figure 9.1:   Two embedded δ-type barrier in the wire which the distance between them is $2.0a^*$, and we plot the transmission as a function of incident energy X for various amplitude of magnetic field from $0.0B^*$ to $1.0B^*$, and the strength of the two barrier are both $1.0E^*$ in (a) and $-1.0E^*$ in (b).
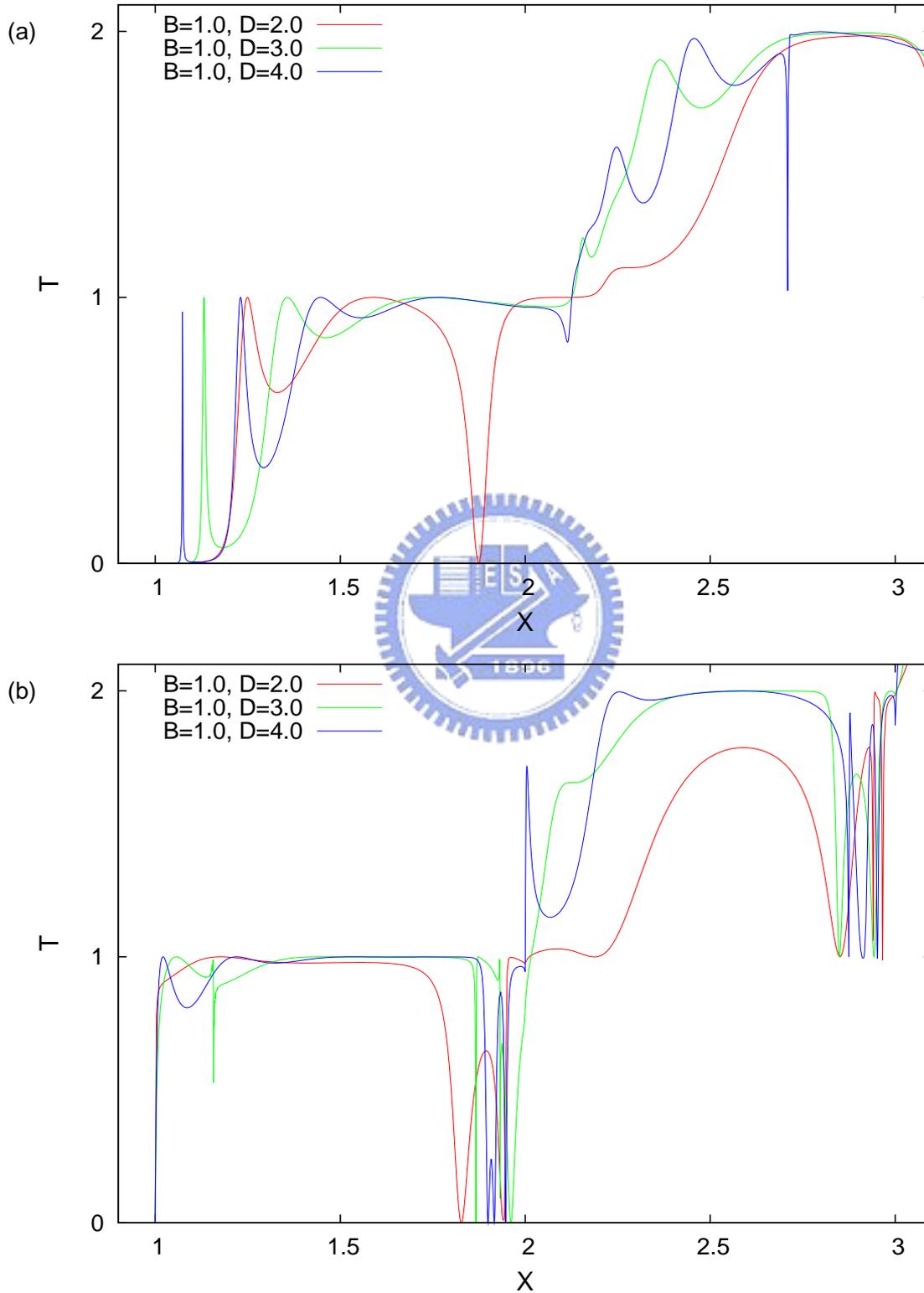
Figure 9.2: The transmission versus the incident energy for double embedded impurity barrier which the strength is $1.0E^*$ in (a) and $-1.0E^*$ in (b), the distance between the two barrier is changed for various distance from $2.0a^*$ to $4.0a^*$.
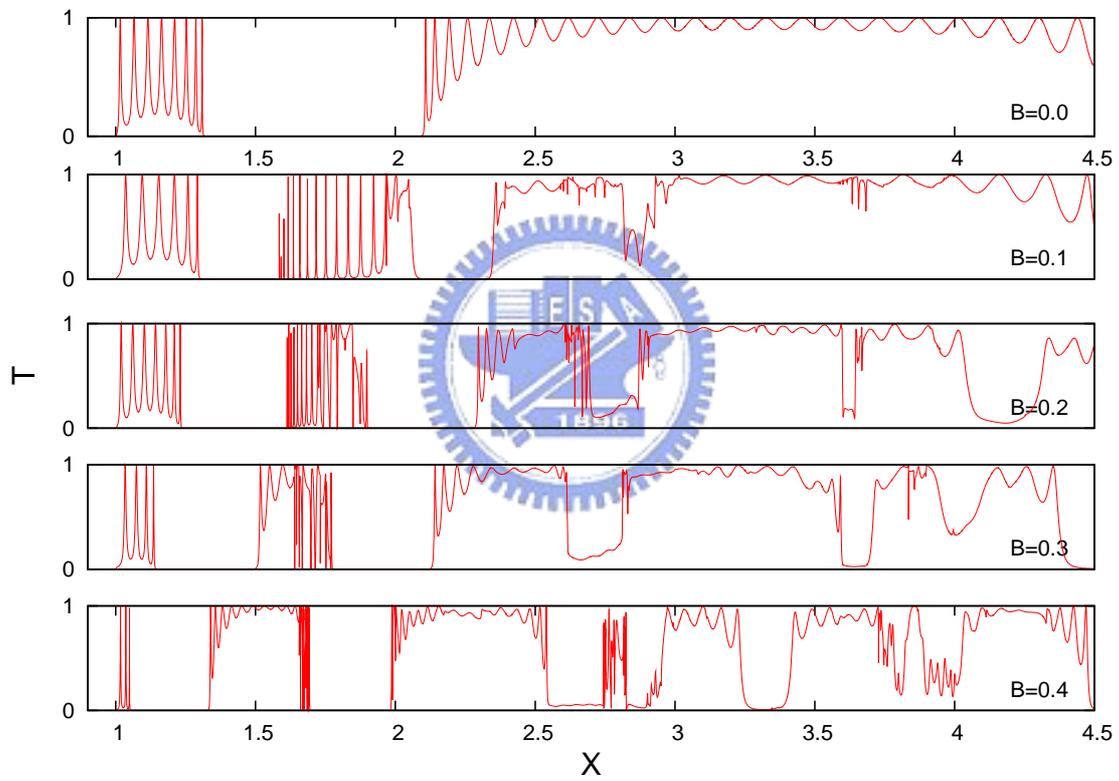
Figure 9.3:   The transmission of the first channel versus the incident energy for 25 slices of δ-type barrier and the distance between two near slices is $3.0a^*$. We change the amplitude of magnetic field from $0.0B^*$ to $0.4B^*$ in series of these five figures.

Appendix A

Detail of the integrations

In this appendix we present the detailed calculation of the integrations we used.

We have three kinds of wavefunctions in y-direction, which $\phi_n^o(y)$ is the ordinary wave-function in the parabolically confined wire with no magnetic field, $\phi_n^\pm(y, k_n)$ is the wave-function in the parabolic wire with magnetic field, and $\phi_n^s(y)$ is the wavefunction which similar to $\phi_n^o(y)$ but replace the parameter ω_y by Ω.

$$\phi_n^o(y) = N_n^o e^{-\frac{1}{2}\omega_y y^2} H_n \left[\sqrt{\omega_y} y \right] \tag{A.1}$$

$$\phi_n^s(y) = N_n^s e^{-\frac{1}{2}\Omega y^2} H_n \left[\sqrt{\Omega} y \right] \tag{A.2}$$

$$\phi_n^\pm(y) = N_n e^{-\frac{1}{2}\Omega(y \mp \alpha_n)^2} H_n \left[\sqrt{\Omega}(y \mp \alpha_n) \right] \tag{A.3}$$

APPENDIX A. DETAIL OF THE INTEGRATIONS
_____

where

$$N_n^o = \left(2^n n! \sqrt{\frac{\pi}{\omega_y}}\right)^{-1/2} \tag{A.4}$$

$$N_n^s = \left(2^n n! \sqrt{\frac{\pi}{\Omega}}\right)^{-1/2} \tag{A.5}$$

$$N_n = N_n^s e^{-\frac{\Omega}{2}\text{Im}(\alpha_n)^2} \left[\sum_{k=0}^{n} \frac{(2\Omega\text{Im}(\alpha_n)^2)^k}{k!}\binom{n}{k}\right]^{-1/2} \tag{A.6}$$

$$= N_n^s e^{-\frac{\Omega}{2}\text{Im}[\alpha_n]^2}\Lambda_n \tag{A.7}$$

$$\Lambda_n = \left[\sum_{k=0}^{n} \frac{(2\Omega\text{Im}[\alpha_n]^2)^k}{k!}\binom{n}{k}\right]^{-1/2} \tag{A.8}$$

There are few integration that have to be calculated, which are
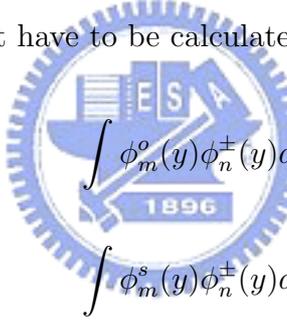
$$\int \phi_m^o(y)\phi_n^\pm(y)dy, \tag{A.9}$$

$$\int \phi_m^s(y)\phi_n^\pm(y)dy, \tag{A.10}$$

$$\int \phi_m^{\pm *}(y)\phi_n^\pm(y)dy, \tag{A.11}$$

$$\int \phi_m^o(y)V_s(y)\phi_n^\pm(y)dy, \tag{A.12}$$

$$\int \phi_m^s(y)V_s(y)\phi_n^\pm(y)dy, \tag{A.13}$$

$$\int \phi_m^{\pm *}(y)V_s(y)\phi_n^\pm(y)dy, \tag{A.14}$$

$$\int y\phi_n^{\pm *}\phi_n^\pm dy = \pm\text{Re}[\alpha_n]. \tag{A.15}$$

98

A.1 $\int \phi_m^o(y)\phi_n^\pm(y)dy$

We first calculate the integration of Eq. (A.9).

$$
\begin{aligned}
&\int \phi_m^o(y)\phi_n^\pm(y)dy \\
=\ &N_m^o N_n \int e^{-\frac{1}{2}\omega_y y^2} H_m(\sqrt{\omega}_y y)e^{-\frac{1}{2}\Omega(y\mp\alpha_n)^2} H_n[\sqrt{\Omega}(y\mp\alpha_n)]dy \qquad \text{(A.16)} \\
&\text{where } N_m^o N_n = 2^{-\frac{m+n}{2}}(m!n!)^{-1/2}\frac{(\omega_y\Omega)^{1/4}}{\sqrt{\pi}}e^{-\frac{\Omega}{2}\mathrm{Im}(\alpha_n)^2}\Lambda_n
\end{aligned}
$$

Since the power of the exponential part can be expressed as:

$$
\begin{aligned}
&-\frac{1}{2}\omega_y y^2 - \frac{1}{2}\Omega(y\mp\alpha_n)^2 \\
=\ &\frac{-1}{2}\left(\omega_y y^2 + \Omega y^2 \mp 2\Omega\alpha_n y + \Omega\alpha_n^2\right) \\
=\ &\frac{-1}{2}\left[(\omega_y+\Omega)y^2 \mp 2\Omega\alpha_n y + \Omega\alpha_n^2\right] \\
&\text{let } \eta = \omega_y + \Omega \\
=\ &\frac{-\eta}{2}\left[y^2 \mp \frac{2\Omega\alpha_n}{\eta}y + (\frac{\Omega\alpha_n}{\eta})^2 - (\frac{\Omega\alpha_n}{\eta})^2 + \frac{\Omega\alpha_n^2}{\eta}\right] \\
=\ &\frac{-\eta}{2}(y\mp\frac{\Omega\alpha_n}{\eta})^2 + \frac{\eta}{2}(\frac{\Omega\alpha_n}{\eta})^2 - \frac{1}{2}\Omega\alpha_n^2 \qquad \text{(A.17)}
\end{aligned}
$$

we get

$$
\int \phi_m^o(y)\phi_n^\pm(y)dy = N_m^o N_n e^{\frac{\eta}{2}(\frac{\Omega\alpha_n}{\eta})^2 - \frac{1}{2}\Omega\alpha_n^2} \int e^{-\frac{\eta}{2}(y\mp\frac{\Omega\alpha_n}{\eta})^2} H_m(\sqrt{\omega}_y y)H_n(\sqrt{\Omega}(y\mp\alpha_n))dy.
$$

$$\text{(A.18)}$$

APPENDIX A. DETAIL OF THE INTEGRATIONS

The integration part:

$$\int e^{-\frac{\eta}{2}(y \mp \frac{\Omega \alpha_n}{\eta})^2} H_m(\sqrt{\omega_y}y) H_n(\sqrt{\Omega}(y \mp \alpha_n)) dy$$

$$= \int e^{-(\sqrt{\frac{\eta}{2}}y \mp \frac{\Omega \alpha_n}{\sqrt{2\eta}})^2} H_m(\sqrt{\omega_y}y) H_n(\sqrt{\Omega}y \mp \sqrt{\Omega}\alpha_n) dy$$

$$\text{let } t = \sqrt{\frac{\eta}{2}}\, y, \; y = \sqrt{\frac{2}{\eta}}\, t$$

$$\Rightarrow \int e^{-(t \mp \frac{\Omega \alpha_n}{\sqrt{2\eta}})^2} H_m(\sqrt{\frac{2\omega_y}{\eta}}t) H_n(\sqrt{\frac{2\Omega}{\eta}}t \mp \sqrt{\Omega}\alpha_n)\sqrt{\frac{2}{\eta}}dt$$

$$\text{let } x = t \mp \frac{\Omega \alpha_n}{\sqrt{2\eta}}, \; t = x \pm \frac{\Omega \alpha_n}{\sqrt{2\eta}}$$

$$\Rightarrow \sqrt{\frac{2}{\eta}} \int e^{-x^2} H_m \left[\sqrt{\frac{2\omega_y}{\eta}}x \pm \frac{\sqrt{\omega_y}\Omega \alpha_n}{\eta} \right] H_n \left[\sqrt{\frac{2\Omega}{\eta}}x \mp \frac{\sqrt{\Omega}\omega_y \alpha_n}{\eta} \right] dx \quad \text{(A.19)}$$

Using this relation $2^{\frac{n}{2}} H_n(x+y) = \sum_{k=0}^{n} \binom{n}{k} H_{n-k}(\sqrt{2}x) H_k(\sqrt{2}y)$

$$\Rightarrow \sqrt{\frac{2}{\eta}} 2^{-\frac{m+n}{2}} \sum_{p=0}^{m} \sum_{q=0}^{n} \binom{m}{m-p}\binom{n}{n-q} H_{m-p}\left[\pm \frac{\sqrt{2\omega_y}\Omega \alpha_n}{\eta} \right] H_{n-q}\left[\mp \frac{\sqrt{2\Omega}\omega_y \alpha_n}{\eta} \right]$$

$$\int e^{-x^2} H_p[2\sqrt{\frac{\omega_y}{\eta}}x] H_q[2\sqrt{\frac{\Omega}{\eta}}x] dx \quad \text{(A.20)}$$

and using the relation of Eqs. (A.75), we have

$$\int \phi_m^o(y)\phi_n^{\pm}(y) dy$$

$$= N_m^o N_n \times \sqrt{\frac{2}{\eta}} 2^{-\frac{m+n}{2}} e^{\frac{1}{2}\eta(\frac{\Omega \alpha_n}{\eta})^2 - \frac{1}{2}\Omega \alpha_n^2}$$

$$\times \sum_{p=0}^{m} \sum_{q=0}^{n} \binom{m}{m-p}\binom{n}{n-q} H_{m-p}\left[\pm \frac{\sqrt{2\omega_y}\Omega \alpha_n}{\eta} \right] H_{n-q}\left[\mp \frac{\sqrt{2\Omega}\omega_y \alpha_n}{\eta} \right]$$

$$\times \begin{cases} \sum_{s}^{(\text{Min}[p,q]-1)/2} \sqrt{\pi}p!q! \frac{[\frac{8}{\eta}\sqrt{\omega_y\Omega}]^{2s+1}}{(2s+1)!} \frac{[\frac{3\omega_y-\Omega}{\eta}]^{\frac{p-2s-1}{2}}}{(\frac{p-2s-1}{2})!} \frac{[\frac{3\Omega-\omega_y}{\eta}]^{\frac{q-2s-1}{2}}}{(\frac{q-2s-1}{2})!} & , m,n \text{ are both odd.} \\ \sum_{s}^{(\text{Min}[p,q])/2} \sqrt{\pi}p!q! \frac{[\frac{8}{\eta}\sqrt{\omega_y\Omega}]^{2s}}{(2s)!} \frac{[\frac{3\omega_y-\Omega}{\eta}]^{\frac{p-2s}{2}}}{(\frac{p-2s}{2})!} \frac{[\frac{3\Omega-\omega_y}{\eta}]^{\frac{q-2s}{2}}}{(\frac{q-2s}{2})!} & , m,n \text{ are both even.} \\ 0 & , m+n \text{ is odd.} \end{cases}$$

where $N_m^o N_n = 2^{-\frac{m+n}{2}} (m!n!)^{-1/2} \frac{(\omega_y\Omega)^{1/4}}{\sqrt{\pi}} e^{-\frac{\Omega}{2}\text{Im}[\alpha_n]^2} \Lambda_n$

and simplify this equation, we obtain:

$$\int \phi_m^o(y)\phi_n^{\pm}(y)dy$$

$$= \sqrt{\frac{2m!n!}{\eta}}\,(\omega_y\Omega)^{1/4}e^{\frac{1}{2}\eta(\frac{\Omega\alpha_n}{\eta})^2-\frac{1}{2}\Omega\mathrm{Re}[\alpha_n]^2}\Lambda_n$$

$$\times\sum_{p=0}^{m}\sum_{q=0}^{n}\frac{H_{m-p}\left[\pm\frac{\sqrt{2\omega_y}\Omega\alpha_n}{\eta}\right]}{2^{m-p}2^p(m-p)!}\frac{H_{n-q}\left[\mp\frac{\sqrt{2\Omega}\omega_y\alpha_n}{\eta}\right]}{2^{n-q}2^q(n-q)!}$$

$$\times\begin{cases}\sum_{s}^{(\mathrm{Min}[p,q]-1)/2}f_{r1}(2s+1)\,f_{r2}(\frac{p-2s-1}{2})\,f_{r3}(\frac{q-2s-1}{2}) & ,\; m,n\;\text{are both odd.}\\[2mm] \sum_{s}^{(\mathrm{Min}[p,q])/2}f_{r1}(2s)\,f_{r2}(\frac{p-2s}{2})\,f_{r3}(\frac{q-2s}{2}) & ,\; m,n\;\text{are both even.}\\[2mm] 0 & ,\; m+n\;\text{is odd.}\end{cases}$$

$$= \sqrt{\frac{2m!n!}{\eta}}\,(\omega_y\Omega)^{1/4}e^{\frac{1}{2}\eta(\frac{\Omega\alpha_n}{\eta})^2-\frac{1}{2}\Omega\mathrm{Re}[\alpha_n]^2}\Lambda_n\sum_{p=0}^{m}\sum_{q=0}^{n}\frac{\bar{H}_{m-p}\left[\pm\frac{\sqrt{2\omega_y}\Omega\alpha_n}{\eta}\right]}{2^p}\frac{\bar{H}_{n-q}\left[\mp\frac{\sqrt{2\Omega}\omega_y\alpha_n}{\eta}\right]}{2^q}$$

$$\times\begin{cases}\sum_{s}^{(\mathrm{Min}[p,q]-1)/2}f_{r1}(2s+1)\,f_{r2}(\frac{p-2s-1}{2})\,f_{r3}(\frac{q-2s-1}{2}) & ,\; m,n\;\text{are both odd.}\\[2mm] \sum_{s}^{(\mathrm{Min}[p,q])/2}f_{r1}(2s)\,f_{r2}(\frac{p-2s}{2})\,f_{r3}(\frac{q-2s}{2}) & ,\; m,n\;\text{are both even.}\\[2mm] 0 & ,\; m+n\;\text{is odd.}\end{cases} \qquad (A.21)$$

where

$$\bar{H}_n(x)\equiv\frac{H_n(x)}{2^n n!},\;\; \eta=\omega_y+\Omega,\;\; \alpha_n=\frac{\omega_c k_n}{\Omega^2} \qquad (A.22)$$

and

$$f_{r1}(n)=(\frac{8\sqrt{\omega_y\Omega}}{\eta})^n/n!,\;\; f_{r2}(n)=(\frac{3\omega_y-\Omega}{\eta})^n/n!,\;\; f_{r3}(n)=(\frac{3\Omega-\omega_y}{\eta})^n/n!. \qquad (A.23)$$

A.2 $\int \phi_m^s(y)\phi_n^{\pm}(y)dy$

Then we calculate the integration of Eq. (A.10).

$$
\int \phi_m^s(y)\phi_n^{\pm}(y)dy
$$

$$
= \ N_m^s N_n \int e^{-\frac{1}{2}\Omega y^2} H_m(\sqrt{\Omega}y) e^{-\frac{1}{2}\Omega(y\mp\alpha_n)^2} H_n[\sqrt{\Omega}(y\mp\alpha_n)]dy \qquad \text{(A.24)}
$$

Since the exponential part can be expressed as:

$$
-\frac{1}{2}\Omega y^2 - \frac{1}{2}\Omega(y\mp\alpha_n)^2 = -\left(\sqrt{\Omega}y \mp \frac{\sqrt{\Omega}\alpha_n}{2}\right)^2 - \frac{\Omega}{4}\alpha_n^2, \qquad \text{(A.25)}
$$

we get

$$
\int \phi_m^s(y)\phi_n^{\pm}(y)dy
$$

$$
= \ N_m^s N_n e^{-\frac{\Omega}{4}\alpha_n^2} \int e^{-(\sqrt{\Omega}y\mp\frac{\sqrt{\Omega}\alpha_n}{2})^2} H_m\left(\sqrt{\Omega}y\right) H_n\left(\sqrt{\Omega}y \mp \sqrt{\Omega}\alpha_n\right) dy.
$$

$$
\text{Define } p = \sqrt{\Omega}y, \text{ and } p' = p \pm \frac{\sqrt{\Omega}\alpha_n}{2},
$$

$$
= \ N_m^s N_n e^{-\frac{\Omega}{4}\alpha_n^2} \int e^{-p^2} H_m\left(p \pm \frac{\sqrt{\Omega}\alpha_m}{2}\right) H_n\left(p \mp \frac{\sqrt{\Omega}\alpha_n}{2}\right)\frac{dp}{\sqrt{\Omega}}. \qquad \text{(A.26)}
$$

Using the identity $\int_{-\infty}^{\infty} e^{-x^2} H_m\left(x+a\right) H_n\left(x+b\right)dx = \sum\limits_{k=0}^{Min[m,n]} 2^{m+n-k}a^{m-k}b^{n-k}\frac{m!n!\sqrt{\pi}}{k!(m-k)!(n-k)!}$,

then we obtain

$$
\int \phi_m^s(y)\phi_n^\pm(y)dy
$$

$$
= N_m^s N_n \sqrt{\frac{\pi}{\Omega}} e^{-\frac{\Omega}{4}\alpha_n^2} \sum_{\kappa=0}^{\mathrm{Min}[m,n]} 2^{m+n-\kappa} \left(\pm\frac{\sqrt{\Omega}\alpha_n}{2}\right)^{m-\kappa} \left(\mp\frac{\sqrt{\Omega}\alpha_n}{2}\right)^{n-\kappa} \frac{m!n!}{\kappa!(m-\kappa)!(n-\kappa)!}
$$

$$
= \sqrt{\frac{\Omega}{\pi}} 2^{-\frac{m+n}{2}} \frac{1}{\sqrt{m!n!}} e^{-\frac{\Omega}{2}\mathrm{Im}(\alpha_n)^2} \Lambda_n
$$

$$
\times \sqrt{\frac{\pi}{\Omega}} e^{-\frac{\Omega}{4}\alpha_n^2} \sum_{\kappa=0}^{\mathrm{Min}[m,n]} 2^{m+n-\kappa} \left(\pm\frac{\sqrt{\Omega}\alpha_n}{2}\right)^{m-\kappa} \left(\mp\frac{\sqrt{\Omega}\alpha_n}{2}\right)^{n-\kappa} \frac{m!n!}{\kappa!(m-\kappa)!(n-\kappa)!}
$$

$$
= \Lambda_n e^{-\frac{\Omega}{4}\mathrm{ABS}(\alpha_n)^2} \sum_{\kappa=0}^{\mathrm{Min}[m,n]} \sqrt{2}^{(m-\kappa)+(n-\kappa)} \left(\pm\frac{\sqrt{\Omega}\alpha_n}{2}\right)^{m-\kappa} \left(\mp\frac{\sqrt{\Omega}\alpha_n}{2}\right)^{n-\kappa} \frac{\sqrt{m!n!}}{\kappa!(m-\kappa)!(n-\kappa)!}
$$

$$
= \Lambda_n e^{-\frac{\Omega}{4}\mathrm{ABS}(\alpha_n)^2} \sum_{\kappa=0}^{\mathrm{Min}[m,n]} \left(\pm\sqrt{\frac{\Omega}{2}}\alpha_n\right)^{m-\kappa} \left(\mp\sqrt{\frac{\Omega}{2}}\alpha_n\right)^{n-\kappa} \frac{\sqrt{m!n!}}{\kappa!(m-\kappa)!(n-\kappa)!} \qquad (A.27)
$$

A.3 $\int \phi_m^{\pm*}(y)\phi_n^\pm(y)dy$
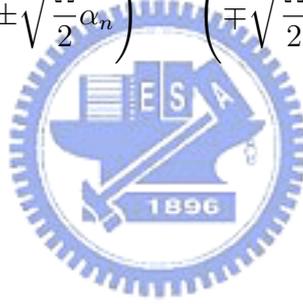
$$
\int \phi_m^{\pm*}(y)\phi_n^\pm(y)dy
$$

$$
= N_m N_n \int e^{-\frac{\Omega}{2}(y\mp\alpha_m^*)^2} H_m^*\left[\sqrt{\Omega}(y\mp\alpha_m)\right] e^{-\frac{\Omega}{2}(y\mp\alpha_n)^2} H_n^*\left[\sqrt{\Omega}(y\mp\alpha_n)\right] dy
$$

$$
\text{let } x = \sqrt{\Omega}y,\ q_n = \sqrt{\Omega}\alpha_n,\ H_m^*(x) = H_m(x^*)
$$

$$
= \frac{N_m N_n}{\sqrt{\Omega}} \int e^{-\frac{1}{2}(x\mp q_m^*)^2 - \frac{1}{2}(x\mp q_n)^2} H_m(x\mp q_m^*)H_n(x\mp q_n)dx \qquad (A.28)
$$

APPENDIX A. DETAIL OF THE INTEGRATIONS

the exponential part:

$$-\frac{1}{2}\{x^2 + q_m^{*\,2} \mp 2q_m^* + x^2 + q_n^2 \mp 2q_n x\}$$

$$= -\{x^2 - (\pm q_m^* \pm q_n)x + \frac{q_m^{*\,2} + q_n^2}{2}\}$$

$$\text{let } a = \pm q_m^* \pm q_n$$

$$= -(x - \frac{a}{2})^2 + \frac{1}{4}\{(\pm q_m^* \pm q_n)^2 - 2(q_m^{*\,2} + q_n^2)\}$$

$$= -(x - \frac{a}{2})^2 - \frac{1}{4}(\pm q_m^* - (\pm q_n))^2$$

$$= -b^2 - (x - \frac{a}{2})^2 \qquad (A.29)$$

$$\text{where } a = \pm q_m^* \pm q_n; \ b = \frac{1}{2}(\pm q_m^* - (\pm q_n)) \qquad (A.30)$$

$$\Rightarrow \quad \int \phi_m^{\pm\,*}(y)\phi_n^{\pm}(y)dy$$

$$= N_m N_n \frac{e^{-b^2}}{\sqrt{\Omega}} \int e^{-(x-\frac{a}{2})^2} H_m(x \mp q_m^*) H_n(x \mp q_n)dx$$

$$\text{let } x' = x - \frac{a}{2}$$

$$= N_m N_n \frac{e^{-b^2}}{\sqrt{\Omega}} \int e^{-x'^2} H_m(x' - \frac{\pm q_m^* - (\pm q_n)}{2}) H_n(x' + \frac{\pm q_m^* - (\pm q_n)}{2})dx'$$

$$= N_m N_n \frac{e^{-b^2}}{\sqrt{\Omega}} \int e^{-x^2} H_m(x - b) H_n(x + b)dx \qquad (A.31)$$

Using the identity $\int_{-\infty}^{\infty} e^{-x^2} H_m(x+a) H_n(x+b) dx = \sum_{k=0}^{Min[m,n]} 2^{m+n-k} a^{m-k} b^{n-k} \frac{m!n!\sqrt{\pi}}{k!(m-k)!(n-k)!}$, and we could get

$$\Rightarrow \quad \int \phi_m^{\pm\,*}(y)\phi_n^{\pm}(y)dy$$

$$= N_m N_n \sqrt{\frac{\pi}{\Omega}} e^{-b^2} \sum_{\kappa=0}^{Min[m,n]} 2^{m+n-\kappa} (-b)^{m-\kappa} b^{n-\kappa} \frac{m!n!}{k!(m-\kappa)!(n-\kappa)!} \qquad (A.32)$$

$$\text{where } b = \frac{1}{2}(\pm q_m^* - (\pm q_n)) = \frac{\sqrt{\Omega}}{2}\{\pm \alpha_m^* - (\pm \alpha_n)\}$$

$$
\begin{aligned}
b &= \frac{\sqrt{\Omega}}{2}\{\pm\alpha_m^* - (\pm\alpha_n)\} \\
b^2 &= \frac{\Omega}{4}\{\alpha_m^{*\,2} + \alpha_n^2 - 2(\pm\alpha_m^*)(\pm\alpha_n)\}
\end{aligned}
$$

and

$$
N_m N_n = \sqrt{\frac{\Omega}{\pi}}\, 2^{-\frac{m+n}{2}}\frac{1}{\sqrt{m!n!}}\, e^{-\frac{\Omega}{2}\mathrm{Im}(\alpha_m)^2 - \frac{\Omega}{2}\mathrm{Im}(\alpha_n)^2}\Lambda_m\Lambda_n \tag{A.33}
$$

$$
\begin{aligned}
\Rightarrow \quad & \int \phi_m^{\pm\,*}(y)\phi_n^{\pm}(y)dy \\
= \ & \Lambda_m\Lambda_n e^{-\frac{\Omega}{4}[\mathrm{ABS}(\alpha_m)^2 + \mathrm{ABS}(\alpha_n)^2] + \frac{\Omega}{2}(\pm\alpha_m^*)(\pm\alpha_n)} \\
& \times \sum_{\kappa=0}^{\mathrm{Min}[m,n]} 2^{\frac{m+n}{2}-\kappa}(-b)^{m-\kappa}b^{n-\kappa}\frac{\sqrt{m!n!}}{k!(m-\kappa)!(n-\kappa)!} \\
= \ & \Lambda_m\Lambda_n e^{-\frac{\Omega}{4}[\mathrm{ABS}(\alpha_m)^2 + \mathrm{ABS}(\alpha_n)^2] + \frac{\Omega}{2}(\pm\alpha_m^*)(\pm\alpha_n)} \\
& \times \sum_{\kappa=0}^{\mathrm{Min}[m,n]} (-\sqrt{2}b)^{m-\kappa}(\sqrt{2}b)^{n-\kappa}\frac{\sqrt{m!n!}}{k!(m-\kappa)!(n-\kappa)!} \tag{A.34}
\end{aligned}
$$

where

$$
b = \frac{\sqrt{\Omega}}{2}\{\alpha_m^* - \alpha_n\}\ \text{for}\ \int \phi_m^{+\,*}(y)\phi_n^{+}(y)dy, \qquad b = \frac{\sqrt{\Omega}}{2}\{\alpha_m^* + \alpha_n\}\ \text{for}\ \int \phi_m^{+\,*}(y)\phi_n^{-}(y)dy,
$$

$$
b = \frac{-\sqrt{\Omega}}{2}\{\alpha_m^* + \alpha_n\}\ \text{for}\ \int \phi_m^{-\,*}(y)\phi_n^{+}(y)dy, \qquad b = \frac{-\sqrt{\Omega}}{2}\{\alpha_m^* - \alpha_n\}\ \text{for}\ \int \phi_m^{-\,*}(y)\phi_n^{-}(y)dy.
$$

A.4 $\int \phi_m^o(y)V_s(y)\phi_n^{\pm}(y)dy$

$$
\begin{aligned}
& \int_{-\infty}^{\infty} \phi_m^o(y)V_s(y)\phi_n^{\pm}(y)dy \\
= \ & N_m^o N_n V_0 \int e^{-\frac{1}{2}\omega_y y^2} H_m(\sqrt{\omega_y}y) e^{-\beta(y-y_0)^2} e^{-\frac{1}{2}\Omega(y\mp\alpha_n)^2} H_n[\sqrt{\Omega}(y\mp\alpha_n)]dy. \tag{A.35}
\end{aligned}
$$

The power of the exponential part:

$$-\frac{1}{2}\omega_y y^2 - \beta(y-y_0)^2 - \frac{1}{2}\Omega(y \mp \alpha_n)^2$$

$$= -\frac{1}{2}\omega_y y^2 - \beta y^2 + 2\beta y_0 y - \beta y_0^2 - \frac{1}{2}\Omega y^2 \pm \Omega\alpha_n y - \frac{1}{2}\Omega\alpha_n^2$$

$$= y^2(-\frac{1}{2}\omega_y - \frac{1}{2}\Omega - \beta) + y(2\beta y_0 \pm \Omega\alpha_n) - \beta y_0^2 - \frac{1}{2}\Omega\alpha_n^2$$

$$= -\eta y^2 + 2\xi^{\pm}y - \beta y_0^2 - \frac{1}{2}\Omega\alpha_n^2$$

$$\text{where } \eta = \frac{\omega_y + \Omega}{2} + \beta, \ \xi^{\pm} = \beta y_0 \pm \frac{\Omega\alpha_n}{2}$$

$$= -(\sqrt{\eta}y - \frac{\xi^{\pm}}{\sqrt{\eta}})^2 + \frac{\xi^{\pm 2}}{\eta} - \beta y_0^2 - \frac{1}{2}\Omega\alpha_n^2 \qquad (A.36)$$

$$\int_{-\infty}^{\infty} \phi_m^o(y) V_s(y) \phi_n^{\pm}(y) dy$$

$$= N_m^o N_n \exp(\frac{\xi^{\pm 2}}{\eta} - \beta y_0^2 - \frac{1}{2}\Omega\alpha_n^2)$$

$$\int e^{-(\sqrt{\eta} - \frac{\xi^{\pm}}{\sqrt{\eta}})^2} H_m(\sqrt{\omega_y}y) H_n(\sqrt{\Omega}(y \mp \alpha_n)) dy \qquad (A.37)$$

$$t = \sqrt{\eta}y - \frac{\xi^{\pm}}{\sqrt{\eta}}, \ \sqrt{\eta}y = t + \frac{\xi^{\pm}}{\sqrt{\eta}},$$

$$y = \frac{t}{\sqrt{\eta}} + \frac{\xi^{\pm}}{\eta}, \ dy = \frac{dt}{\sqrt{\eta}}.$$

$$e^{-(\sqrt{\eta}y - \frac{\xi^{\pm}}{\sqrt{\eta}})^2} H_m(\sqrt{\omega_y}y) H_n(\sqrt{\Omega}(y \pm \alpha_n)) dy$$

$$\rightarrow e^{-t^2} H_m\left[\sqrt{\frac{\omega_y}{\eta}}t + \frac{\sqrt{\omega_y}\xi^{\pm}}{\eta}\right] H_n\left[\sqrt{\frac{\Omega}{\eta}}t + \frac{\sqrt{\Omega}\xi^{\pm}}{\eta} \mp \sqrt{\Omega}\alpha_n\right] \frac{dt}{\sqrt{\eta}}$$

$$= e^{-t^2} H_m\left[\sqrt{\frac{\omega_y}{\eta}}t + \frac{\sqrt{\omega_y}}{\eta}[\beta y_0 \pm \frac{\Omega\alpha_n}{2}]\right]$$

$$\times H_n\left[\sqrt{\frac{\Omega}{\eta}}t + \frac{\sqrt{\Omega}}{\eta}[\beta y_0 \mp \frac{\omega_y\alpha_n}{2} \mp \beta\alpha_n]\right] \frac{dt}{\sqrt{\eta}} \qquad (A.38)$$

APPENDIX A. DETAIL OF THE INTEGRATIONS

$$\Rightarrow \quad \frac{1}{\sqrt{\eta}} 2^{-\frac{m+n}{2}} \sum_{p=0}^{m} \sum_{q=0}^{n} \binom{m}{m-p}\binom{n}{n-q} H_{m-p}\left[\frac{\sqrt{2\omega_y}}{\eta}(\beta y_0 \pm \frac{\Omega\alpha_n}{2})\right]$$

$$\times H_{n-q}\left[\frac{\sqrt{2\Omega}}{\eta}(\beta y_0 \mp \frac{\omega_y\alpha_n}{2} \mp \beta\alpha_n)\right] \int e^{-t^2} H_p(\sqrt{\frac{2\omega_y}{\eta}}t) H_q(\sqrt{\frac{2\Omega}{\eta}}t) dt \quad (A.39)$$

And then, we obtain the integration :

$$\int_{-\infty}^{\infty} \phi_m^o(y) V_s(y) \phi_n^{\pm}(y) dy$$

$$= \left[2^{-\frac{m+n}{2}}(m!n!)^{-1/2}\frac{(\omega_y\Omega)^{1/4}}{\sqrt{\pi}} e^{-\frac{\Omega}{2}\mathrm{Im}(\alpha_n)^2}\Lambda_n\right] \exp(\frac{\xi^{\pm 2}}{\eta} - \beta y_0^2 - \frac{1}{2}\Omega\alpha_n^2)\sqrt{\frac{1}{\eta}}2^{-\frac{m+n}{2}}$$

$$\times \sum_{p=0}^{m}\sum_{q=0}^{n}\frac{m!n!}{p!(m-p)!q!(n-q)!}$$

$$\times H_{m-p}\left[\frac{\sqrt{2\omega_y}}{\eta}(\beta y_0 \pm \frac{\Omega\alpha_n}{2})\right] H_{n-q}\left[\frac{\sqrt{2\Omega}}{\eta}(\beta y_0 \mp \frac{\omega_y\alpha_n}{2} \mp \beta\alpha_n)\right]$$

$$\times \begin{cases} \sum_s^{\mathrm{Min}[p,q]/2} \sqrt{\pi}p!q!\frac{(\frac{4}{\eta}\sqrt{\omega_y\Omega})^{2s}}{(2s)!}\frac{(\frac{2\omega_y}{\eta}-1)^{\frac{p-2s}{2}}}{(\frac{p-2s}{2})!}\frac{(\frac{2\Omega}{\eta}-1)^{\frac{q-2s}{2}}}{(\frac{q-2s}{2})!} & , p, q, \text{ are both even}; \\[2em] \sum_s^{(\mathrm{Min}[p,q]-1)/2} \sqrt{\pi}p!q!\frac{(\frac{4}{\eta}\sqrt{\omega_y\Omega})^{2s+1}}{(2s+1)!}\frac{(\frac{2\omega_y}{\eta}-1)^{\frac{p-2s-1}{2}}}{(\frac{p-2s-1}{2})!}\frac{(\frac{2\Omega}{\eta}-1)^{\frac{q-2s-1}{2}}}{(\frac{q-2s-1}{2})!} & , p, q, \text{ are both odd}; \\[2em] 0 & , p + q \text{ is odd}. \end{cases}$$

$$= \sqrt{\frac{m!n!\sqrt{\omega_y\Omega}}{\eta}}\Lambda_n \exp(\frac{\xi^{\pm 2}}{\eta} - \beta y_0^2 - \frac{1}{2}\Omega\mathrm{Re}[\alpha_n]^2)$$

$$\times \sum_{p=0}^{m}\sum_{q=0}^{n}\frac{H_{m-p}\left[\frac{\sqrt{2\omega_y}}{\eta}(\beta y_0 \pm \frac{\Omega\alpha_n}{2})\right]}{2^{m-p}(m-p)!2^p}\frac{H_{n-q}\left[\frac{\sqrt{2\Omega}}{\eta}(\beta y_0 \mp \frac{\omega_y\alpha_n}{2} \mp \beta\alpha_n)\right]}{2^{n-q}(n-q)!2^q}$$

$$\times \begin{cases} \sum_s^{\mathrm{Min}[p,q]/2} f_{r1}(2s)\, f_{r2}(\frac{p-2s}{2})\, f_{r3}(\frac{q-2s}{2}) & , p, q, \text{ are both even}; \\[2em] \sum_s^{(\mathrm{Min}[p,q]-1)/2} f_{r1}(2s+1)\, f_{r2}(\frac{p-2s-1}{2})\, f_{r3}(\frac{q-2s-1}{2}) & , p, q, \text{ are both odd}; \\[2em] 0 & , p + q \text{ is odd}. \end{cases}$$

$$= \sqrt{\frac{m!n!\sqrt{\omega_y\Omega}}{\eta}}\Lambda_n \exp(\frac{\xi^{\pm 2}}{\eta} - \beta y_0^2 - \frac{1}{2}\Omega\mathrm{Re}[\alpha_n]^2)$$

$$\times \sum_{p=0}^{m}\sum_{q=0}^{n}\frac{\bar{H}_{m-p}\left[\frac{\sqrt{2\omega_y}}{\eta}(\beta y_0 \pm \frac{\Omega\alpha_n}{2})\right]}{2^p}\frac{\bar{H}_{n-q}\left[\frac{\sqrt{2\Omega}}{\eta}(\beta y_0 \mp \frac{\omega_y\alpha_n}{2} \mp \beta\alpha_n)\right]}{2^q}$$

$$\times \begin{cases} \sum_{s}^{\mathrm{Min}[p,q]/2} f_{r1}(2s)\, f_{r2}(\frac{p-2s}{2})\, f_{r3}(\frac{q-2s}{2}) & , p,q, \text{ are both even;} \\ \sum_{s}^{(\mathrm{Min}[p,q]-1)/2} f_{r1}(2s+1)\, f_{r2}(\frac{p-2s-1}{2})\, f_{r3}(\frac{q-2s-1}{2}) & , p,q, \text{ are both odd;} \\ 0 & , p+q \text{ is odd.} \end{cases} \quad \text{(A.40)}$$

and

$$\frac{\xi^{\pm 2}}{\eta} - \beta y_0^2 - \frac{1}{2}\Omega\mathrm{Re}[\alpha_n]^2 = -\frac{\Omega}{2}\mathrm{Re}[\alpha_n]^2(\frac{\omega_y + 2\beta}{2\eta}) - \frac{\Omega^2}{4\eta}\mathrm{Im}[\alpha_n]^2 - \beta y^2(\frac{\omega_y + \Omega}{2\eta}) + \frac{\beta\Omega\alpha_n}{\eta}y \tag{A.41}$$

where we define that

$$\eta = \frac{\omega_y + \Omega}{2} + \beta,\ \xi^{\pm} = \beta y_0 \pm \frac{\Omega\alpha_n}{2} \tag{A.42}$$

$$f_{r1}(n) = (\frac{4}{\eta}\sqrt{\omega_y\Omega})^n/n! \tag{A.43}$$

$$f_{r2}(n) = (\frac{2\omega_y}{\eta} - 1)^n/n! \tag{A.44}$$

$$f_{r3}(n) = (\frac{2\Omega}{\eta} - 1)^n/n! \tag{A.45}$$

The approach as $\beta \to \infty$, we have the limiting case of V_s is a Dirac delta function

$$\int_{-\infty}^{\infty} \phi_m^o(y)V_s(y)\phi_n^{\pm}(y)dy$$

$$\to e^{-\frac{1}{2}\omega_y y^2}H_m(\sqrt{\omega_y}y)e^{-\frac{\Omega}{2}(y\mp\alpha_n)^2}H_n(\sqrt{\Omega}(y\mp\alpha_n)) \cdot N_m^s N_n$$

$$= 2^{-\frac{m+n}{2}}(m!n!)^{-1/2}\frac{(\omega_y\Omega)^{1/4}}{\sqrt{\pi}}e^{-\frac{\Omega}{2}\mathrm{Im}[\alpha_n]^2}e^{-\frac{\omega_y}{2}y^2 - \frac{\Omega}{2}(y^2 + \alpha_n^2 \mp 2\alpha_n y)}H_m(\sqrt{\omega_y}y)H_n(\sqrt{\Omega}(y\mp\alpha_n)) \times \Lambda_n$$

$$= \sqrt{\frac{2^{m+n}}{m!n!}}\frac{(\omega_y\Omega)^{1/4}}{\sqrt{\pi}}e^{-\frac{1}{2}(\omega_y+\Omega)y^2 \pm \Omega\alpha_n y - \frac{\Omega}{2}\mathrm{Re}[\alpha_n]^2}\tilde{H}_m(\sqrt{\omega_y}y)\tilde{H}_n(\sqrt{\Omega}(y\mp\alpha_n)) \times \Lambda_n \tag{A.46}$$

A.5 $\int \phi_m^s(y)V_s(y)\phi_n^\pm(y)dy$

$$\int_{-\infty}^{\infty} \phi_m^s(y)V_s(y)\phi_n^\pm(y)dy$$
$$= N_m^s N_n V_0 \int e^{-\frac{1}{2}\Omega y^2} H_m(\sqrt{\Omega}y)e^{-(y-y_0)^2}e^{-\frac{1}{2}\Omega(y\mp\alpha_n)^2} H_n[\sqrt{\Omega}(y\mp\alpha_n)]. \quad (A.47)$$

The power of the exponential part:

$$-\frac{1}{2}\Omega y^2 - \beta(y-y_0)^2 - \frac{1}{2}\Omega(y\mp\alpha_n)^2$$
$$= -\frac{1}{2}\Omega y^2 - \beta y^2 + 2\beta y_0 y - \beta y_0^2 - \frac{\Omega}{2}y^2 \pm \Omega\alpha_n y - \frac{\Omega}{2}\alpha_n^2$$
$$= -(\Omega+\beta)y^2 + (2\beta y_0 \pm \Omega\alpha_n)y - \beta y_0^2 - \frac{\Omega}{2}\alpha_n^2$$

let $\eta = \Omega+\beta$; $\xi^\pm = 2\beta y_0 \mp \Omega\alpha_n = 2\beta y_0 \mp \frac{\omega_c}{\Omega}k_n$.

$$= -\eta\left[y^2 - \frac{\xi^\pm}{\eta}y + \left(\frac{\xi^\pm}{2\eta}\right)^2\right] + \frac{\xi^{\pm2}}{4\eta} - \beta y_0^2 - \frac{\Omega}{2}\alpha_n^2$$
$$= -\eta\left[y - \frac{\xi^\pm}{2\eta}\right]^2 + \frac{\xi^{\pm2}}{4\eta} - \beta y_0^2 - \frac{\Omega}{2}\alpha_n^2 \quad (A.48)$$
$$= -\eta\left[y - \frac{\xi^\pm}{2\eta}\right]^2 - \frac{1}{4\eta}\left\{2\beta\Omega(y_0\pm\alpha_n)^2 + 2\beta\Omega y_0^2 + \Omega^2\alpha_n^2\right\} \quad (A.49)$$

then:

$$\int_{-\infty}^{\infty} \phi_m^s(y) V_s(y) \phi_n^{\pm}(y) dy$$

$$= N_m^s N_n \, e^{\frac{\xi^{\pm 2}}{4\eta} - \beta y_0^2 - \frac{\Omega}{2}\alpha_n^2} \int \exp[-\eta \left(y - \frac{\xi^{\pm}}{2\eta}\right)^2] H_m(\sqrt{\Omega}y) H_n[\sqrt{\Omega}(y \mp \alpha_n)] dy \quad \text{(A.50)}$$

let $y' = y - \dfrac{\xi^{\pm}}{2\eta}$, then the integration became

$$= \sqrt{\frac{\Omega}{\pi}} 2^{-\frac{m+n}{2}} \frac{1}{\sqrt{m!n!}} e^{-\frac{\Omega}{2}\text{Im}[\alpha_n]^2} \Lambda_n e^{\frac{\xi^{\pm 2}}{4\eta} - \beta y_0^2 - \frac{\Omega}{2}\alpha_n^2}$$

$$\times \int e^{-\eta y'^2} H_m[\sqrt{\Omega}(y' + \frac{\xi^{\pm}}{2\eta})] H_n[\sqrt{\Omega}(y + \frac{\xi^{\pm}}{2\eta} \mp \alpha_n)] dy'$$

let $t = \sqrt{\eta}y'$; $dy' = \dfrac{dt}{\sqrt{\eta}}$.

$$= 2^{-\frac{m+n}{2}} \frac{1}{\sqrt{m!n!}} \Lambda_n \sqrt{\frac{\Omega}{\pi\eta}} e^{\frac{\xi^{\pm 2}}{4\eta} - \beta y_0^2 - \frac{\Omega}{2}\text{Re}[\alpha_n]^2}$$

$$\times \int e^{-t^2} H_m[\sqrt{\frac{\Omega}{\eta}}t + \frac{\sqrt{\Omega}\xi^{\pm}}{2\eta}] H_n[\sqrt{\frac{\Omega}{\eta}}t + \sqrt{\Omega}(\frac{\xi^{\pm}}{2\eta} \mp \alpha_n)] dt \quad \text{(A.51)}$$

and using this identity $H_n(x+y) = 2^{-n/2} \sum_{\kappa=0}^{n} \binom{n}{\kappa} H_{n-\kappa}(\sqrt{2}x) H_\kappa(\sqrt{2}y)$, Gradshteyn 8.958, we can get that the part of the integration become

$$2^{-\frac{m+n}{2}} \sum_{p=0}^{m} \binom{m}{p} H_{m-p}\left(\frac{\sqrt{2\Omega}\xi^{\pm}}{2\eta}\right) \sum_{q=0}^{n} \binom{n}{q} H_{n-q}\left(\sqrt{2\Omega}(\frac{\xi^{\pm}}{2\eta} \mp \alpha_n)\right)$$

$$\times \int e^{-t^2} H_p\left(\sqrt{\frac{2\Omega}{\eta}}t\right) H_q\left(\sqrt{\frac{2\Omega}{\eta}}t\right) dt$$

$$= 2^{-\frac{m+n}{2}} \sqrt{\pi} \sum_{p=0}^{m} \sum_{q=0}^{n} \binom{m}{p}\binom{n}{q} H_{m-p}\left(\frac{\sqrt{2\Omega}\xi^{\pm}}{2\eta}\right) H_{n-q}\left(\sqrt{2\Omega}(\frac{\xi^{\pm}}{2\eta} \mp \alpha_n)\right)$$

$$\times \sum_{k=0}^{\text{Min}[p,q]} 2^k k! \binom{p}{k}\binom{q}{k}\left(\frac{\beta-\Omega}{\beta+\Omega}\right)^{\frac{p+q}{2}-k} H_{p+q-2k}(0). \quad \text{(A.52)}$$

Then we obtain

$$\int_{-\infty}^{\infty} \phi_m^s(y) V_s(y) \phi_n^{\pm}(y) dy$$

$$= 2^{-\frac{m+n}{2}} \frac{1}{\sqrt{m!n!}} \Lambda_n \sqrt{\frac{\Omega}{\pi\eta}} e^{\frac{\xi^{\pm 2}}{4\eta} - \beta y_0^2 - \frac{\Omega}{2} \text{Re}[\alpha_n]^2}$$

$$\times \int e^{-t^2} H_m[\sqrt{\frac{\Omega}{\eta}} t + \frac{\sqrt{\Omega}\xi^{\pm}}{2\eta})] H_n[\sqrt{\frac{\Omega}{\eta}} t + \sqrt{\Omega}(\frac{\xi^{\pm}}{2\eta} \mp \alpha_n)] dt$$

$$= 2^{-(m+n)} \frac{1}{\sqrt{m!n!}} \Lambda_n \sqrt{\frac{\Omega}{\eta}} e^{\frac{\xi^{\pm 2}}{4\eta} - \beta y_0^2 - \frac{\Omega}{2} \text{Re}[\alpha_n]^2}$$

$$\times \sum_{p=0}^{m} \sum_{q=0}^{n} \binom{m}{p} \binom{n}{q} H_{m-p} \left(\frac{\sqrt{2\Omega}\xi^{\pm}}{2\eta} \right) H_{n-q} \left(\sqrt{2\Omega}(\frac{\xi^{\pm}}{2\eta} \mp \alpha_n) \right)$$

$$\times \sum_{k=0}^{\text{Min}[p,q]} 2^k k! \binom{p}{k} \binom{q}{k} \left(\frac{\beta - \Omega}{\beta + \Omega} \right)^{\frac{p+q}{2} - k} H_{p+q-2k}(0).$$

$$= \Lambda_n \sqrt{\frac{\Omega}{\eta}} e^{\frac{\xi^{\pm 2}}{4\eta} - \beta y_0^2 - \frac{\Omega}{2} \text{Re}[\alpha_n]^2} \sum_{p=0}^{m} \sum_{q=0}^{n} H_{m-p} \left(\frac{\sqrt{2\Omega}\xi^{\pm}}{2\eta} \right) H_{n-q} \left(\sqrt{2\Omega}(\frac{\xi^{\pm}}{2\eta} \mp \alpha_n) \right)$$

$$\times \sum_{k=0}^{\text{Min}[p,q]} 2^{k-m-n} \frac{\sqrt{m!n!}}{(m-p)!(p-k)!(n-q)!(q-k)!k!} \left(\frac{\beta - \Omega}{\beta + \Omega} \right)^{\frac{p+q}{2} - k} H_{p+q-2k}(0).$$

$$= \Lambda_n \sqrt{\frac{\Omega}{\eta}} e^{\frac{\xi^{\pm 2}}{4\eta} - \beta y_0^2 - \frac{\Omega}{2} \text{Re}[\alpha_n]^2} \sum_{p=0}^{m} \sum_{q=0}^{n} \frac{2^{p-m}}{(m-p)!} H_{m-p} \left(\frac{\sqrt{2\Omega}\xi^{\pm}}{2\eta} \right) \frac{2^{q-n}}{(n-q)!} H_{n-q} \left(\sqrt{2\Omega}(\frac{\xi^{\pm}}{2\eta} \mp \alpha_n) \right)$$

$$\times \sum_{\kappa=0}^{\text{Min}[p,q]} 2^{-\kappa} \frac{\sqrt{m!n!}}{(p-\kappa)!(q-\kappa)!\kappa!} \left(\frac{\beta - \Omega}{\beta + \Omega} \right)^{\frac{p+q}{2} - k} 2^{2\kappa - p - q} H_{p+q-2\kappa}(0). \tag{A.53}$$

And finally we have

$$\int_{-\infty}^{\infty} \phi_m^s(y) V_s(y) \phi_n^{\pm}(y) dy$$

$$= \Lambda_n \sqrt{\frac{\Omega}{\eta}} \, e^{\frac{\xi^{\pm 2}}{4\eta} - \beta y_0^2 - \frac{\Omega}{2} \text{Re}[\alpha_n]^2} \times \sum_{p=0}^{m} \sum_{q=0}^{n} \bar{H}_{m-p} \left(\frac{\sqrt{2\Omega}\xi^{\pm}}{2\eta} \right) \bar{H}_{n-q} \left(\sqrt{2\Omega}(\frac{\xi^{\pm}}{2\eta} \mp \alpha_n) \right)$$

$$\times \sum_{\kappa=0}^{\text{Min}[p,q]} 2^{-\kappa} \tilde{H}_{p+q-2\kappa}(0) \left(\frac{\beta - \Omega}{\beta + \Omega} \right)^{\frac{p+q}{2} - k} \frac{\sqrt{m!n!}}{(p-\kappa)!(q-\kappa)!\kappa!}. \tag{A.54}$$

A.6 $\int \phi_m^{\pm *}(y) V_s(y) \phi_n^{\pm}(y) dy$

$$\int_{-\infty}^{\infty} \phi_m^{\pm *}(y) V_s(y) \phi_n^{\pm}(y) dy$$

$$= \sqrt{\frac{\beta}{\pi}} V_0 N_m N_n \int e^{-\frac{\Omega}{2}(y \mp \alpha_m^*)^2} H_m^* \left[\sqrt{\Omega}(y \mp \alpha_m) \right] e^{-\beta(y-y_0)^2} e^{-\frac{\Omega}{2}(y \mp \alpha_n)^2} H_n \left[\sqrt{\Omega}(y \mp \alpha_n) \right] dy \tag{A.55}$$

The exponetial part:

$$-\Omega \{ \frac{1}{2}(y^2 + \alpha_m^{*\,2} \mp 2\alpha_m^* y) + \frac{1}{2}(y^2 + \alpha_n{}^2 \mp 2\alpha_n y) + \frac{\beta}{\Omega}(y^2 + y_0^2 - 2y_0 y) \}$$

$$= -\{ y^2(\Omega + \beta) - y \left[\Omega(\pm \alpha_m^* \pm \alpha_n) + 2\beta y_0 \right] + \frac{\Omega}{2}(\alpha_m^{*\,2} + \alpha_n^2) + \beta y_0^2 \}$$

$$\text{let } \eta = \Omega + \beta, \ \xi^{\pm\pm} = \Omega(\pm \alpha_m^* \pm \alpha_n) + 2\beta y_0,$$

$$= -\eta \{ y^2 - y \frac{\xi^{\pm\pm}}{\eta} + \left(\frac{\xi^{\pm\pm}}{2\eta} \right)^2 \} + \frac{\xi^{\pm\pm 2}}{4\eta} - \frac{\Omega}{2}(\alpha_m^{*\,2} + \alpha_n^2) - \beta y_0^2$$

$$= -\eta \left(y - \frac{\xi^{\pm\pm}}{2\eta} \right)^2 + \{ \frac{\xi^{\pm\pm 2}}{4\eta} - \frac{\Omega}{2}(\alpha_m^{*\,2} + \alpha_n^2) - \beta y_0^2 \} \tag{A.56}$$

The Hermite part:

$$H_m \left[\sqrt{\Omega}(y \mp \alpha_m^*)\right] H_n \left[\sqrt{\Omega}(y \mp \alpha_n)\right]$$

$$= 2^{-\frac{m}{2}} \sum_{p=0}^{m} \binom{m}{p} H_{m-p}(\mp\sqrt{2\Omega}\alpha_m^*) H_p(\sqrt{2\Omega}y) \times 2^{-\frac{n}{2}} \sum_{q=0}^{n} \binom{n}{q} H_{n-q}(\mp\sqrt{2\Omega}\alpha_n) H_q(\sqrt{2\Omega}y)$$

$$= 2^{-\frac{m+n}{2}} \sum_{p=0}^{m} \sum_{q=0}^{n} \binom{m}{p} \binom{n}{q} H_{m-p}(\mp\sqrt{2\Omega}\alpha_m^*) H_{n-q}(\mp\sqrt{2\Omega}\alpha_n) H_p(\sqrt{2\Omega}y) H_q(\sqrt{2\Omega}y) \quad (A.57)$$

$$\Rightarrow \int_{-\infty}^{\infty} \phi_m^{\pm *}(y) V_s(y) \phi_n^{\pm}(y) dy$$

$$= \sqrt{\frac{\beta}{\pi}} V_0 N_m N_n \exp[\frac{\xi^{\pm\pm 2}}{4\eta} - \frac{\Omega}{2}(\alpha_m^{* \, 2} + \alpha_n^2) - \beta y_0^2]$$

$$\times 2^{-\frac{m+n}{2}} \sum_{p=0}^{m} \sum_{q=0}^{n} \binom{m}{p} \binom{n}{q} H_{m-p}(\mp\sqrt{2\Omega}\alpha_m^*) H_{n-q}(\mp\sqrt{2\Omega}\alpha_n)$$

$$\times \int e^{-\eta(y - \frac{\xi^{\pm\pm}}{2\eta})^2} H_p(\sqrt{2\Omega}y) H_q(\sqrt{2\Omega}y) dy \quad (A.58)$$

and the integration part in the above equation:

$$\int e^{-\eta(y - \frac{\xi^{\pm\pm}}{2\eta})^2} H_p(\sqrt{2\Omega}y) H_q(\sqrt{2\Omega}y) dy \quad \text{let } \sqrt{\eta}y = t,$$

$$= \int e^{-(t - \frac{\xi^{\pm\pm}}{2\sqrt{\eta}})^2} H_p(\sqrt{\frac{2\Omega}{\eta}}y) H_q(\sqrt{\frac{2\Omega}{\eta}}y) \frac{dt}{\sqrt{\eta}}$$

$$= \sqrt{\frac{\pi}{\eta}} \sum_{\kappa=0}^{\text{Min}(p,q)} 2^{\kappa} \kappa! \binom{p}{\kappa} \binom{q}{\kappa} \left(\frac{\beta - \Omega}{\beta + \Omega}\right)^{\frac{p+q}{2} - \kappa} H_{p+q-2\kappa} \left(\frac{\sqrt{\Omega}\xi^{\pm\pm}}{\sqrt{2(\beta^2 - \Omega^2)}}\right) \quad (A.59)$$

by using this identity, Gradshteyn 7.374.9 ,

$$\int_{-\infty}^{\infty} e^{-(x-y)^2} H_m(\alpha x) H_n(\alpha x) dx = \sqrt{\pi} \sum_{\kappa=0}^{\text{Min}(m,n)} 2^{\kappa} \kappa! \binom{m}{\kappa} \binom{n}{\kappa} \left(1 - \alpha^2\right)^{\frac{m+n}{2} - \kappa} H_{m+n-2\kappa} \left[\frac{\alpha y}{(1 - \alpha^2)^{1/2}}\right].$$
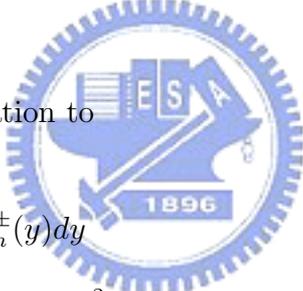
$$(A.60)$$

APPENDIX A. DETAIL OF THE INTEGRATIONS

And then we could obtain

$$
\int_{-\infty}^{\infty} \phi_m^{\pm\,*}(y)V_s(y)\phi_n^{\pm}(y)dy
$$

$$
= \sqrt{\frac{\beta}{\pi}}V_0 N_m N_n \sqrt{\frac{\pi}{\eta}}\; e^{\frac{\xi^{\pm\pm\,2}}{4\eta}-\frac{\Omega}{2}(\alpha_m^{*\,2}+\alpha_n^2)-\beta y_0^2}
$$

$$
\times 2^{-\frac{m+n}{2}}\sum_{p=0}^{m}\sum_{q=0}^{n}\binom{m}{p}\binom{n}{q}H_{m-p}(\mp\sqrt{2\Omega}\alpha_m^*)H_{n-q}(\mp\sqrt{2\Omega}\alpha_n)
$$

$$
\times \sum_{\kappa=0}^{\text{Min}(p,q)} 2^{\kappa}\kappa!\binom{p}{\kappa}\binom{q}{\kappa}\left(\frac{\beta-\Omega}{\beta+\Omega}\right)^{\frac{p+q}{2}-\kappa} H_{p+q-2\kappa}\left(\frac{\sqrt{\Omega}\xi^{\pm\pm}}{\sqrt{2(\beta^2-\Omega^2)}}\right) \quad \text{(A.61)}
$$

where $\eta = \Omega + \beta$, $\xi^{\pm\pm} = \Omega(\pm\alpha_m^* \pm \alpha_n) + 2\beta y_0$.

or we could simplify this equation to

$$
\int_{-\infty}^{\infty} \phi_m^{\pm\,*}(y)V_s(y)\phi_n^{\pm}(y)dy
$$

$$
= \sqrt{\frac{\beta}{\pi}}V_0\sqrt{\frac{\Omega}{\eta}}\Lambda_m \Lambda_n \exp[\frac{\xi^{\pm\pm\,2}}{4\eta}-\frac{\Omega}{2}(\text{Re}(\alpha_m)^2+\text{Re}(\alpha_n)^2)-\beta y_0^2]
$$

$$
\times \sum_{p=0}^{m}\sum_{q=0}^{n}\bar{H}_{m-p}(\mp\sqrt{2\Omega}\alpha_m^*)\bar{H}_{n-q}(\mp\sqrt{2\Omega}\alpha_n)
$$

$$
\times \sum_{\kappa=0}^{\text{Min}(p,q)} \frac{\sqrt{m!n!}}{\kappa!(p-\kappa)!(q-\kappa)!}\left(\frac{\beta-\Omega}{\beta+\Omega}\right)^{\frac{p+q}{2}-\kappa} 2^{-\kappa}\tilde{H}_{p+q-2\kappa}\left(\frac{\sqrt{\Omega}\xi^{\pm\pm}}{\sqrt{2(\beta^2-\Omega^2)}}\right)\text{(A.62)}
$$

A.7 $\quad \int y\phi_n^{\pm*}\phi_n^{\pm}dy = \pm\mathrm{Re}[\alpha_n]$

$$\int yN_n e^{-\frac{\Omega}{2}(y\mp\alpha_n^*)^2}H_n[\sqrt{\Omega}(y\mp\alpha_n^*)]\cdot N_n e^{-\frac{\Omega}{2}(y\mp\alpha_n)^2}H_n[\sqrt{\Omega}(y\mp\alpha_n)]dy$$

$$\text{let } x = \sqrt{\Omega}y,\ q_n = \sqrt{\Omega}\alpha_n$$

$$= \ N_n^2 \int \frac{dx}{\Omega}xe^{-\frac{1}{2}(x\mp q_n^*)^2-\frac{1}{2}(x\mp q_n)^2}H_n(x\mp q_n^*)H_n(x\mp q_n)$$

$$= \ N_n^2\frac{e^{-b^2}}{\Omega}\int xe^{-(x-\frac{a}{2})^2}H_n(x\mp q_n^*)H_n(x\mp q_n)dx$$

$$\text{let } a = \pm q_n^* \pm q_n;\ b = \frac{1}{2}[\pm q_n^* - (\pm q_n)]$$

$$= \ N_n^2\frac{e^{-b^2}}{\Omega}\int xe^{-x^2}H_n(x-b)H_n(x+b)dx + \frac{a}{2\sqrt{\Omega}}N_n^2\frac{e^{-b^2}}{\sqrt{\Omega}}\int e^{-x^2}H_n(x-b)H_n(x+b)dx$$

$$= \ \frac{a}{2\sqrt{\Omega}} = \frac{\sqrt{\Omega}}{2\sqrt{\Omega}}(\pm q_n^* \pm q_n) = \pm\frac{1}{2}(\alpha_n^* + \alpha_n)$$

$$= \ \pm\mathrm{Re}[\alpha_n] = \pm\frac{\omega_c\mathrm{Re}[k_n]}{\Omega^2} \tag{A.63}$$

where $\int xe^{-x^2}H_n(x-b)H_n(x+b)dx = 0$ and $N_n^2\frac{e^{-b^2}}{\sqrt{\Omega}}\int xe^{-x^2}H_n(x-b)H_n(x+b)dx = 1$.

$$\int xe^{-x^2}H_n(x-b)H_n(x+b)dx = \frac{-1}{2}\int H_n(x-b)H_n(x+b)d(e^{-x^2})$$

$$= \ \frac{-1}{2}\left\{H_n(x-b)H_n(x+b)e^{-x^2}\Big|_{-\infty}^{\infty} - \int e^{-x^2}d[H_n(x-b)H_n(x+b)]\right\}$$

$$= \ \frac{n}{2}\left\{\int e^{-x^2}H_n(x-b)H_{n-1}(x+b)dx + \int e^{-x^2}H_n(x+b)H_{n-1}(x-b)dx\right\}$$

$$= \ 0 \tag{A.64}$$

$$\text{and} \quad \int e^{-x^2}H_n(x-b)H_{n-1}(x+b)dx = 2^n n!\sqrt{\pi}\sum_{k=0}^{n-1}\frac{(-2b^2)^{n-k}}{2b}\frac{n!(n-k)}{k!(n-k)!^2 n}$$

$$\int e^{-x^2}H_n(x+b)H_{n-1}(x-b)dx = 2^n n!\sqrt{\pi}\sum_{k=0}^{n-1}\frac{(-2b^2)^{n-k}}{-2b}\frac{n!(n-k)}{k!(n-k)!^2 n}$$

$$= \ -\int e^{-x^2}H_n(x-b)H_{n-1}(x+b)dx \tag{A.65}$$

A.8 $\displaystyle\int_{-\infty}^{\infty} \phi_m^{o\,*}(y)V_s(y)\phi_n^o(y)dy$

$$\int_{-\infty}^{\infty} \phi_m^{o\,*}(y)V_s(y)\phi_n^o(y)dy$$

$$= \quad (2^m m! 2^n n! \frac{\pi}{\omega_y})^{-1/2} \int e^{-\frac{\omega_y}{2}y^2} H_m(\sqrt{\omega_y}y) e^{-\beta(y-y_0)^2} e^{-\frac{\omega_y}{2}y^2} H_n(\sqrt{\omega_y}y)dy$$

$$= \quad N_m N_n \int e^{-\omega_y y^2 - \beta(y-y_0)^2} H_m(\sqrt{\omega_y}y) H_n(\sqrt{\omega_y}y)dy$$

$$\text{let } \ t^2 = (\omega_y + \beta)y^2, \ y = \frac{t}{\sqrt{\omega_y + \beta}}$$

$$\text{and the expential part}: \ -\omega_y y^2 - \beta(y-y_0)^2 = -(t - \frac{\beta y_0}{\sqrt{\omega_y + \beta}})^2 - \frac{\beta \omega_y}{\omega_y + \beta}$$

$$= \quad N_m N_n e^{\frac{-\beta \omega_y}{\omega_y + \beta}y_0^2} \int e^{-(t-\frac{\beta y_0}{\sqrt{\omega_y+\beta}})^2} H_m(\sqrt{\frac{\omega_y}{\omega_y + \beta}}t) H_n(\sqrt{\frac{\omega_y}{\omega_y + \beta}}t) \frac{dt}{\sqrt{\omega_y + \beta}} \qquad \text{(A.66)}$$

Using this mathematic relation

$$\int_{-\infty}^{\infty} e^{-(x-y)^2} H_m(\alpha x) H_n(\alpha x)dx$$

$$= \quad \pi^{1/2} \sum_{\kappa=0}^{\text{Min}[m,n]} 2^\kappa \kappa! \binom{m}{\kappa}\binom{n}{\kappa}(1-\kappa^2)^{\frac{m+n}{2}-\kappa} H_{m+n-2\kappa}\left[\frac{\alpha y}{(1-\alpha^2)^{1/2}}\right] \qquad \text{(A.67)}$$

We have

$$
\int_{-\infty}^{\infty} \phi_m^{o\,*}(y) V_s(y) \phi_n^o(y) dy
$$

$$
= \sqrt{\frac{1}{2^{m+n} m! n!}} \sqrt{\frac{\omega_y}{\omega_y \beta}} e^{-\frac{\beta \omega_y}{\omega_y + \beta} y_0^2}
$$

$$
\times \sum_{\kappa=0}^{\mathrm{Min}[m,n]} 2^{\kappa} \frac{m! n!}{(m-\kappa)!(n-\kappa)!\kappa!} \left(\frac{\beta}{\omega_y + \beta}\right)^{\frac{m+n}{2}-\kappa} H_{m+n-\kappa} \left[\sqrt{\frac{\omega_y \beta}{\omega_y + \beta}} y_0 \right]
$$

$$
= \sqrt{\frac{m! n!}{2^m 2^n}} \sqrt{\frac{\omega_y}{\omega_y + \beta}} e^{-a^2} \sum_{\kappa=0}^{\mathrm{Min}[m,n]} \frac{2^{\kappa}}{\kappa!} \frac{\left(\frac{\beta}{\omega_y + \beta}\right)^{m-\kappa}}{m-\kappa} \frac{\left(\frac{\beta}{\omega_y + \beta}\right)^{n-\kappa}}{n-\kappa} H_{m+n-\kappa}[a] \qquad (A.68)
$$

$$
\text{where } a = \sqrt{\frac{\beta \omega_y}{\omega_y + \beta}} y_0. \qquad (A.69)
$$

A.9   Recurrence relations of Hermite polynomial

In order to get the better accuracy in numerial analysis,

We change the $H_n(x)$ in the calculation to $\tilde{H}_n(x)$, where $\tilde{H}_n(x) = 2^{-n} H_n(x)$.

$$
H_0(x) = 1, \ H_1(x) = 2x,
$$

$$
H_{n+1}(x) - 2x H_n(x) + 2n H_{n-1}(x) = 0,
$$

$$
H_n(x) - 2x H_{n-1}(x) + 2(n-1) H_{n-2}(x) = 0,
$$

$$
2^{-n} H_n(x) - 2^{-(n-1)} x H_{n-1}(x) + 2^{-(n-1)}(n-1) H_{n-2}(x) = 0,
$$

$$
\Rightarrow \quad \tilde{H}_n(x) - x \tilde{H}_{n-1}(x) + \frac{n-1}{2} \tilde{H}_{n-2}(x) = 0, \qquad (A.70)
$$

$$
\text{and } \tilde{H}_0(x) = 1, \ \tilde{H}_1(x) = 2^{-1} H_1(x) = x,
$$

$$
\text{where } \tilde{H}_n(x) = 2^{-n} H_n(x).
$$

or

$$\frac{H_n(x)}{2^n} - \frac{x H_{n-1}(x)}{2^{n-1}} + \frac{(n-1)H_{n-2}(x)}{2 \cdot 2^{n-2}} = 0$$

$$\frac{H_n(x)}{2^n n!} - \frac{x}{n}\frac{H_{n-1}(x)}{2^{n-1}(n-1)!} + \frac{1}{2n}\frac{H_{n-2}(x)}{2^{n-2}(n-2)!} = 0$$

let $\bar{H}_n(x) \equiv \dfrac{H_n(x)}{2^n n!}$, and then, we have

$$\bar{H}_n(x) - \frac{x}{n}\bar{H}_{n-1}(x) + \frac{1}{2n}\bar{H}_{n-2}(x) = 0$$

and $\bar{H}_0(x) = 1$, $\bar{H}_1(x) = \dfrac{H_1(x)}{2^1 1!} = x$.
$$\tag{A.71}$$

A.10 $\int e^{-x^2} H_m(ax) H_n(bx) dx$

$$\int e^{-x^2} H_m(ax) H_n(bx) dx = \begin{cases} \text{m + n is even. m, n are both even.} \\ \sum\limits_{s}^{Min[m,n]/2} \frac{(2ab)^{2s}\sqrt{\pi}m!n!(a^2-1)^{\frac{m-2s}{2}}(b^2-1)^{\frac{n-2s}{2}}}{(\frac{m-2s}{2})!(\frac{n-2s}{2})!(2s)!} \\ \text{m + n is even. m, n are both odd.} \\ \sum\limits_{s}^{(Min[m,n]-1)/2} \frac{(2ab)^{2s+1}\sqrt{\pi}m!n!(a^2-1)^{\frac{m-2s-1}{2}}(b^2-1)^{\frac{n-2s-1}{2}}}{(\frac{m-2s-1}{2})!(\frac{n-2s-1}{2})!(2s+1)!} \\ \text{m + n is odd.} \\ 0 \end{cases} \tag{A.72}$$

Using the definition of Hermite polynomial function

$$e^{-t^2+2tx} = \sum_{k=0}^{\infty} \frac{t^k}{k!} H_k(x) \tag{A.73}$$

and we has this relation:

$$e^{-x^2} e^{-t^2+2tax} e^{-u^2+2ubx} = e^{-x^2} \sum_{m=0}^{\infty} \frac{t^m}{m!} H_m(ax) \sum_{n=0}^{\infty} \frac{t^n}{n!} H_n(bx) \tag{A.74}$$

Integrate over x, and we obtain:

$$\sum_{m,n=0}^{\infty} \frac{t^m u^n}{m!n!} \int e^{-x^2} H_m(ax) H_n(bx) dx = e^{-t^2-u^2} \int e^{-x^2+2tax+2ubx} dx \tag{A.75}$$

118

APPENDIX A. DETAIL OF THE INTEGRATIONS

The exponential part can be simplified to:

$$-x^2 + 2tax + 2ubx = -[x^2 - 2(ta+ub)x + (ta+ub)^2 - (ta+ub)^2]$$

$$= -[x - (ta+ub)]^2 + (ta+ub)^2$$

And then Eq. (A.75) become

$$e^{-t^2-u^2+(ta+ub)^2} \int_{-\infty}^{\infty} e^{-(x-(ta-ub))^2} dx$$

which the integration part is a error function and equal to $\sqrt{\pi}$.

$$= \sqrt{\pi} e^{-t^2-u^2+(ta+ub)^2}$$

$$= \sqrt{\pi} e^{t^2(a^2-1)+u^2(b^2-1)+2taub}$$

using the series expansion $e^x = \sum_{k=0}^{\infty} \frac{x^k}{k!}$

$$= \sqrt{\pi} \sum_{p=0}^{\infty} \frac{t^{2p}(a^2-1)^p}{p!} \sum_{q=0}^{\infty} \frac{t^{2q}(b^2-1)^q}{q!} \sum_{r=0}^{\infty} \frac{t^r u^r (2ab)^r}{r!}$$

$$= \sqrt{\pi} \sum_{p,q,r} \frac{t^{2p+r}u^{2q+r}(a^2-1)^p(b^2-1)^q(2ab)^r}{p!q!r!} \tag{A.76}$$

Then we have to reduce the parameter 'p, q, r' to 'm, n'.

Let
$$\begin{cases} m = 2p+r, \quad p = \frac{m-r}{2}, \\ n = 2q+r, \quad q = \frac{n-r}{2}, \end{cases} \quad r < \text{MIN}[m,n]$$

and $m+n = 2p+2q+2r = 2(p+q+r) \rightarrow m+n$ is even,

$$m-r = 2p \qquad \rightarrow m-r \text{ is even,}$$

$$n-r = 2q \qquad \rightarrow n-r \text{ is even.}$$

There are three case satisfied the conditions

119

1) m+n is even; m,n are both even; and r → even.

$$\text{Eq. (A.76)} = \sum_{m,n=0}^{\infty} \sum_{r}^{\text{MIN[m,n]}} \frac{t^m u^n}{m!n!} \frac{(2ab)^r m!n!(a^2-1)^{\frac{m-r}{2}}(b^2-1)^{\frac{n-r}{2}}}{(\frac{m-r}{2})!(\frac{n-r}{2})!r!}$$

let $r = 2s$,

$$= \sum_{m,n=0}^{\infty} \sum_{s}^{\text{MIN[m,n]}/2} \frac{t^m u^n}{m!n!} \frac{(2ab)^{2s} m!n!(a^2-1)^{\frac{m-2s}{2}}(b^2-1)^{\frac{n-2s}{2}}}{(\frac{m-2s}{2})!(\frac{n-2s}{2})!(2s)!}$$

2) m+n is even; m,n are both odd; and r → odd. Let r=2s+1.

$$\text{Eq. (A.76)} = \sum_{m,n=0}^{\infty} \sum_{s}^{(\text{MIN[m,n]}-1)/2} \frac{t^m u^n}{m!n!} \frac{(2ab)^{2s+1} m!n!(a^2-1)^{\frac{m-2s-1}{2}}(b^2-1)^{\frac{n-2s-1}{2}}}{(\frac{m-2s-1}{2})!(\frac{n-2s-1}{2})!(2s+1)!}$$

3) m+n is odd.

$$\text{Eq. (A.76)} = 0.$$

Finally we have

$$\int e^{-x^2} H_m(ax) H_n(bx) dx$$

$$= \begin{cases} \sum_{s}^{\text{MIN[m,n]}/2} \frac{(2ab)^{2s} m!n!(a^2-1)^{\frac{m-2s}{2}}(b^2-1)^{\frac{n-2s}{2}}}{(\frac{m-2s}{2})!(\frac{n-2s}{2})!(2s)!} & ; m, n \text{ are both even.} \\ \sum_{s}^{(\text{MIN[m,n]}-1)/2} \frac{(2ab)^{2s+1} m!n!(a^2-1)^{\frac{m-2s-1}{2}}(b^2-1)^{\frac{n-2s-1}{2}}}{(\frac{m-2s-1}{2})!(\frac{n-2s-1}{2})!(2s+1)!} & ; m, n \text{ are both odd.} \\ 0 & ; m+n \text{ is odd.} \end{cases} \quad (A.77)$$

A.11 $\int e^{-x^2} H_m(x+a) H_n(x+b) dx$

Proof of Mathematic equation

$$\int_{-\infty}^{\infty} e^{-x^2} H_m(x+a) H_n(x+b) dx = \sum_{p=0}^{\text{Min}(m,n)} 2^{m+n-p} a^{m-p} b^{n-p} \frac{\sqrt{\pi} m!n!}{p!(m-p)!(n-p)!} \quad (A.78)$$

Using the definition of Hermite polynomial $e^{2xt-t^2} = \sum_{n=0}^{\infty} \frac{H_n(x)}{n!} t^n$ and we can have this

relation:

$$e^{-x^2}e^{2(x+a)t-t^2}e^{2(x+b)u-u^2} = \sum_{n=0}^{\infty}\sum_{n=0}^{\infty}e^{-x^2}\frac{H_m(x+a)}{m!}t^m\frac{H_n(x+b)}{n!}u^n \qquad (A.79)$$

And integrate over x, we can obtain

$$\sum_{n=0}^{\infty}\sum_{n=0}^{\infty}\frac{t^m}{m!}\frac{u^n}{n!}\int e^{-x^2}H_m(x+a)H_n(x+b)dx$$

$$= e^{-t^2-u^2}\int e^{-x^2+2(x+a)t+2(x+b)u}dx$$

$$= e^{-t^2-u^2+2at+2bu}\int e^{-x^2+2xt+2xu}dx$$

$$= e^{-t^2-u^2+2at+2bu+(t+u)^2}\int e^{-(x-(t+u))^2}dx$$

$$= e^{2at+2bu+2tu}\sqrt{\pi} \qquad (A.80)$$

$$\text{where } \int_{-\infty}^{\infty}e^{-(x-(t+u))^2}dx = \int_{-\infty}^{\infty}e^{-x^2}dx = \sqrt{\pi}$$

$$\text{and } -t^2-u^2+2at+2bu+(t+u)^2 = 2at+2bu+2tu$$

$$e^{2at+2bu+2tu}$$

$$= \sum_{p}^{\infty}\frac{2^p(tu)^p}{p!}\sum_{q}^{\infty}\frac{2^q(at)^q}{q!}\sum_{r}^{\infty}\frac{2^r(bu)^r}{r!}$$

$$= \sum_{p,q,r}^{\infty}\frac{2^{p+q+r}a^qb^rt^{p+q}u^{p+r}}{p!q!r!} \qquad (A.81)$$

$$\text{Let } m = p+q, \ n = p+r.$$

$$= \sum_{m,n}^{\infty}\sum_{p=0}^{\text{Min}[m,n]}\frac{2^{m+n-p}a^{m-p}b^{n-p}t^mu^n}{p!(m-p)!(n-p)!} \qquad (A.82)$$

Finally we have

$$\int_{-\infty}^{\infty}e^{-x^2}H_m(x+a)H_n(x+b) = \sum_{p=0}^{\text{Min}[m,n]}2^{m+n-p}a^{m-p}b^{n-p}\frac{m!n!\sqrt{\pi}}{p!(m-p)!(n-p)!} \qquad (A.83)$$

A.12 $\quad \int e^{-(x-y)^2} H_m(\alpha x) H_n(\alpha x) dx$

Proof of Mathematic equation

$$
\int\limits_{-\infty}^{\infty} e^{-(x-y)^2} H_m(\alpha x) H_n(\alpha x) dx
$$

$$
= \sum_{c=0}^{\text{Min}[m,n]} \sum_{a=0}^{(m-c)/2} \sum_{b=0}^{(n-c)/2} m! n! \sqrt{\pi} \frac{(\alpha^2-1)^a}{a!} \frac{(\alpha^2-1)^b}{b!} \frac{(2\alpha^2)^2}{c!} \frac{(2\alpha y)^{m-2a-c}}{(m-2a-c)!} \frac{(2\alpha y)^{m-2b-c}}{(m-2b-c)!}
$$

$$
\text{(A.84)}
$$

Using the definition of Hermite polynomial $e^{2xt-t^2} = \sum_{n=0}^{\infty} \frac{H_n(x)}{n!} t^n$ and we can have this relation:

$$
\int \sum_{m=0}^{\infty} \frac{H_m(x)}{m!} s^m \sum_{n=0}^{\infty} \frac{H_n(x)}{n!} t^n e^{-(x-y)^2} dx
$$

$$
= \sum_{m=0}^{\infty} \sum_{n=0}^{\infty} \frac{s^m}{m!} \frac{t^n}{n!} \int e^{-(x-y)^2} H_m(\alpha x) H_n(\alpha x) dx = \int e^{-s^2+2s\alpha x} e^{-t^2+2t\alpha x} e^{-(x-y)^2} dx
$$

$$
= e^{-s^2-t^2-y^2} \int e^{2s\alpha x+2t\alpha x-x^2+2xy} dx = e^{-s^2-t^2-y^2+(s\alpha+t\alpha+y)^2} \int e^{-(x-a)^2} dx
$$

$$
= \sqrt{\pi} e^{-s^2-t^2-y^2+(s\alpha+t\alpha+y)^2} \qquad \text{(A.85)}
$$

the exponential part of the Eq. (A.85) could be simplify to:

$$
-s^2 - t^2 - y^2 + (s\alpha+t\alpha+y)^2 = (\alpha^2-1)s^2 + (\alpha^2-1)t^2 + 2\alpha^2 st + 2\alpha ty + 2\alpha sy \quad \text{(A.86)}
$$

and using the series expansion of $e^x = \sum_{k=0}^{\infty} \frac{x^k}{k!}$

$$e^{(\alpha^2-1)s^2+(\alpha^2-1)t^2+2\alpha^2 st+2\alpha ty+2\alpha sy}$$

$$= \sum_{a=0}^{\infty} \frac{(\alpha^2-1)^a s^{2a}}{a!} \sum_{b=0}^{\infty} \frac{(\alpha^2-1)^b t^{2b}}{b!} \sum_{c=0}^{\infty} \frac{2^c \alpha^{2c} s^c t^c}{c!} \sum_{c=0}^{\infty} \frac{2^d \alpha^d t^d y^d}{d!} \sum_{c=0}^{\infty} \frac{2^f \alpha^f s^f y^f}{f!}$$

$$= \sum_{a,b,c,d,f} \frac{1}{a!b!c!d!f!} s^{2a+c+d} t^{2b+c+f} (\alpha^2-1)^{a+b} \alpha^{2c+d+f} y^{d+f} 2^{c+d+f}$$

$$\text{let} \begin{cases} m = 2a+c+d \\ n = 2b+c+f \end{cases}, \text{and} \begin{cases} d = m-2a-c \\ f = n-2b-c \end{cases}. \tag{A.87}$$

$$= \frac{s^m}{m!} \frac{t^n}{n!} \sum_{a,b,c,m-2a-c,n-2b-c} \frac{m!n!(\alpha^2-1)^{a+b} \alpha^{m+n-2a-2b} y^{m+n-2a-2b-2c} 2^{m+n-2a-2b}}{a!b!c!(m-2a-c)!(n-2a-c)!}$$

$$\tag{A.88}$$

we have:

$$\begin{cases} d = m-2a-c \in N \ge 0 \\ f = n-2b-c \in N \ge 0 \end{cases} \Rightarrow \begin{cases} m \ge 2a+c \\ n \ge 2b+c \end{cases} \Rightarrow \begin{cases} m \ge c, & m-c \ge 2a, & \frac{m-c}{2} \ge a \\ n \ge c, & n-c \ge 2b, & \frac{n-c}{2} \ge b \end{cases}.$$

$$\tag{A.89}$$

Here we confine the range of c first, and then we can also know the range of a and b.

$$\sum_{a,b,c,m-2a-c,n-2b-c}^{\infty} = \sum_{m=0}^{\infty} \sum_{n=0}^{\infty} \sum_{c=0}^{\text{Min}[m,n]} \sum_{a=0}^{(m-c)/2} \sum_{b=0}^{(n-c)/2} \tag{A.90}$$

And finally we have:

$$\int e^{-(x-y)^2} H_m(\alpha x) H_n(\alpha x) dx$$

$$= \sum_{c=0}^{\text{Min}[m,n]} \sum_{a=0}^{(m-c)/2} \sum_{b=0}^{(n-c)/2} m!n!\sqrt{\pi} \frac{(\alpha^2-1)^a}{a!} \frac{(\alpha^2-1)^b}{b!} \frac{(2\alpha^2)^2}{c!} \frac{(2\alpha y)^{m-2a-c}}{(m-2a-c)!} \frac{(2\alpha y)^{m-2b-c}}{(m-2b-c)!}$$

$$\tag{A.91}$$

Bibliography

[1] H. van Houten, C. W. J. Beenakker, and B. J. van Wees, in Semiconductors and Semimetals, edited by M. A. Reed (Academic, New York, 1990), Vol. 35, p. 9.

[2] G. Timp, in Semiconductors and Semimetals, edited by M. A. Reed (Academic, New York, 1990), Vol. 35, p. 113.

[3] C. W. J. Beenakker and H. van Houten, in Solid State Physics: Advances in Research and Applications, edited by H. Ehrenreich and D. Turnbull (Academic, New York, 1992), Vol. 44, p. 1.

[4] Y. Hirayama, T. Saku and Y. Horikoshi, Phys. Rev. B 39, 5535 (1989).

[5] J. Faist, P. Guèret and H. Rothuizen, Phys. Rev. B 42, 3217 (1990).

[6] G. L. Timp and R. E. Howard, Proc. IEEE 79, 1188 (1991) .

[7] J. Masek and B. Kramer, Z. Phys. B 75, 37 (1989).

[8] J. Masek, P. Lipavsky and B. Kramer, J. Phys. Condens. Matter. 1, 6395 (1989).

[9] D. van Marel and E. G. Haanapel, Phys. Rev. B 39, 7811 (1989).

[10] P. L. McEuen, B. W. Alphenaar, R. G. Wheeler and R. N. Sacks, Surf. Sci. 229, 312 (1990).

[11] I. Kander, Y. Imry and U. Sivan, Phys. Rev. B 41, 12941 (1990).

[12] C. S. Chu and R. S. Sorbello, Phys. Rev. B 40, 5941 (1989).

[13] P. F. Bagwell, Phys. Rev. B 41, 10354 (1990).

[14] E. Tekman and S. Ciraci, Phys. Rev. B 42, 9098 (1990).

[15] A. Kumar and P. F. Bagwell, Phys. Rev. B 43, 9012 (1991).

[16] A. Kumar and P. F. Bagwell, Phys. Rev. B 44, 1747 (1991).

[17] A. Kumar and P. F. Bagwell, Solid State Commun. 75, 949 (1990).

[18] J. A. Nixon, J. H. Davies and H. U. Baranger, Phys. Rev. B 43, 12638 (1991).

[19] Y. B. Levinson, M. I. Lubin and E. V. Sukhorukov, Piśma Zh. Eksp. Teor. Fiz. 54, 405 (1991) [JETP Lett. 54, 401 (1991)].

[20] Y. B. Levinson, M. I. Lubin and E. V. Sukhorukov, Phys. Rev. B 45, 11936 (1992).

[21] M. W. Dellow, P. H. Beton, C. J. G. Langerak, T. J. Foster, P. C. Main, L. Eaves, M. Henini, S. P. Beamount, and C. D. W. Wilkinson, Phys. Rev. Lett. 68, 1754 (1992).

[22] M. Buttiker, Phys. Rev. B. 38,9375 (1988)

[23] K. v. Klitzing, G. Dorda, and M. Pepper, Phys. Rev. Lett. 45, 494 (1980).

[24] The Quantum Hall Effect, edited by P. R. Prange and S. M. Girvin (Springer-Verlag, New York, 1990).

[25] T. Chakraborty and P. Pietiläinen, The Quantum Hall Effects: Integral and Fractional (Springer-Verlag, Berlin, 1995).

[26] A. H. MacDonald, in Mesoscopic Quantum Physics, edited by E. Akkermans, G. Montambaux, J.-L. Pichard, and J. Zinn-Justin, Proceedings of the 1994 Les Houches Summer School, Session LXI (Elsevier, Amsterdam, 1995), p. 659.

[27] K. I. Wysokinski, Eur. J. Phys. 21, 535 (2000).

[28] T. Koma, Rev. Math. Phys. 16, 1115 (2004).

BIBLIOGRAPHY

[29] J. K. Jain and S. A. Kivelson, Phys. Rev. B 37, 4276 (1988).

[30] P. H. M. van Loosdrecht, C. W. J. Beenakker, H. van Houten, J. G. Williamson, B. J. van Wees, J. E. Mooij, C. T. Foxon, and J. J. Harris, Phys. Rev. B 38, 10162 (1988).

[31] F. M. Peeters, Phys. Rev. Lett. 61, 589 (1988).

[32] G. Kirczenow, Phys. Rev. Lett. 62, 1920 (1989); 62, 2993 (1989); Phys. Rev. B 42, 5357 (1990).

[33] D. G. Ravenhall, H. W. Wyld, and R. L. Schult, Phys. Rev. Lett. 62, 1780 (1989); R. L. Schult, H. W. Wyld, and D. G. Ravenhall, Phys. Rev. B 41, 12760 (1990).

[34] H. U. Baranger, D. P. DiVincenzo, R. A. Jalabert, and A. D. Stone, Phys. Rev. B 44, 10637 (1991).

[35] A. H. MacDonald and P. Streda, Phys. Rev. B 29, 1616 (1984).

[36] W. Zawadzki, Semicond. Sci. Technol. 2, 550 (1987);

[37] O. Z. Olendskii, Fiz. Tverd. Tela (S.-Peterburg) 34, 3087 (1992) [Sov. Phys. Solid State 34, 1653 (1992)].

[38] C. S. Kim and O. Olendski, Appl. Phys. Lett. 69, 2575 (1996); Semicond. Sci. Technol. 12, 788 (1997).

[39] U. Fano, Phys. Rev. 124, 1866 (1961).

[40] J. U. Nöckel, Phys. Rev. B 46, 15348 (1992).

[41] R. Akis, P. Vasilopoulos, and P. Debray, Phys. Rev. B 56, 9594 (1997).

[42] P. Duclos, P. Exner, and B. Meller, Rep. Math. Phys. 47, 253 (2001).

[43] V. Vargiamidis and H. M. Polatoglou, Phys. Rev. B 67, 245303 (2003).

[44] V. Gudmundsson, Y.-Y. Lin, C.-S. Tang, V. Moldoveanu, J. H. Bardarson, and A. Manolescu, Phys. Rev. B 71, 235302 (2005).

[45] J. U. Nöckel and A. D. Stone, Phys. Rev. B 51, 17219 (1995).

[46] C. W. J. Beenakker and H. van Houten, Phys. Rev. Lett. 60, 2406 (1988)

[47] R. E. Prange and T.-W. Nee, Phys. Rev. 168, B779 (1968).

[48] M. S. Khaikin, Adv. Phys. 18, 1 (1969).

[49] B. R. Snell, K. S. Chan, F. W. Sheard, L. Eaves, G. A. Toombs, D. K. Maude, J. C. Portal, S. J. Bass, P. Claxton, G. Hill, and M. A. Pate, Phys. Rev. Lett. 59, 2806 (1987) .

[50] B. I. Halperin, Phys. Rev. B 25, 2185 (1982).

[51] P. Streda, J. Kurcera, and A. H. MacDonald, Phys. Rev. Lett. 59, 1973 (1987) .

[52] M. L. Roukes, A. Scherer, S. J. Allen, Jr., H. G. Craighead, R. M. Ruthen, E. D. Beebe, and J. P. Harbison, Phys. Rev. Lett. 59, 3011 (1987) .

[53] R. E. Prange, Phys. Rev. 171, B737 (1968).

[54] R. Landauer, IBM J. Res. Dev. 1,223(1957)

[55] R. Landauer, Phil. Mag. 21,863 (1970)

[56] P.W. Anderson, D.J. Thouless, E. Abrahams, and D.S.Fisher, Phys. Rev. B 22,3519 (1980)

[57] A.D. Stone and A. Szafer, IBM J. Res. Dev. 32,384(1988)

[58] E.N. Economon and C.M. Soukoulis, Szafer, Phys. Rev. Lett. 46,618 (1981)

[59] *Introduction to Mesoscopic Physics*, Y.Imry (Oxford 1997), pp94

[60] M. Buttiker, Y.Imry, R.Landauer, and S.Pinhas, Phys. Rev. B 31,6207 (1985)

BIBLIOGRAPHY

[61] M. Buttiker, Phys. Rev. Lett. 57,1761 (1986)

[62] A.D. Benoit, S. Washburn, C.P. Umbach, R. B. Laibowitz, and R.A. Webb, Phys. Rev. Lett. 57,1765 (1986)

[63] U. Sivan and Y. Imry, Phys. Rev. B. 33, 551 (1986)

[64] *Gradshteyn and Ryzhik's Table of Integrals, Series, and Products*, Alan Jeffrey and Daniel Zwillinger(eds.), Sixth edition (July 2000)

[65] S.A. Gurvitz, Y.B. Levinson, Phys. Rev. B. 47, 10578 (1993)

[66] S.A. Gurvitz, Phys. Rev. B. 51, 7123 (1995).

[67] H. Tamura and T. Ando, Phys. Rev. B. 44, 1792 (1991).

[68] E.V. Sukhorukov and M.I. Lubin C. Kunze Y. Levinson, Phys. Rev. B. 49, 17191 (1994).

[69] Y. Takagaki and K. Ploog, Phys. Rev. B. 51, 7017 (1995).

[70] Vidar Gudmundsson, Yu-yu Lin, Chi-Shung Tang, Valeriu Moldoveanu, Jens Hjorleifur Bardarson, and Andrei Manolescu, Phys. Rev. B. 72, 235302 (2005).

[71] Shi-Shung Tang, Wing Wa Yu, and Vidar Gudmundsson, Phys. Rev. B. 72, 195331 (2005).